Dr. J. Allen 541

AS&E

ASE-1919

FINAL REPORT - CONTRACT NAS 5-11086

LUNAR SURFACE EXPLORATION BY SATELLITE

JUNE 1968

Prepared for

NATIONAL AERONAUTICS and SPACE ADMINISTRATION

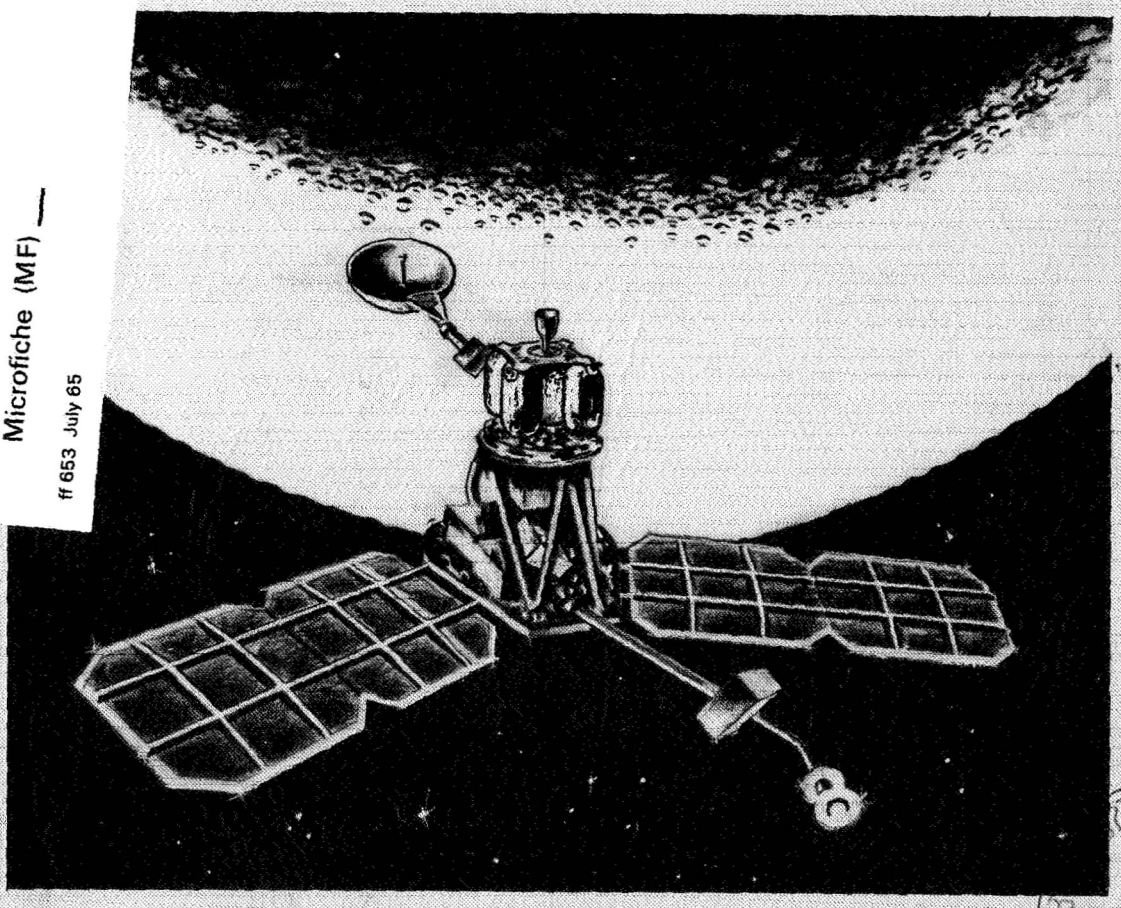

6805-1

AMERICAN SCIENCE and ENGINEERING, Inc.

FINAL REPORT

LUNAR SURFACE EXPLORATION BY SATELLITE

An Integrated Experiment Package

To Perform

Measurements Of The Composition Of The Lunar Surface

Contract NAS 5-11086

J. Carpenter, P. Gorenstein, H. Gursky
B. Harris, J. Jordan, T. McCallum, M. Ortmann, L. Sodickson

Prepared For

National Aeronautics and Space Administration
Goddard Space Flight Center
Greenbelt, Maryland 20771

Prepared By

American Science and Engineering, Inc.
11 Carleton Street
Cambridge, Massachusetts 02142

JUNE 1968

CONTENTS

Section			Page
1.0	INTRODUCTION		1-1
	1.1	Scientific Objectives	1-1
	1.2	Relation of the Manned Missions and Other Areas of Selenological Research	1-2
2.0	STATE OF PRESENT LUNAR KNOWLEDGE		2-1
	2.1	Current Status of the Observational Data Relating to the Moon	2-1
	2.2	Selenological Observations from Earth and Space	2-3
	2.3	Surveyor and Luna 10 Results	2-4
3.0	THE RADIATION ENVIRONMENT AT THE LUNAR SURFACE		3-1
	3.1	Various Physical Phenomena	3-1
		3.1.1 Radioactive Elements	3-2
		3.1.2 Cosmic Ray Interactions On The Lunar Surface	3-6
		3.1.3 Solar X-Rays and Lunar Fluorescence	3-8
		3.1.4 Infrared Radiation	3-13
	3.2	Physical Significance of These Phenomena	3-16
		3.2.1 Resultant Nuclear and Atomic Radiation	3-16
		3.2.2 Relation to Chemical Abundances	3-16
		3.2.3 Relation to Other Lunar Characteristics	3-19
		3.2.4 Sampling Depth of the Various Radiation	3-20
		3.2.5 Suitability of Moon Habitation and as a Scientific Observatory	3-21
	3.3	Interrelation Among the Various Radiations	3-22
		3.3.1 Increased Number of Elemental Ratios	3-22
		3.3.2 Consistency Among the Experiments	3-22

CONTENTS (continued)

Section			Page
	3.3.3	Background Measurements	3-23
	3.3.4	Instrumentation Compatibility	3-23
	3.3.5	Measurement Compatibility	3-24
	3.3.6	Spacecraft and Mission Compatibility	3-24
4.0	FLUXES, BACKGROUND, EXPERIMENTAL TECHNIQUES AND INSTRUMENTATION		4-1
4.1	Introduction		4-1
4.2	Gamma Ray Experiment		4-2
	4.2.1	Fluxes and Background	4-2
	4.2.2	Gamma Ray Detectors	4-6
	4.2.3	Electronics	4-13
	4.2.4	Expected Performance	4-13
4.3	X-Ray Fluorescence Experiment		4-20
	4.3.1	Fluxes and Background	4-20
	4.3.2	Detectors	4-21
	4.3.3	Electronics	4-25
	4.3.4	Estimated Counting Rates	4-28
4.4	Alpha Particle Experiment		4-35
	4.4.1	Fluxes and Background	4-35
	4.4.2	Detectors	4-42
	4.4.3	Electronics	4-42
	4.4.4	Expected Performance	4-44
4.5	Neutron Albedo Experiment		4-47
	4.5.1	Fluxes and Background	4-47
	4.5.2	Neutron Detectors	4-49
	4.5.3	Electronics	4-51
	4.5.4	Expected Performance	4-51

CONTENTS (continued)

Section			Page
	4.6	Observational Aspects of Lunar Radiations	4-54
	4.7	Expected Results	4-59
		4.7.1 Resolution of Spectral Lines	4-59
		4.7.2 Figure of Merit of Detector Systems	4-60
		4.7.3 Background Measurements, Auxiliary Monitors and Measurements	4-60
5.0	SPACECRAFT SELECTION		5-1
	5.1	Physical Characteristics of Experiment	5-1
	5.2	Environmental Constraints	5-6
	5.3	Spacecraft/Experiment Electrical System	5-7
	5.4	Mounting and Orientation Considerations	5-7
	5.5	Possible Spacecraft	5-9
		5.5.1 Pioneer	5-9
		5.5.2 Anchored IMP	5-9
		5.5.3 Lunar Orbiter	5-9
6.0	FLIGHT REQUIREMENTS, SPACECRAFT ATTITUDE AND ORBITAL PARAMETERS		6-1
	6.1	Basic Plan of the Experiment	6-1
	6.2	Spacecraft Stabilization Modes	6-6
	6.3	Detector Orientation	6-6
	6.4	Orbital Effects	6-7
		6.4.1 Lunar Rotation	6-7
		6.4.2 Changes During the Year	6-9
		6.4.3 Effect of Orbit Inclination	6-9
		6.4.4 Methods of Increasing Moon-Viewing Time	6-12

CONTENTS (continued)

Section		Page
6.5	Sun Inclination	6-13
6.6	Other Orientation Considerations	6-14
6.7	Data Handling System	6-15
7.0	CONCLUSIONS AND RECOMMENDATIONS	7-1
7.1	Overall Program Conclusions	7-1
7.2	Definitions of Areas of Work	7-3
7.3	Recommendations for Future Work	7-6
REFERENCES		7-8

APPENDICES

A	SATELLITE ENVIRONMENT	A-1
B	A/IMP STORAGE CAPABILITY (MODELS D & E)	B-1
C	TABLE OF ABUNDANCES	C-1
D	INFRARED EXPERIMENT	D-1
E	MASS SPECTROMETER EXPERIMENT	E-1

ILLUSTRATIONS

Figure		Page
1-1	Lunar Map Showing Proposed Mission Sites and Sequence	1-3
2-1	Measurements of Lunar Composition at Landing Sites of Surveyors V, VI, and VII[8]	2-5
2-2	Gamma Ray Spectra From the Moon as Observed From the Soviet Spacecraft Luna 10	2-6
3-1	Gamma-Ray Spectrum of Soil Showing the Contribution of Uranium + Daughters, Thorium + Daughters, and Potassium-40	3-5
3-2	Solar and Galactic Cosmic Ray Proton Flux	3-7
3-3	Comparison of Solar X-Ray Spectrum Between 6.3 and 20 Å Obtained During a Flare on March 22, 1967 With a Spectrum Obtained on the Previous Day When No Flares Were in Progress	3-9
3-4	The Solar X-Ray Spectrum in the Region 1.3 - 3.1 Å as Observed by Neupert, Gates, Swartz and Young[12] During the Increasing Phase of an X-Ray Burst on March 22, 1967	3-10
3-5	Calculated Yield of Fluorescent Kα and Scattered X-Rays from Ideal Smooth Lunar Surface Material of Basaltic and Granite Composition	3-12
3-6	Calculated Fluorescent and Scattered X-Ray Intensity During Typical Solar Flare	3-14
4-1	Typical Y^{88} Gamma Ray Spectrum Obtained with a 3" Dia x 3" Thick Thallium Activated Sodium Iodide Crystal	4-7
4-2	Gamma Ray Detector with Active Shield and Collimator	4-9
4-3	Geometry of Gamma Rays Entering Detector	4-11
4-4	Calculated Response for Several Energies of Gamma Ray Detector Shown in Figure 4-3	4-12
4-5	Functional Block Diagram of Gamma Ray Experiment	4-14
4-6	Gamma Ray Spectrum from Moon as It Would be Observed in a Low Resolution Detector	4-15
4-7	The X-Ray Transmission as a Function of Wavelength for Several Metallic Filters of Selected Thickness	4-24

ILLUSTRATIONS (continued)

Figure		Page
4-8	X-ray Detector Consisting of Collimator, Proportional Counters, and Filter Wheel	4-26
4-9	Function Block Diagram of X-ray Experiment	4-27
4-10	Functional Block Diagram of Charge Particle Experiment	4-43
4-11	Alpha Particle Background at Surveyor V Landing Site	4-45
4-12	The Calculated Neutron Equilibrium Leakage Spectrum for the Lunar Surface for Compositions A, Chondritic Material; B, Chondritic Material with a 10 Per Cent Increase in the Total 1/v Capture; E, Chondritic Material with 0.1 H/Si Atom; and F, with 1.0 H/Si Atom	4-48
4-13	Functional Block Diagram of Neutron Experiment	4-52
4-14	Calculated Neutron Counting Rate Ratios in Detectors (a) and (b)	4-53
4-15	Coverage of Lunar Surface From Orbiting Vehicle With Detectors Limited to 60° Cone-Shaped Field of View	4-56
5-1	Sensors/DHS/Communications System Block Diagram	5-3
5-2	Logic Block Diagram Experiment Processing Electronics	5-4
5-3	Spacecraft/Experiment System Electronic Interface Block Diagram	5-8
6-1	Conceptual View of X-Ray Fluorescence Data Sensing from Orbiting Satellite	6-2
6-2	Plan View of Orbiting Satellite	6-3
6-3	View Area Parameters	6-4
6-4	Scanned Area for Equator-Polar Orbit	6-5
6-5	Scanning of Polar Regions with Detector Axes Fixed in Perpendicular Orientation to Solar Direction	6-8
6-6	View Looking Down on Pole	6-10
6-7	Satellite and Orbital Relationships Over Solar Year	6-11

TABLES

Table		Page
III-1	Uranium (Radium) Series	3-3
III-2	Thorium Series	3-4
III-3	Results of a Calculation of the Yield of Fluorescent X-Rays	3-11
IV-1	Energies and Relative Yields of Natural Gammas	4-2
IV-2	Window Transmissions	4-22
IV-3	Expected Counting Rates	4-29
IV-4	Estimates of Terrestrial and Meteoritic Sources Of Alpha-Emission	4-36
IV-5	Expected Counting Rates	4-40
V-1	Experimental Physical Characteristics and Parameters	5-2
V-2	Spacecraft Characteristics	5-10
VI-1	Data System Parameters	6-16

FOREWORD

This document is the final report on a study of an integrated group of experiments whose objective is a geochemical survey of the lunar surface to be performed from a lunar orbiting spacecraft. The study was performed under NASA Contract NAS 5-11086 for the Goddard Space Flight Center.

The central idea in this program is that a certain amount of atomic and nuclear radiation is naturally emitted from the moon that is characteristic of the elements comprising the surface layer and that the detection and analysis of this radiation can be used to determine chemical composition. Geochemical prospecting with nuclear radiation detectors is a recognized technique, and its application to the moon has been discussed for at least ten years. Experimental attempts to detect certain species of this radiation extend almost as far back. The x-ray astronomy group at American Science and Engineering attempted, during 1961 and 1962, to detect fluorescence x-rays from the moon with instruments flown on sounding rockets. During the same time period a group of the University of California and the Jet Propulsion Laboratory attempted to measure gamma radition from the moon with instruments on the Ranger spacecraft series. During the intervening time the technology required to detect these radiations has greatly improved. In addition, other observations have been proposed that appear to have merit, such as the measurement of neutrons and alpha particles. Specific proposals to perform these measurements have generally had favorable reviews from various scientific committees.

Concurrently, it has been recognized that it is useful to consider an integrated experiment package in which the various observations are performed simultaneously. Not only is there a certain economy of technology in the sense that the several instruments can share common hardware and present similar constraints to the mission, but also it can be demonstrated that more information on the moon can be obtained by this

approach as opposed to performing single experiments. An integrated experiment, in fact, was given a high priority by the geochemical panel of the Santa Cruz study group, meeting during the summer of 1967.

Much of the material in this document is common knowledge; some of it, however, particularly discussions of certain background radiation, has not been generally available. Also, the interrelationships between the various instruments are discussed in detail, as are the requirements of an actual space mission.

Technical monitorship of this report was provided by Dr. Isidore Adler and Dr. J. I. Trombka of the Goddard Space Flight Center. The authors gratefully acknowledge the many fruitful discussions with them and their fellow staff members.

1.0 INTRODUCTION

1.1 Scientific Objectives

Exploration of the moon is a major objective of our space effort. The scientific significance of this activity has been widely discussed in literature beginning long before the possibility existed. Particular objectives for various aspects of lunar exploration were presented at the 1967 and 1965 NASA Summer Conference on Lunar Exploration and Science held at Santa Cruz, California and Falmouth, Massachusetts[1,2]. The motivation for this study originated with the recommendation by the Geochemistry Group at the Santa Cruz conference that a compositional remote sensing package be given a high priority and be flown at the earliest opportunity.

The absence of an atmosphere about the moon allows the use of an orbiting vehicle for widespread exploration of the lunar surface through the observation of charged particles, neutrons, as well as non-optical electromagnetic radiations. If several of these observations are made simultaneously from a single integrated experiment package, the total result assumes a greater selenological importance. This report describes a set of experiments for a lunar orbiting vehicle providing spatial resolution. Essential performance characteristics of the experiments and the requirements of the vehicle are considered. The principal objective of the integrated experiment is to conduct a compositional survey of the lunar surface. Inhomogeneities will be evident to a scale of about 50 Km. In particular, it will be possible to discriminate between areas that are basaltic and granitic. In addition, the experiment will be sensitive to the presence of hydrogeneous material near the surface and to the spatial distribution of natural radioactivity which is proportional to the concentrations of uranium and thorium. Both of these factors are relevant to the suitability of selected regions of the moon for habitation and as sites for an x-ray or γ-ray observatory.

1.2 Relation of the Manned Missions and Other Areas of Selenological Research

The ultimate in lunar study will result from the manned expeditions to selected points. Several lunar sites that have been proposed for such investigation are shown in Figure 1-1. Detailed measurements of the composition will result from analysis in situ and on returned samples. This program of research would complement those measurements in the following ways.

a) Perform a Measurement of the Moon's Composition as a Whole

Limitations upon the astronaut's range of mobility will mean that the manned expeditions can survey only a very small fraction of the moon. However, knowledge of the gross composition is needed to explain many important lunar characteristics possibly including several local topographic features. These measurements would establish or place limiting values upon the mean chemical composition of the lunar surface.

b) Extrapolation of the Findings of the Manned Missions

Correlation of these results with those obtained in manned missions would provide a sound basis for extrapolating the results of the detailed analysis at selected points to larger regions of the moon.

c) Indicate New Regions of Outstanding Interest

To date the topography has been the basis for selecting regions of outstanding interest for further investigation under the manned program. This program will produce a mapping of the moon in terms of geochemical indices and natural radioactivity levels. As a result, new regions of outstanding interest may emerge. These findings will also be important to lunar research from earth based observatories. It has been established that the optical character of irradiated rocks can be similar in appearance to the lunar color and

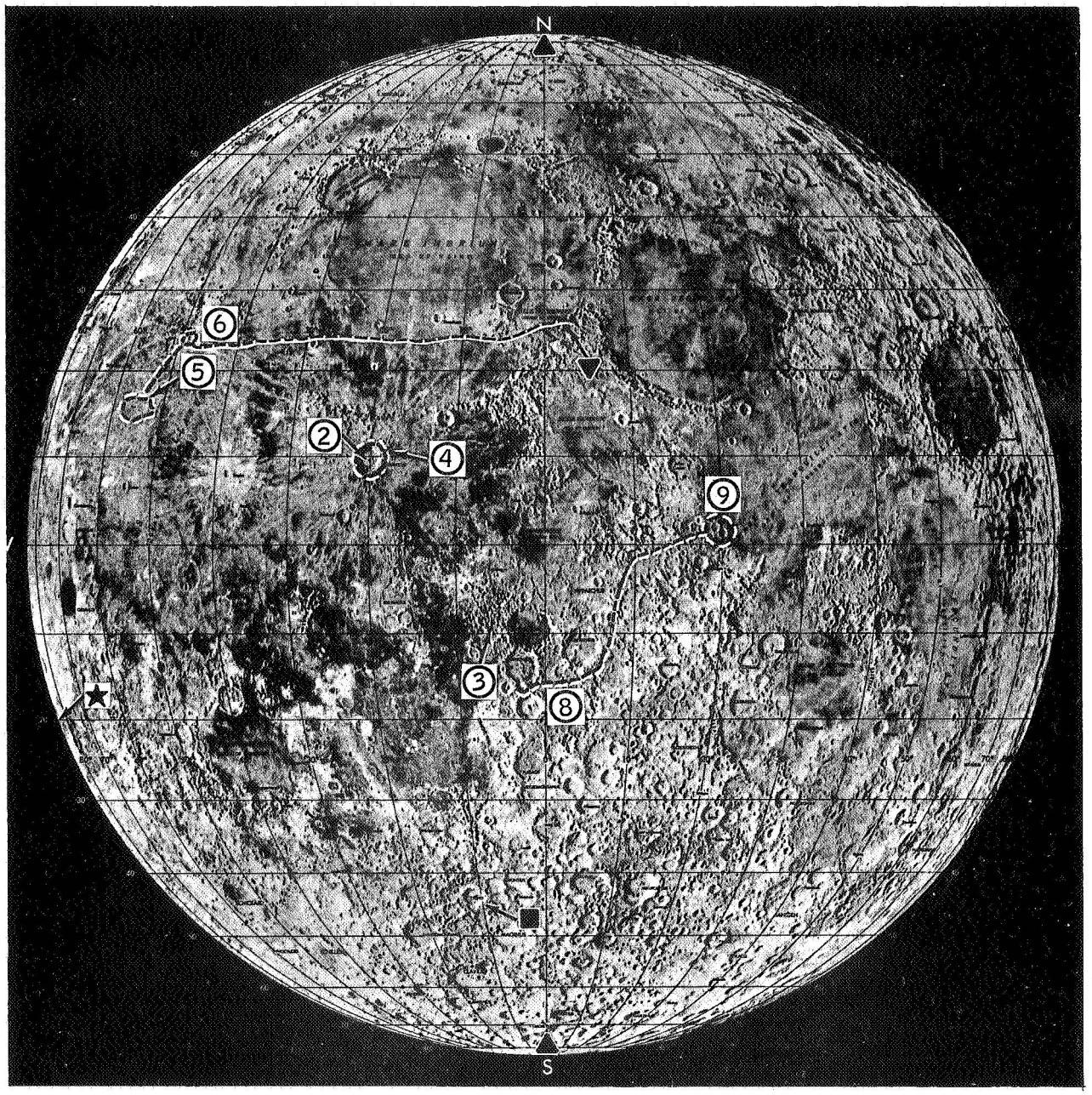

Figure 1-1. Lunar map showing proposed mission sites and sequence.

albedo. If different regions which are shown to have the same chemical composition can be distinguished on the basis of their optical properties, the results can be interpreted on the basis of difference in the amounts of solar radiation they have received and hence their history.

2.0 STATE OF PRESENT LUNAR KNOWLEDGE

2.1 Current Status of the Observational Data Relating to the Moon

To date the majority of the observations on the moon have had to do with surface properties, although certain measurements such as the radar reflectivity and the thermal emission (infrared and radio) give some information down to depths of perhaps meters. The outstanding piece of information on the moon as a bulk object is its density; more recently it has become possible to measure its bulk electrical characteristics. The magnetic field is directly measurable (it is found to be absent), and its electrical conductivity is measurable through the study of the interaction of the moon and the solar wind[3].

Prior to the measurements at the Surveyor landing sites, estimates of the chemical composition of the lunar surface had been speculation, usually based on models of the formation of the moon. It has long been assumed that the lunar highlands consist mostly of granitic material and that the maria are basaltic, as in the continents and oceans of the earth's crust. To date no firm geochemical evidence exists which suggests that the composition of the maria is different from that of the highlands. A study of the depth-diameter ratios of lunar craters indicate that the material in the maria exhibits less shear strength than that of the continental material. This has been interpreted by some as indicating that the maria are composed of vesicular lava and that the highlands are compacted rubble.

Clearly, the presently available information cannot provide an accurate analysis of the composition of the lunar surface.

The Surveyor program has provided photographs down to a scale of millimeters, and certainly improvements will be made in infrared and radar studies to yield pictures with as good a scale as is obtained in visible

light from the earth. These studies of the surface have made possible the assessment of a variety of geophysical processes. Of particular significance is the fact that certain features, such as the craters, Tycho and Copernicus, display anomalous radar reflectivity and infrared emission. Tycho has long been regarded as the classic example of an impact crater; however, based on recent lunar orbiter photographs, Strom and Fielder[4] find evidence for lava flows and, thus, volcanic eruptions. Also transient optical phenomena involving color changes, bright spots, and obscurations as have been summarized recently by Middlehurst[5] must be the result of disturbances in the lunar crust. The significance of these modern observations of the moon is that they begin to reveal a host of dynamical processes and in sufficient detail to begin to make realistic quantitative models.

The alpha-scattering experiments performed during the Surveyor Missions have provided the first quantitative geochemical data on the moon's surface, although observations made during the Soviet Lunik series have a geochemical interpretation. Aside from telling us what elements comprise the moon, geochemical observations give us information on the origin of the moon, its thermal history, and the mass flows on the surface.

2.2 Selenological Observations from Earth and Space

As with many other branches of the space sciences, many of the important results in the study of the moon will be obtained from earthbound observations. The infrared and radio emission from the moon, studied in high resolution, yields the thermal conductivity of the surface and may indicate the existence of real subsurface hot regions. The infrared emission studies may also yield geochemical information, although it has not been established that they can do so. High resolution radar studies provide point-by-point measures of the local conductivity which is indicative of the character (e.g., compaction) of the local material. Of course, there is a continuing interest in the study of transient phenomena.

Efforts have been made to infer composition measurements through earth based optical observations. A similarity has been noted between the properties of the lunar albedo in the visible region and species of terrestrial rock that have been subjected to solar-like irradiation[6].

The presence of man on the moon, the return of rock samples, and the placement of sophisticated instruments on the surface will represent the high point of lunar research. However, no matter how many times the moon is visited, trips to the surface can provide information only on a microscopic fraction of the total. The availability of lunar-orbiting vehicles allow the accumulation of all kinds of data in addition to the high resolution photographs to which they have been almost exclusively devoted. In particular, measurements of the high energy environment of the moon, high resolution infrared imagery, detection of a lunar atmosphere by mass spectroscopy, the study of the lunar interaction with the solar wind, and presumably other observations become feasible and desirable in view of the fact that they allow study of the entire lunar surface and the determination other than just purely topographic features.

2.3 Surveyor and Luna 10 Results

Measurements on the lunar chemical composition have emerged from the results of the Surveyor series and the Soviet spacecraft Luna 10.

Three Surveyor missions, V, VI, and VII, have performed a chemical analysis of the landing sites by means of an alpha-scattering technique. Several light and middle Z elements were identified and their abundances were determined to an accuracy of several percent[7]. Findings of the three missions are summarized in Figure 2-1. The Surveyor V and VI landing sites were in the maria regions. The chemical analysis indicates that the soil at the site is a silicate rock similar to basaltic materials available on the earth. The Surveyor VII measurement was performed in a highlands area site. The analysis indicates a somewhat different chemical composition containing less iron.

In 1967 gamma-rays emitted by the moon were detected with a spectrometer aboard the Soviet lunar orbiter Luna 10[8]. The objective was to determine the chemical composition and the degree of natural radioactivity. Typical gamma-ray spectra from the moon as seen in that experiment are shown in Figure 2-2. The authors attribute "peaks" in the spectra to the presence of certain elements. It was found that on the average no more than 10 percent of the total intensity of lunar gamma radiation was due to the decay of potassium, thorium, and uranium, and that over 90 percent was the result of cosmic ray effects. By comparing those spectra with that for terrestrial standards the authors conclude that the lunar rocks are of a basic (basaltic) and/or ultra-basic (dunite and chondritic) composition. They did not confirm the existence of large areas characterized by a granitic composition.

ELEMENT	SURVEYOR V		SURVEYOR VI		SURVEYOR VII	
CARBON	< 3 %		< 2 %		< 2 %	
OXYGEN	58	± 5	57	± 5	58	± 5
SODIUM	< 2		< 2			
MAGNESIUM	3	± 3	3	± 3	4	± 3
ALUMINUM	6.5	± 2	6.5	± 2	8	± 3
SILICON	18.5	± 3	22	± 4	18.5	± 3
"CALCIUM"	13	± 3	6	± 2	6	± 2
"IRON"			5	± 2	2	± 1

Figure 2-1 Measurements of Lunar Composition at Landing Sites of Surveyors V, VI, and VII (7)

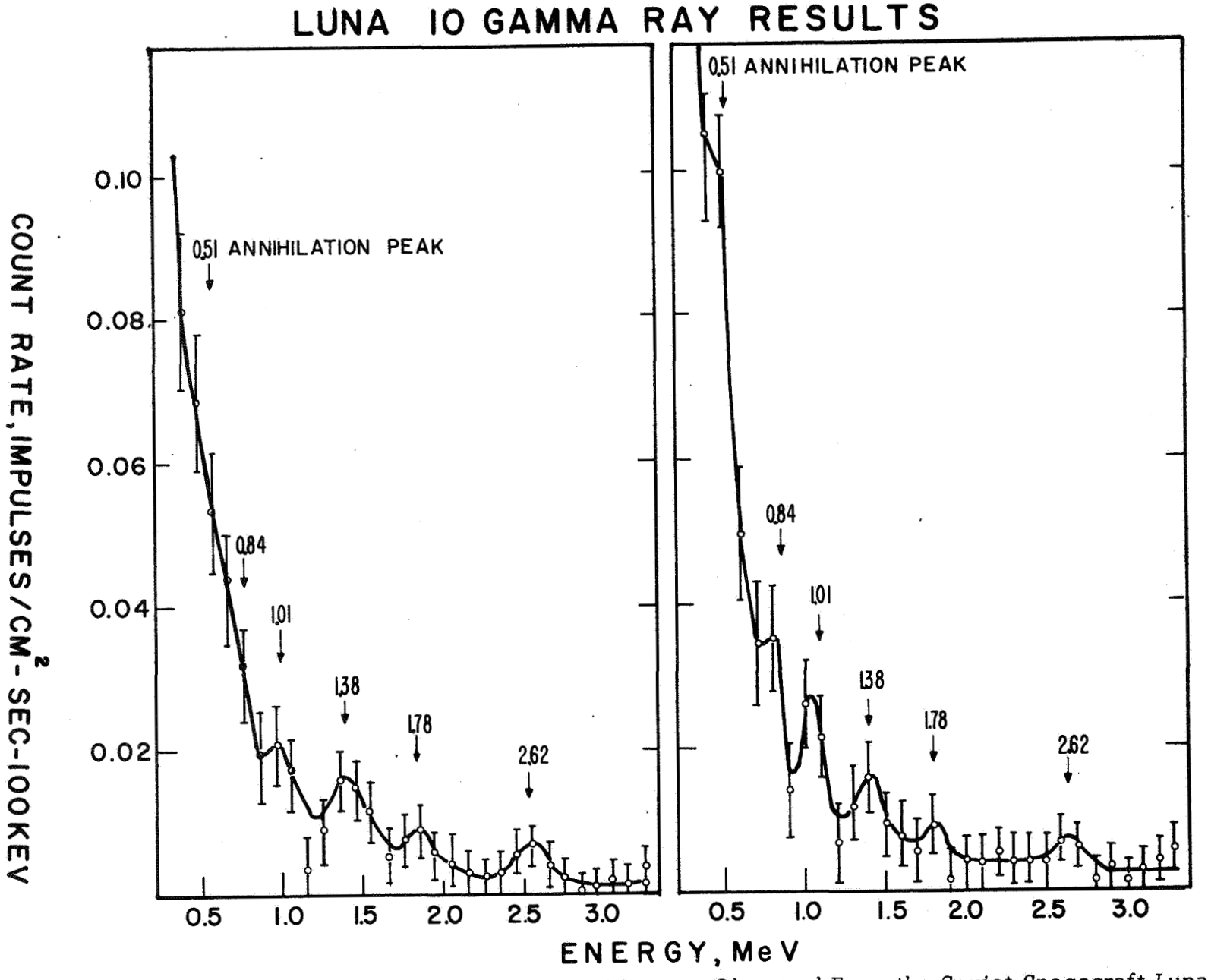

Figure 2-2 Gamma Ray Spectra From the Moon as Observed From the Soviet Spacecraft Luna 10 (Reproduced from article by Vinogradov et al [8])

3.0 THE RADIATION ENVIRONMENT AT THE LUNAR SURFACE

3.1 Various Physical Phenomena

Both natural and induced sources of radiation are expected at the lunar surface. Among the principal natural radioactive constituents are presumably those long lived nuclides found on the earth, such as K^{40}, U^{238}, and Th^{232} and their decay products which emit alpha, beta, and gamma radiation of various energies. Special processes may occur such as the radon diffusion mechanism suggested by Kraner, Schroeder, Davidson, and Carpenter[9] which greatly enhance the radioactivity at the surface. Bombardment of the lunar surface by galactic cosmic rays and energetic protons associated with solar flare events lead to the production of a variety of shorter lived nuclides on the lunar surface. The result is an induced radioactivity.

Interactions of cosmic rays also yield a prompt albedo of charged particles, neutrons, and photons through inelastic processes and the breakup of highly excited nuclei. The great complexity in the spectra of highly excited states cause large variations in the energy and nature of the emitted nuclear radiation.

Solar x-rays absorbed on the lunar surface will cause fluorescence x-rays to be emitted. These x-rays will be characteristic of the elements expected to be found on the surface such as O, Na, Mg, Al, Si, K, Ca, Mn and Fe. The relative yield of their characteristic x-rays is then conditioned by the relative abundance of these elements. Other factors such as the shape of the incident solar x-ray spectrum and the size of the lunar particles will also have a strong influence. In the absence of solar activity there is a much smaller contribution to the production of lunar x-rays through natural radioactivity and cosmic ray bombardment, and solar wind effects.

Observation of nuclear radiation from the lunar surface is of fundamental interest when the results are interpretable in terms of chemical composition. Such interpretation is possible when the spectrum contains discrete lines. In the subsequent discussion it is explained that a substantial fraction of the outgoing x- and γ- radiation is discrete. There is also reason to believe that the radon diffusion mechanism will produce significant amounts of monoenergetic alpha particles at the surface.

3.1.1 Radioactive Elements

(a) Natural Radioactivity

Expectations concerning lunar radioactivity are conditioned by our experience with natural radioactivity in the earth's crust. The principal elements that contribute to the radiation emanating from rocks are K^{40}, and the members of the uranium series and the thorium series. Gamma rays result from all three while the latter two produce a variety of alpha and beta rays as well. The decay chains of uranium and thorium are given in Tables III-1 and III-2. Several of the rare earth elements contribute a very much smaller share to the total radioactivity. A typical gamma ray spectrum from a soil sample is shown in Figure 3-1.

On the earth the ratio of K^{40} to K^{39} is fairly constant at 1:8500 so that the gamma activity is an indication of the total amount of potassium. Generally speaking, the concentrations of potassium vary from 2% to 6% in granite and 0.4% to 1.5% in basalt. Various sub-classes in these two categories such as "oceanic" or "plateau" basalt can be distinguished by their potassium concentrations. The granite rocks are also richer in uranium and thorium than the basalts. Consequently, granite will exhibit significantly more gamma activity than basalts. Most data indicates that the concentration of Th and U and the Th/U ratio increases with the degree of rock differentiation. In igneous rock the concentration of all three gamma emitters varies roughly with the percentage of silica.

TABLE III-1

URANIUM (RADIUM) SERIES

Isotope	Symbol	Historical Name	Half-life	Radiation	Energy (mev.)
Uranium-238..	$_{92}U^{238}$	Uranium I	4.5×10^{9} yr.	α	4.18(77), 4.13(23)
Thorium-234..	$_{90}Th^{234}$	Uranium X_1	24.1 day	β	0.19(65), 0.10(35)
				γ	0.09(15), 0.06(7), 0.03(7)
Protactinium-234.....	$_{91}Pa^{234}$	Uranium X_2	1.18 min.	β	2.31(93), 1.45(6), 0.55(1)
				γ	1.01(2), 0.77(1), 0.04(3)
Uranium-234..	$_{92}U^{234}$	Uranium II	2.50×10^{5} yr.	α	4.77(72), 4.72(28)
				γ	0.05(28)
Thorium-230..	$_{90}Th^{230}$	Ionium	8.0×10^{4} yr.	α	4.68 (76), 4.62(24)
Radium-226...	$_{88}Ra^{226}$	Radium	1622 yr.	α	4.78(94), 4.59(6)
				γ	0.19(4)
Radon-222....	$_{86}Rn^{222}$	Radon	3.82 day	α	5.48(100)
Polonium-218..	$_{74}Po^{218}$	Radium A	3.05 min.	α	6.00(100)
Lead-214.....	$_{82}Pb^{214}$	Radium B	26.8 min.	β	1.03(6), 0.66(40), 0.46(50), 0.40(4)
				γ	0.35(44), 0.29(24), 0.24(11), 0.05(2)
Bismuth-214..	$_{83}Bi^{214}$	Radium C	19.7 min.	β	3.18(15), 2.56(4), 1.79(8), 1.33(33), 1.03(22), 0.74(20)
				γ	2.43(2), 2.20(6), 2.12(1), 1.85(3), 1.76(19), 1.73(2), 1.51(3), 1.42(4), 1.38(7), 1.28(2), 1.24(7), 1.16(2), 1.12(20), 0.94(5), 0.81(2), 0.77(7), 0.61(45)
Polonium-214..	$_{84}Po^{214}$	Radium C'	160×10^{-6} sec.	α	7.68(100)
Lead-210.....	$_{82}Pb^{210}$	Radium D	19.4 yr.	β	0.06(17), 0.02(83)
				γ	0.05(4)
Bismuth-210..	$_{83}Bi^{210}$	Radium E	5.0 day	β	1.16(100)
Polonium-210..	$_{84}Po^{210}$	Radium F	138.4 day	α	5.30(100)
Lead-206.....	$_{82}Pb^{206}$	Radium G	Stable		

Reference: The Natural Radiation Environment, Ed. by J. A. S. Adams and W. M. Lowder, Rice University Semicentennial Publication, University of Chicago Press, Chicago 1964.

TABLE III-2

THORIUM SERIES

Isotope	Symbol	Historical Name	Half-life	Radiation	Energy (mev.)
Thorium-232..	$_{90}Th^{232}$	Thorium	1.41×10^{10} yr.	α	4.01(76), 3.95(24)
				γ	0.06(24)
Radium-228...	$_{88}Ra^{228}$	Mesothorium I	6.7 yr.	β	0.05(100)
Actinium-228..	$_{89}Ac^{228}$	Mesothorium II	6.13 hr.	β	2.18(10), 1.85(9), 1.72(7), 1.13(53), 0.64(8), 0.45(13)
				γ	1.64(13), 1.59(12), 1.10, 1.04, 0.97(18), 0.91(25), 0.46(3), 0.41(2), 0.34(11), 0.23, 0.18(3), 0.13(6), 0.11, 0.10, 0.08
Thorium-228..	$_{90}Th^{228}$	Radiothorium	1.91 yr.	α	5.42(72), 5.34(28)
				γ	0.08(2)
Radium-224...	$_{88}Ra^{224}$	Thorium X	3.64 day	α	5.68(95), 5.45(5)
				γ	0.24(5)
Radon-220....	$_{86}Rn^{220}$	Thoron	54.5 sec.	α	6.28(99+)
Polonium-216..	$_{84}Po^{216}$	Thorium A	0.158 sec.	α	7.68(100)
Lead-212.....	$_{82}Pb^{212}$	Thorium B	10.64 hr.	β	0.58(14), 0.34(80), 0.16(6)
				γ	0.30(5), 0.24(82), 0.18(1), 0.12(2)
Bismuth-212..	$_{83}Bi^{212}$	Thorium C	60.5 min.	α	6.09(10), 6.04(25)
				β	2.25(56), 1.52(4), 0.74(1), 0.63(2)
				γ	0.04(1), with α 2.20(2), 1.81(1), 1.61(3), 1.34(2), 1.04(2), 0.83(8), 0.73(10), with β
Polonium-212..	$_{84}Po^{212}$	Thorium C'	0.30×10^{-6} sec.	α	8.78(100)
Thallium-208..	$_{81}Tl^{208}$	Thorium C''	3.1 min.	β	2.37(2), 1.79(47), 1.52, 1.25
				γ	2.62(100), 0.86(14), 0.76(2), 0.58(83), 0.51(25), 0.28(9), 0.25(2)
Lead-208.....	$_{82}Pb^{208}$	Thorium D	Stable		

Reference: (See page 3-3).

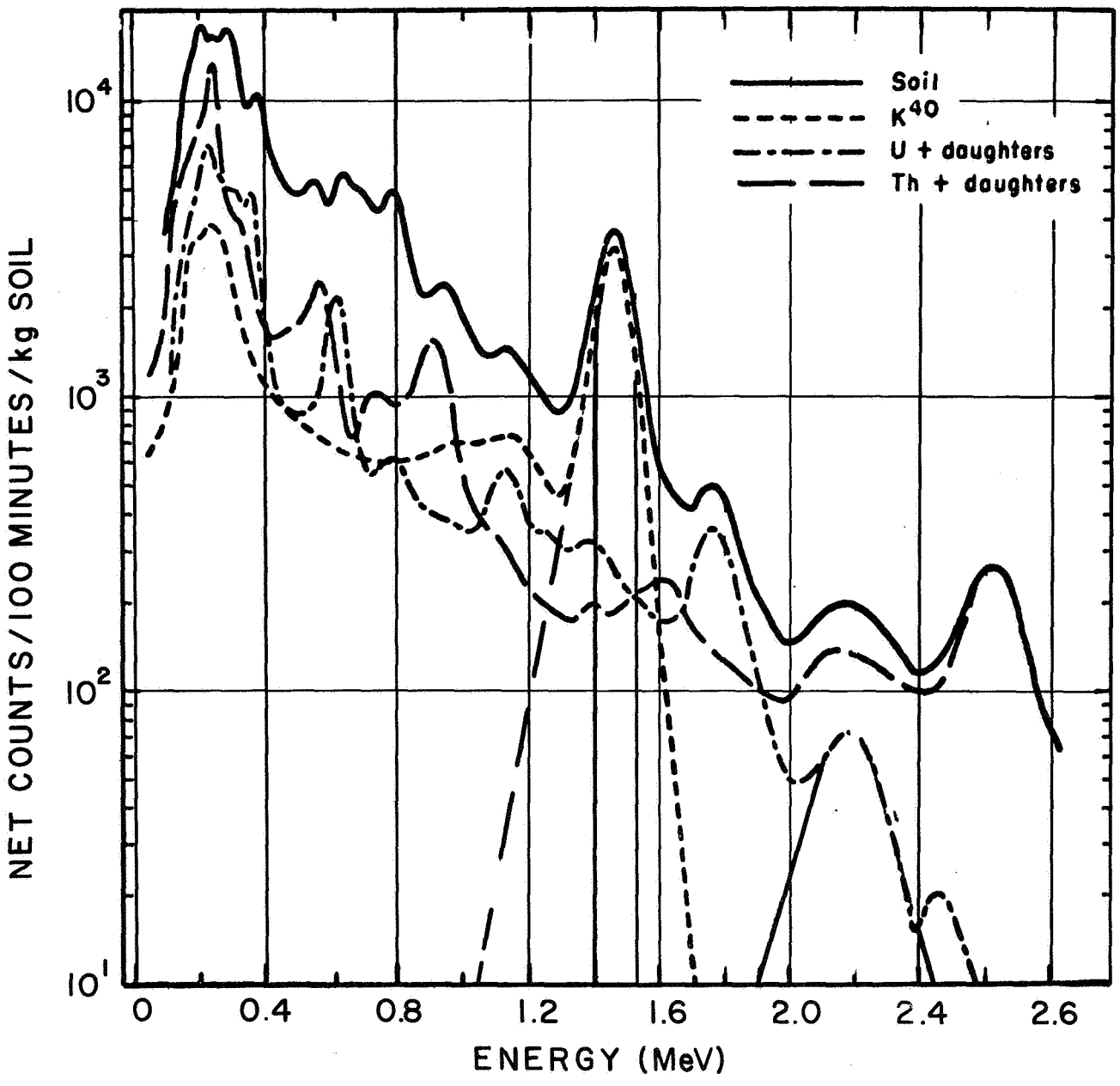

Figure 3-1 Gamma-Ray Spectrum of Soil Showing the Contribution of Uranium + Daughters, Thorium + Daughters, and Potassium - 40. This figure appears in an article by Gustafson and Biar (10)

(b) Radon Diffusion Mechanism

A process by which radon diffuses through the upper surface layer of the moon and subsequently deposits some of its decay products on the surface has been suggested as mechanism for producing sizable surface activity. Recent measurements on earth samples of the radon and thoron diffusion allow estimates of this effect to be made. If the process is comparable in effectiveness on the moon, the natural radioactivity at the surface will be substantially above that predicted by the distributed concentrations of uranium and thorium. In addition to increasing the total amount of alpha, beta and gamma activity, the diffusion process is a means by which alpha particles can leave the lunar surface without degradation through ionization. The result is alpha particles with discrete kinetic energies.

3.1.2 Cosmic Ray Interactions On The Lunar Surface

Strongly interacting particles are perpetually striking the lunar surface. Most of these are protons; they originate from the sun and outside of the solar system ("galactic" component). Figure 3-2 shows the measured proton flux from these two sources. The absence of an atmosphere and a magnetic field leads to a situation that is quite different from that prevailing at the earth's surface. Charged particles of low momentum are not magnetically deflected away from the moon, and strong interactions of the primaries take place directly on the surface. An interacting primary undergoes a complex series of nuclear reactions that will ultimately yield several decay products. These reactions include meson production, "knock on" and evaporation mechanisms. Inelastic processes produce excited nuclei which subsequently emit gamma rays, charged particles, and neutrons. The neutrons in turn may escape or be captured by nuclei and produce gamma rays. The initial kinetic energy of the proton primary will eventually be transferred to an abundance of gamma rays, neutrons, and charged particles. Their spectral distribution is for the most part a large number of lines that are characteristic of the elements

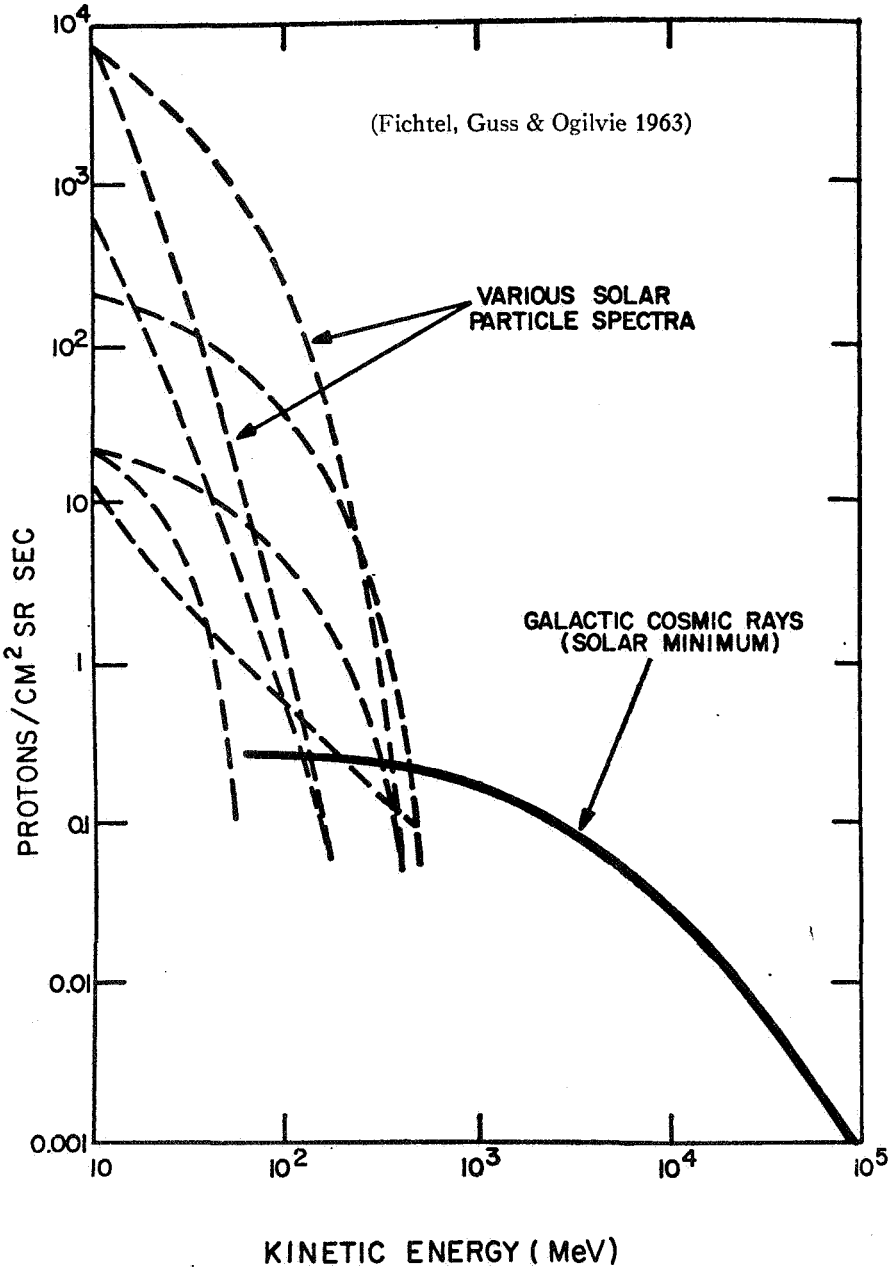

Figure 3-2 Solar and Galactic Cosmic Ray Proton Flux (Fichtel, Guss, and Ogilvie)[11]

found on the lunar surface. However, the density of lines is large and if they are not resolved, the spectrum will appear to be a continuum. The residual nuclei are unstable, generally short lived beta and gamma emitters. Some of the nuclides that will be formed are longer lived, such as $Al^{26}(T_{1/2} = 7.4 \times 10^5$ yr.) and $Ca^{41}(T_{1/2} = 1.1 \times 10^5$ yr.). Departures from equilibrium could be used in principle to date events or processes on that time scale which have occured on the surface. The concentrations of those two elements would be small so that this would best be done with returned samples. Copius amounts of charged and neutral particles will be emitted from the lunar surface. However, the charged particles suffer continuous slowing down inside the lunar material, and the spectral information is lost. On the other hand, the gamma rays will in part leave the lunar surface as lines. However, the spectral distribution is extremely dense and complex due to the large variety of excited nuclei decaying by stages to the ground state.

3.1.3 Solar X-Rays and Lunar Fluorescence

The absorption of solar x-rays by the lunar surface creates fluorescent x-rays of the constituent chemical elements. The normal solar x-ray spectrum is sufficiently hard to produce significant amount of fluorescent Kα x-rays from the more abundant elements such as oxygen, sodium, aluminum, magnesium, and silicon. In addition, there are very soft Lα x-rays from iron, calcium, and potassium. Solar x-ray spectra are shown in Figures 3-3 and 3-4. Harder incident x-rays from occasional solar flare outbursts will produce the more easily observable Kα radiation of these three elements. Deriving quantitative chemical composition from the observation of these x-rays requires a great deal of caution. The amount produced is not large enough to allow the use of Bragg Spectrometers for precise wavelength selection. Hence, one is required to use low resolution techniques such as proportional counters with pulse height analysis plus filters. Fluorescent x-rays are

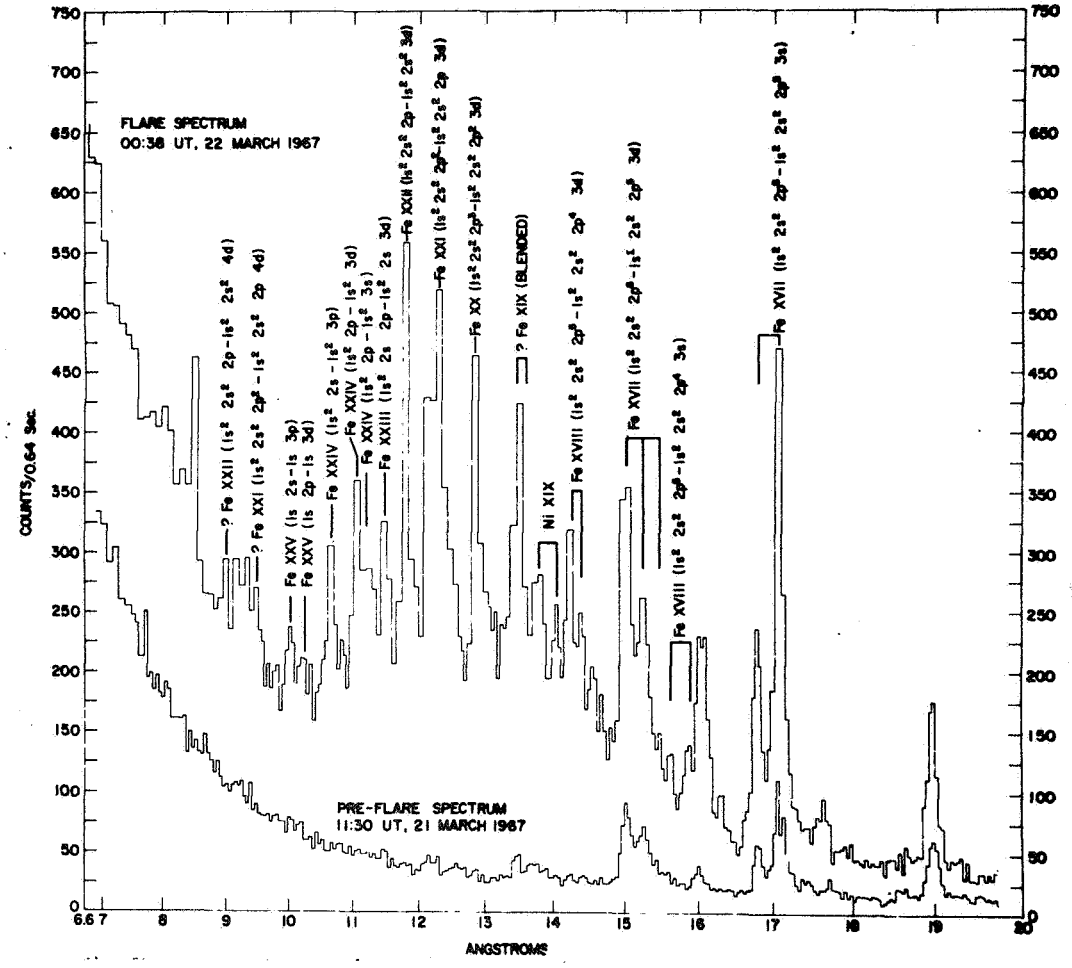

Figure 3-3 Comparison of Solar X-Ray Spectrum Between 6.3 and 20 Å Obtained During a Flare on March 22, 1967 With a Spectrum Obtained on the Previous Day When No Flares Were in Progress.

Note: Spectral resolution is insufficient to allow resolution of lines within each array. (From article by Neupert, Gates, Swartz and Young[12])

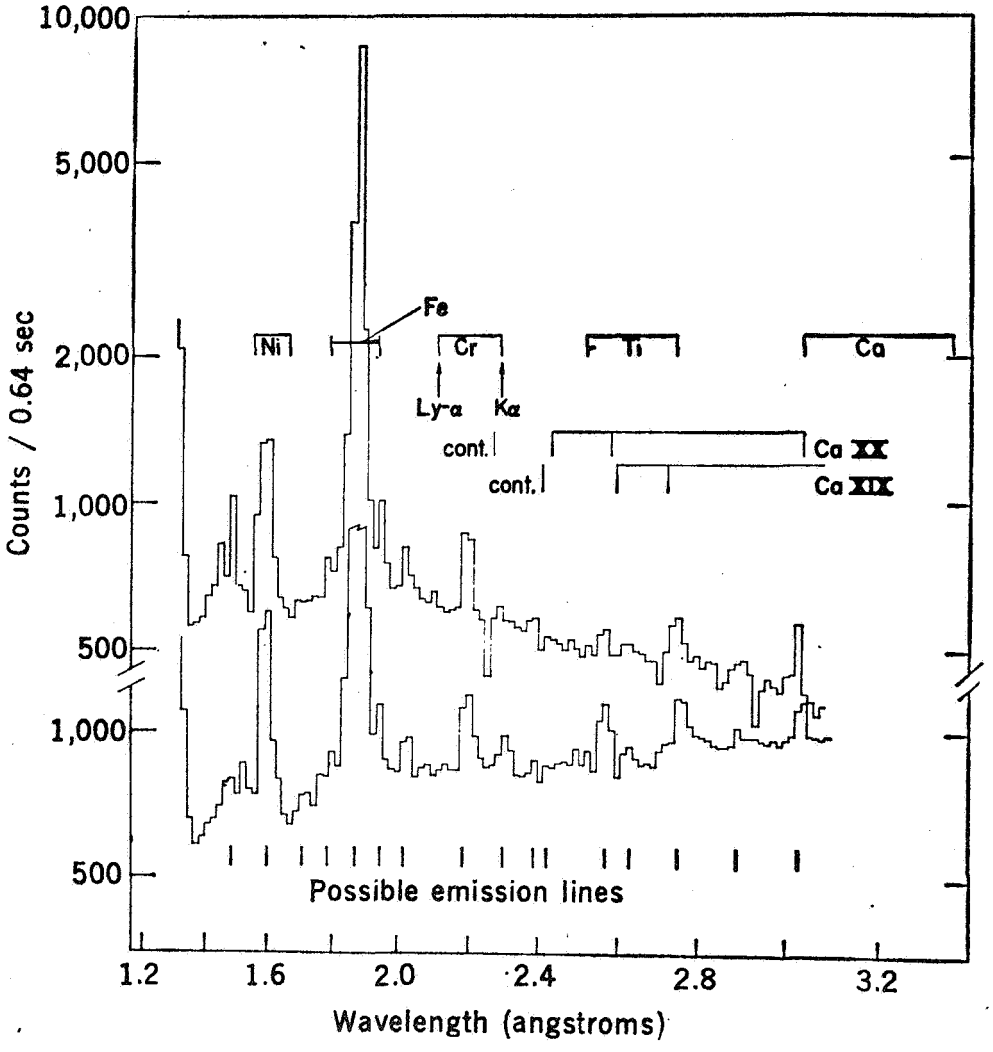

Figure 3-4 The Solar X-Ray Spectrum in the Region 1.3 - 3.1 Å as Observed by Neupert, Gates, Swartz and Young [12] During the Increasing Phase of an X-ray Burst on March 22, 1967.

Note: Apparent differences in spectral distribution are due to the increase in intensity of the x-ray burst in the time (5 min.) required to make the two scans.

accompanied by a backward scattering of the incident solar flux. In addition to a continuum, the scattered spectrum may contain lines that are quite similar in energy to the fluorescent x-rays. The yields will depend not only upon the chemical composition but upon the nature of the solar x-ray spectrum plus the the size of the particles upon the lunar surface.

The results of a calculation of the yield of fluorescent x-rays are summarized in Table III-3 for a granitic and a basaltic composition. The solar x-ray flux used in the computation is taken from the OSO-III daily averages for April, 1967, a time when the solar activity was still about three years before the expected maximum. A continuum non-flare solar flux was assumed whose spectral shape characterized by free-free emission with $T = 6 \times 10^6 {}^oK$. The solar flux and the direction of observation are assumed to be normally incident to the lunar surface. Absorption effects from all the elements are included. Grain size effects are neglected. The results are also shown in Figure 3-5.

TABLE III-3

Results of a Calculation of the Yield of Fluorescent X-Rays

	Element	K_α	Fraction by Wt.	Yield of Fluorescent Photons
Basalt	O	23Å	.38	314 cm^{-2}-sec^{-1} $ster^{-1}$
	Fe(L)	17	.14	197
	Na	11.9	.02	24
	Mg	9.9	.05	53
	Al	8.3	.09	31
	Si	7.1	.19	46
	K	3.7	.01	.17
	Ca	3.35	.09	.68
	Fe(K)	1.9	.14	0
Granite	O		.44	430
	Fe(L)		.05	84
	Na		.03	42
	Mg		.01	7.2
	Al		.09	34.9
	Si		.30	82.7
	K		.05	.7
	Ca		.03	.2
	Fe(k)		.05	0

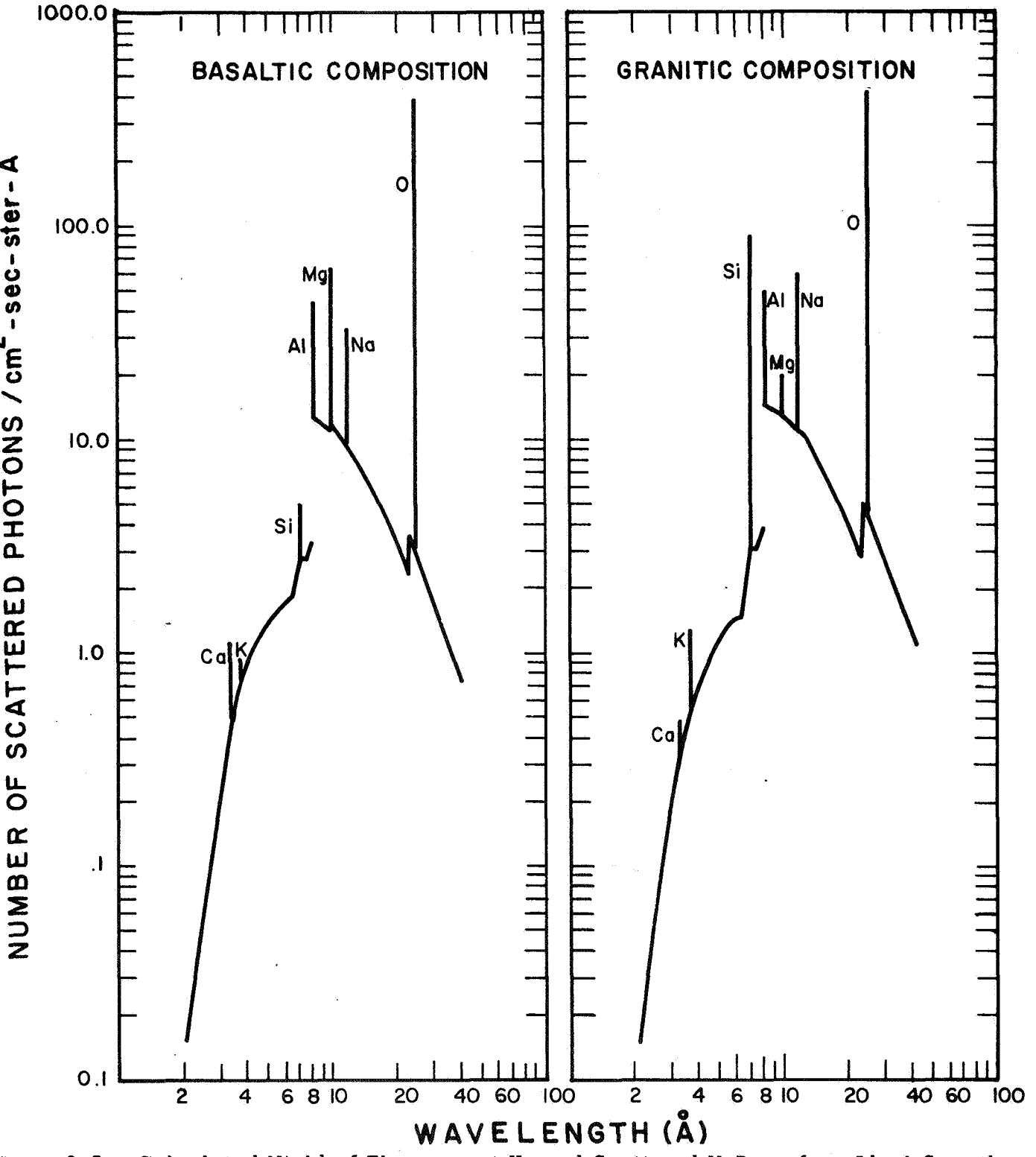

Figure 3-5 Calculated Yield of Fluorescent Kα and Scattered X-Rays from Ideal Smooth Lunar Surface Material of Basaltic and Granite Composition.

Note: The incident Solar Spectrum is presumed to be a free-free emission continuum characterized by T = 6 x 10^6oK whose total integrated intensity between 2 and 8Å and 8-20Å is equal to the mean of the OSO-III daily averages for April 1967. The curves represent the back-scattered Solar Flux.

The two compositions are readily distinguishable on the basis of the Mg/Si fluorescence ratio. The yield of fluorescence radiation from K, Ca, and Fe is not sufficient under excitation from normal solar radiation.

Figure 3-6 shows the photon yield from these same two compositions when a flare occurs. The effects derived from the difference in abundance of K, Ca, and Fe are evident.

3.1.4 Infrared Radiation

Spectral analysis of absorption and reflection of infrared radiation has been shown to characterize the composition of minerals. Such measurements, however, require carefully prepared samples for precise identification and are therefore of questionable value for remote sensing of the lunar surface. Measurement of the infrared emission from the lunar surface is feasible and has been investigated for its usefulness as a tool for compositional mapping.

The infrared spectrum emitted from mineral samples consists of the blackbody radiation corresponding to the sample temperature with superimposed bands characteristic of the sample material. One such band represents the fundamental O-Si stretching vibration and has been shown to shift from about 9 microns for acidic material like quartz to near 12 microns for ultrabasic minerals. Thus, the position of this band, if observable, can determine the lithologic type of the rock although the spectral position of these bands are difficult to locate with accuracy (they appear as broad minima in the spectrum). They can nevertheless provide compositional information. The O-Si-O bending modes appear in the 16-40 micron range and their spectral position also changes with mineral composition but in a less orderly manner.

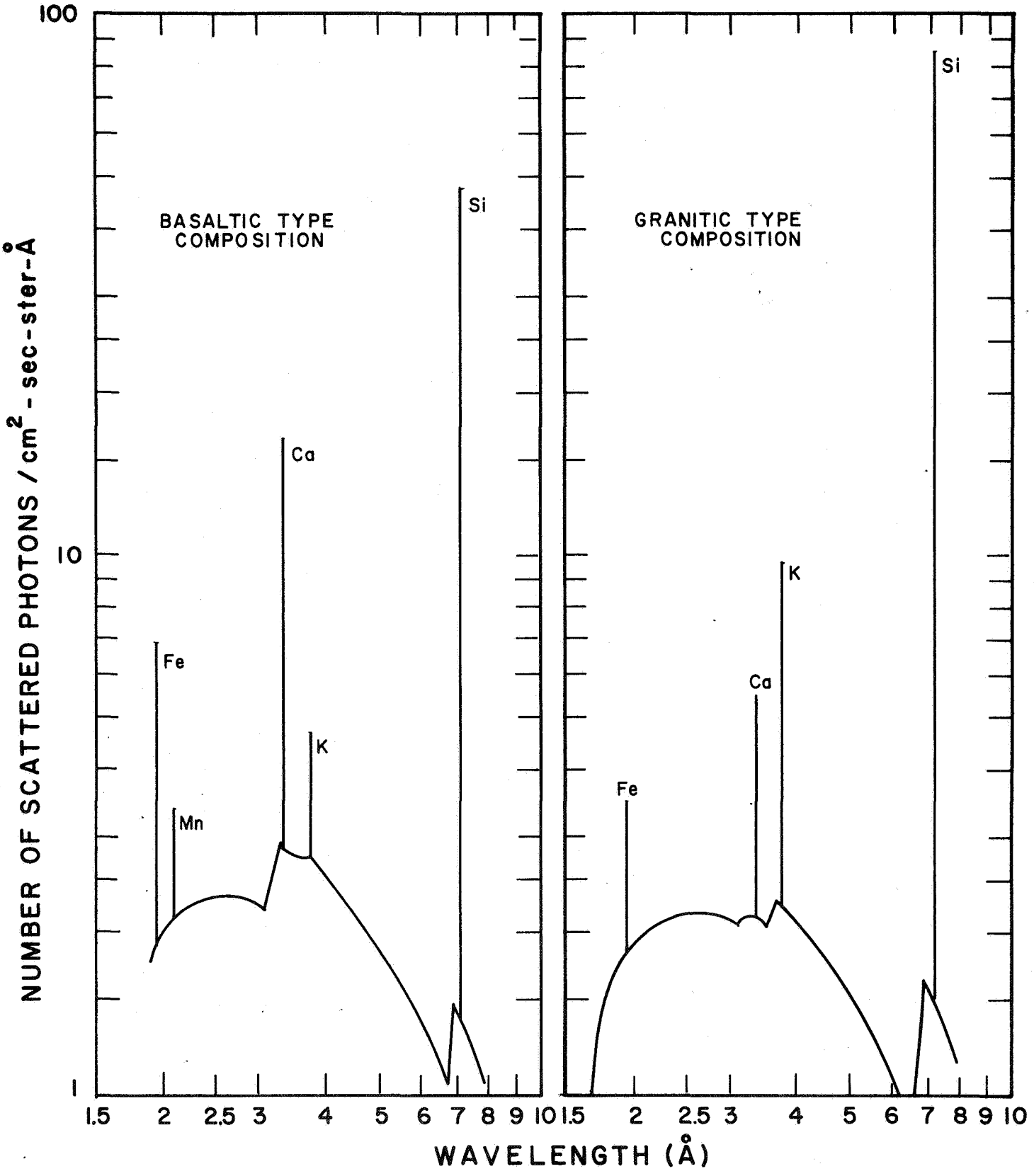

Figure 3-6 Calculated Fluorescent and Scattered X-Ray Intensity During Typical Solar Flare (Presence of lines in Solar Flux Spectrum is neglected)

Since the moon has no absorbing atmosphere, it is an ideal object for radiometric observations, but it is at present uncertain that compositional mapping from infrared emission will be successful. It has been demonstrated both experimentally and theoretically that the spectral information found in sand size or larger rock disappears as the samples are more finely divided. Hence, interpretation of infrared data is hindered by the uncertainty in particle size.

Until further information is available, it appears necessary to conclude that measurement of the infrared emission may be a questionable technique of determining the lunar composition, although it is still useful in providing radiometric data. It would seem relatively easy to place a thermister bolometer on board a lunar satellite for this purpose. A bolometer has the advantages of wide spectral response, compactness, and is compensated for changes in ambient temperature.

A radiometer capable of observing the temperature range expected and with spatial resolution suggested by the Geophysics Group at the Santa Cruz conference would, however, be a complex device which would not seem to coordinate well with the other experiments.

3.2 Physical Significance of These Phenomena

3.2.1 Resultant Nuclear and Atomic Radiation

As a consequence of the natural radioactivity and the cosmic ray interactions, there are various nuclear radiations emanating from the lunar surface. Charged particles, neutrons, and gamma rays are ejected. In principle, since a great amount of the radiation is generated from the decay of excited nuclei, it is in the form of line spectra. In practice, slowing down in the lunar material degrades the charged particles into continuous distributions. The neutron energies cannot be measured precisely. Only in the case of gammas is there the possibility of identifying some of these lines. However, in the absence of direct experimental data it is not clear which energies would be the most prominent. Certainly positron annihilation radiation would be included. Various (n,γ) processes from the most abundant isotopes will contribute.

Expectations for the alpha-spectra are different if the radon diffusion mechanism is effective. Discrete alpha particle lines would be visible from an increased number of decays taking place above the surface. Accompanying the alphas would be an enhanced gamma activity.

Fluoresence x-rays will be observable from the sunlit portion of the moon. The quantity is directly proportional to the solar x-ray flux. Hence it will exhibit the same time variations, varying in periods of the order of one hour. A scattered solar x-ray flux will also be present, within a given proportional counter resolution interval it will usually be much smaller than the yield of a fluorescent line. Nevertheless, the presence of a strong solar line near an x-ray edge of a lunar element can lead to misleading results.

3.2.2 Relation to Chemical Abundances

(a) Gamma Rays

Natural radioactive decay is indicative of the chemical abundances of K^{40}, U^{238}, and Th^{232}. If the relevant lines are identified, the strengths are directly proportional to the concentrations of those elements.

There is one qualification which should be noted if the radon diffusion mechanism is operative. This is discussed below in the section on charged particles. The cosmic ray produced gamma spectrum may be sensitive to the chemical abundance, but the quantitative relation between the two has not yet been demonstrated. Even so, without very high resolution detectors it may be difficult to extract the chemical information. Experimental work with proton accelerators is needed in this area.

(b) X-Rays

Fluorescent x-rays are sensitive to the chemical composition but not in a simple way. For a fixed chemical abundance a variation in the spectral hardness of the solar spectrum will change the ratio of the fluorescent lines. Increases in hardness will enhance the yield from elements of higher Z. This means the solar x-ray spectrum must be simultaneously viewed in a detector system that provides energy resolution from about 1-20 Å.

Chemical effects also complicate the interpretation of fluorescent line ratios in terms of relative abundance. The presence of an element of atomic number Z will absorb outgoing radiation from element Z + 1 much more strongly than that of element Z-1. For example, the ratio of SiKα/MgKα is reduced as the concentration of aluminum is increased.

To study the influence of the solar spectra and of varying chemical abundances, a computer code has been written that calculates the yield of fluorescent x-rays for complex chemical mixtures. The scattering is also included. If the program succeeds in predicting the yields in the laboratory from simulated solar spectra impinging on rock samples, it will be useful in helping to extract quantitative chemical information from the fluorescent line ratios. Calculations based on the program appear in Section 3.1.3 where the expected x-ray fluxes are calculated.

(c) Charged Particles

Because charged particles suffer energy degradation in passing through the lunar material, their spectra is not expected to yield useful information concerning the chemical composition. With the loss of spectral information it will not be possible to separate the contributions of natural radioactive decay from that of the cosmic ray processes.

Existence of the radon diffusion mechanism (to be discussed in Section 4.3) will lead to monoenergetic alpha particles above the surface. Increased gamma activity from the daughter products of U^{238} and Th^{232} past radon will accompany the alphas. The effectiveness of a possible diffusion mechanism is not known, other than what is indicated by the observations on the earth where a significant effect is seen. Hence the observed strengths of the alpha lines cannot be immediately interpreted in terms of uranium and thorium concentrations. Consequently, this mechanism should be looked for on the moon. If it were a factor in the radiation environment on the lunar surface and were to remain undetected, the natural gamma activity would be given a spurious interpretation.

(d) Neutrons

The calculated equilibrium leakage spectrum at the lunar surface that is produced by the interaction of cosmic rays is dependent on the assumed composition and is particularly sensitive to the hydrogen content. Lingenfelter, Canfield, and Hess[13] have applied neutron diffusion theory to the description of the escaping flux. The source terms include the nuclear evaporation mechanism, "knock-on events", and a contribution from the absorption of π mesons. They find the following relation between mineral type and the fraction of the neutrons which leak into space.

Mineral Type	Neutron Leakage
Chondrites	35.9 %
Basalt	29.7
Granite	32.3
Tektites	40.0

Moreover, there is a significant variation of the ratio of fast to slow neutrons with the ratio of hydrogen to silicon atoms. These effects are discussed in more detail in Section 4.4.

3.2.3 Relation to Other Lunar Characteristics

The data obtained from the various radiation experiments have a direct interpretation in terms of the chemical abundances of the material comprising the surface of the moon whereas many of the other lunar characteristics (optical, albedo, electrical and thermal conductivity) are not particularly sensitive to the exact elemental composition of the surface layer. The primary importance of these results is that they will yield the most widespread information on the bulk composition of the moon. For example, the presence of large amounts of water near the surface is directly indicated; secondly, variations in composition on the surface should be interpretable in terms of impacts uncovering base material, lava or ash flows, or age differences. If the fresh material has a different chemical composition over a sufficiently large area (50Km x 50Km), it will be detectable. Hence differences in chemical composition are related to catostrophic events and erosion processes which have taken place on the moon.

The degree of natural radioactivity has implications concerning the thermal history of the moon. There is disagreement as to whether the moon has undergone substantial melting at any time in its history. Taking earth as an analogy, high temperatures promoting differentiation would be produced by

the radioactive decay of potassium, uranium, and thorium. In addition to causing the differentiation, these elements would themselves be differentiated. Acidic rocks, as they are found on Earth, contain concentrations of these three elements that are an order of magnitude or more greater than in the undifferentiated primordial material. Consequently, if a high natural gamma activity is observed in certain regions, the implication is that differentiation has occurred and that possibly the moon has had a thermal history similar to that of the earth.

Extrapolating from our experience on the earth, the radon diffusion mechanism should be quite effective in bringing additional radioactivity above the surface. If the diffusion rate is vastly different than our expectations, this may imply something about the state of compactness or porosity of the material below the surface; or it may simply be that the extremely high vacuums prevailing in the moon retard the radon movement through the lunar material.

3.2.4 Sampling Depth of the Various Radiation

The various experiments carried aboard the integrated experiment package sample the lunar surface to different depths. Generally speaking, for the gamma ray, x-ray, and neutron experiments the sampling depth is equal to the mean free path of the radiation in the lunar surface material. For the gamma rays this is equal to about 20-25 grams/cm^2; for the x-rays about 2 milligrams/cm^2, and the neutrons about 100 grams/cm^2.

The existence of the radon diffusion mechanism would allow radon from a distance of some 10 feet or several Kg/cm^2 to reach the surface. Otherwise the alpha sampling depth would be similar to that of the x-rays.

Chemical differences as a function of depth should give information on age, the existence of significant flows, such as lava or ash flows, or the debris from nearby craters. The lunar surface throughout its history has been churned up to depths of hundreds of meters as a result of craters. Since the mass of infalling material should be small compared to the amount of churned up matter, the composition of even the topmost layer is a proper sample of the lunar material to a considerable depth. Thus, differences in composition with depth must be interpretable in terms of some process other than cratering that altered the chemical composition.

3.2.5 Suitability of Moon Habitation and as a Scientific Observatory

Although the primary objectives of the measurements are to provide geochemical data concerning the distribution of various elements on the moon, the results may also be of interest in other areas. In particular, the presence of hydrogen near the surface would provide a source of water if the moon were to be eventually populated. From this point of view it is important to locate accessible supplies of hydrogen.

Measurements of the gamma ray activity has important implications concerning the desirability of selected locations as sites for gamma ray and x-ray astronomy observatories. Minimum background is desired for maximum sensitivity. The result from these measurements might prove useful in choosing from among possible sites.

Measurements of the moon's cosmic ray albedo as provided by the gamma, neutron, and charged particle experiments may yield some pertinent data to experimenters planning large scale cosmic ray studies on the moon. Ultimately it will be desirable to conduct such observations from large platforms outside the earth's magnetosphere.

3.3 Interrelation Among the Various Radiations

3.3.1 Increased Number of Elemental Ratios

The gamma-ray measurement will be sensitive to U, Th, and K. Possibly some gammas from the decay of highly excited states of the more abundant elements can be identified. The x-ray observation will be sensitive to the Al, Mg, and Si abundances and that of Ca, K, and Fe where there is sufficient solar flare activity. The neutron measurement will indicate the amount of hydrogen. Hence simultaneous measurements provide more elemental ratios with which to classify lunar regions. For example, the K/Ca ratio where the K is obtained from the gamma ray and the Ca from the x-ray measurements is a good index for describing chemical variation.

3.3.2 Consistency Among the Experiments

If the experimental results are correct, in general there should be no disagreement concerning the abundances of the elements that they share in common. Consistency on individual elements can be checked only to an extent, since one type of radiation is a more sensitive indicator of a particular element than another.

Consistency should be more clearly evident in the conclusions concerning the overall rock type. Basaltic characteristics should be reflected both in a low gamma activity and by a higher MgKα/SiKα ratio in the x-ray experiment.

Over some lunar regions a real disagreement may exist because of the difference in sampling depth. Special events or processes may have taken place on the lunar surface that affect depths to several microns but not to several decimeters. The difference may help delimit the epoch of the event or the time scale of the processes.

3.3.3 Background Measurements

Fluxes measured in one experiment provide background information for another. Examples are listed.

(a) Alpha and Gamma Measurements

If significant spectral lines are seen in the alpha measurement, the existence of the radon diffusion mechanism is established. This would lead to a gamma activity at certain energies that is higher than that warranted by the composition.

(b) Gamma and Neutron

The largest background in the neutron experiment will be gamma's from the moon and spacecraft which are accepted as neutrons. The gamma measurement will determine the flux from both sources. In turn, neutron induced events constitute a significant fraction of the background in the gamma detector.

(c) X-Ray and Neutron

Interpretation of the neutron experiment is dependent on the concentration of certain elements. The most important abundance to ascertain for determining the thermal neutron capture cross section is that of iron. This would be accomplished in the x-ray experiment.

3.3.4 Instrumentation Compatibility

All the measurements will require nucleonic instrumentation that is quite similar. Gating and storage logic will be similar. Pulse height analysis is needed in all cases. Hence a considerable saving is achieved by developing and qualifying a single set of logic modules and a single type of pulse height analyzer that is interchangeable between the different experiments.

3.3.5 Measurement Compatibility

All the measurements will have about the same spatial resolution and view direction. Hence one aspect solution is sufficient for all measurements. Even if some failure occurs that makes the lunar coordinates uncertain, there can be no doubt that the view directions of all detectors were aligned during the measurement.

3.3.6 Spacecraft and Mission Compatibility

The experiments require different locations in the spacecraft. The gamma and neutron experiments desire placement on a boom; this leaves space in-board for the x-ray, charged particle, and other experiments.

All the measurements desire about the same duration of the mission for a significant result.

4.0 FLUXES, BACKGROUND, EXPERIMENTAL TECHNIQUES AND INSTRUMENTATION

4.1 Introduction

The processes described in 3.1 lead to measurable fluxes of gamma rays, x-rays, alpha particles, and neutrons that can be detected in instruments placed aboard a lunar orbiting vehicle. If the field of view of the instruments is limited by a collimator or its equivalent, the observations are restricted at any time to a well-defined portion of the lunar surface. Only in the case of the neutron experiment is this difficult to attain. In the following discussion it is assumed that the common field of view is a cone whose full opening angle is 60°. This corresponds to an element of spatial resolution whose full width at half maximum is approximately equal to the altitude when the instruments are looking normally to the surface.

All the experimental techniques referred to are well known in the nucleonic technology. Most have already been used in space and other rigorous environments. A great deal of the electronic logic is common to all the experiments. In particular all require pulse height analysis. Pulse height analyzers of varying degrees of sophistication have been used in a large variety of space experiments including the Surveyor alpha-particle scattering measurements.[14]

The proposed detector configurations are preliminary. Several modifications and adjustments will undoubtedly occur as the instruments are tested with simulated solar x-ray spectra and particle beams. Certain aspects of the instrumentation are discussed only in those cases where they are especially important. For example, weight is an important consideration for the gamma detector because of the dense materials it requires and of the desirability of locating the instrument on a boom. For the other experiments it is much less important.

4.2 Gamma Ray Experiment

4.2.1 Fluxes and Background

The naturally occuring gamma radiation originates from K^{40} and the U^{238} and Th^{232} decay chains. The energies and relative yields of the more important gammas are summarized in Table IV-1. Only gammas whose energy exceeds 0.3 MeV and whose yield is greater than 10 percent are included.

TABLE IV-1

Energies and Relative Yields of Natural Gammas

Constituent	$T_{1/2}$	Range of Abundance in Earth's Crust	Yields of Gamma Rays with E > 0.3 MeV	
			Gamma Energy	Yield
K^{40}	1.3×10^9 yr	$1 - 6 \times 10^{-6}$ per gram	1.46 MeV	11%
			0.35	44
U^{238} plus decay products	4.5×10^9	0 - 5 ppm	1.76	19
			1.12	20
			0.61	45
Th^{232} plus decay products	14.1×10^9	0 - 20 ppm	2.62	100
			1.64	13
			1.59	12
			0.97	18
			0.91	25
			0.34	11
			0.73	10
			0.86	14
			0.53	83
			0.51	25

The natural activity due to potassium for one gram of basaltic material may be calculated as follows:

Assumed potassium concentration = 1%

$$K^{40}/\text{all K} = 1.18 \times 10^{-4}$$

Yield of 1.46 MeV γ = 0.11

λ, decay constant = $L_N\, 2/T_{1/2} = 5.33 \times 10^{-10}\,\text{yr}^{-1} = 1.7 \times 10^{-17}\,\text{sec}^{-1}$

$$\text{gamma activity/gm} = 0.11 \times 1.18 \times 10^{-4} \times 1.7 \times 10^{-17} \times \frac{6 \times 10^{23}}{40} \times 0.01$$

$$= \frac{0.033 \text{ photons/gram sec}}{4\pi}$$

Hence,

$$dN_\gamma/d\Omega\, dT = 2.6 \times 10^{-3} \text{ photons/gm-sec-ster}$$

The K^{40} activity in granitic materials would be about a factor of 5 greater. The total gamma flux leaving the lunar surface will originate from a depth that is equal to the mean free path, about 20 grams/cm^2. Hence, the flux of 1.46 MeV photons from basaltic material is equal to 5.2×10^{-2} photons/cm^2-sec-ster. The U and Th contributions to the total gamma flux are about equal to material containing 1%K when their concentrations are about 1.25 ppm and 3.1 ppm, respectively. "Buildup" effects from compton interaction of exiting gammas will create a distribution of softer photons that accompanies the primary.

There are two important sources of gamma ray background in the measurement of these natural gammas.

(a) Gamma rays from the lunar surface produced as a result of cosmic ray (galactic and solar) interaction. A very large gamma albedo is generated. Results from the Soviet spacecraft Luna 10 indicate that the observed gamma flux from the

moon exceeds the value expected from terrestial basalt by a factor of 10 and is 1.5 to 2 times that of granite. (8)

(b) Gamma rays produced in the spacecraft material as a result of cosmic ray interactions.

Item (a) either can or cannot be treated as background depending upon how the measurement is conceived. These gamma photons do contain spectral lines superimposed upon a continuum that are characteristic of the lunar composition. The important lines that are within the energy range of the natural radioactive constituents are derived from the decay of the low lying excited states of O, Al, Si, Ca and Fe. More energetic nuclear gamma are present plus those generated in the decay of neutral pi mesons. Although they themselves fall beyond the range of interest, they will undergo secondary processes that create photons of lower energy. The extent to which the lines can be resolved and exploited to give analytic information should be the subject of further study. Literature searches should be made to summarize what has been learned at accelerators concerning the yield of characteristic gammas from the interaction of high energy protons in various materials. Additional experimental work with known materials and proton beams should be of great value.

Item (b) is an effect which provides absolutely no analytic information concerning the moon. Lines which are characteristic of the materials used aboard the spacecraft will occur in the same energy range as that of the natural radioactive nuclides. Measurement of this background can be carried out during periods when the gamma detectors do not have a view of the moon. Such periods may occur in the course of the mission. It would be occasionally desirable to interrupt periods of lunar data accumulation by changing the attitude to the spacecraft to orientations when no view of the moon is possible, as a means of determining this background.

In addition, neutrons will contribute to the background in the gamma detector. Inelastic scattering of fast neutrons and (n, γ) reactions that occur in the detector itself or the shielding material will produce a background that can be reduced but not entirely eliminated by the judicious use of thin thermal neutron absorbers outside the detector plus active shielding material in the detector.

Four factors in the design of the experiment can be controlled such as to minimize the background.

1) Placement of the detector system away from large masses; for example on a boom, removed from the bulk of the spacecraft.

2) An active shielding device to reduce the charged particle and gamma ray background by a combination of absorption and anti-coincidence.

3) Spatial resolution through the use of an active collimator that limits the gamma detector's field of view to a well defined portion of the moon.

4) Best possible energy resolution. The background spectrum will consist of a continuum plus lines that do not coincide with those of the radioactive nuclides. With respect to a continuum background the required number of counts for determing the strength of a line varies as the square root of the detector resolution. When nearby lines can cause confusion, the ability to resolve and separate the interferring lines is a necessity.

In addition, radioactive materials should not be used aboard the spacecraft nor in any of the experimental systems. In particular,

uranium and thorium alloys are unacceptable unless they are thoroughly disposed of before data taking begins. The photomultiplier tubes of the detector should not contain K^{40}. Rare earth materials in the spacecraft may cause an undue gamma background. Use of rare earths should be minimal.

4.2.2 Gamma Ray Detectors

(a) Choice of Detector Crystal - Two detector systems are currently being used in gamma ray spectroscopy; the one detector consists of a thallium activated sodium iodide scintillating crystal (NaI(Tl)) and the other of a lithium drifted germanium crystal cooled by liquid nitrogen Ge (Li). The former converts the gamma ray into light that is detected by a photomultiplier tube, while the latter converts the gamma directly into a number of electron-hole pairs which appear as a current pulse. The Ge (Li) devices have the very important advantage of substantially better resolution. At 1.33 MeV the resolution of a large detector is 4 keV (FWHM) compared to about 120 keV for a 3-inch diameter x 3-inch NaI(Tl) crystal. The relative superiority in resolution is offset by an inferiority in efficiency of a factor of 25. Overall, in the presence of a background continuum given a sufficient number of counts, the Ge(Li) devices offer greater sensitivity for detecting the presence of a line and determining its strength. When the background contains lines of unknown strength that lie close by, as is the case in this measurement, the high resolution detector is clearly to be preferred. However, the low quantum efficiency of single detectors plus the cooling requirement, appears to preclude their immediate use in space.

This leaves the NaI (Tl) as the choice for the detector. The response of a 3-inch diameter x 3-inch unit with good operational characteristic is shown in Figure 4-1. A pure line source of gamma radiation produces a peak that is accompanied by a lower energy compton continuum. The

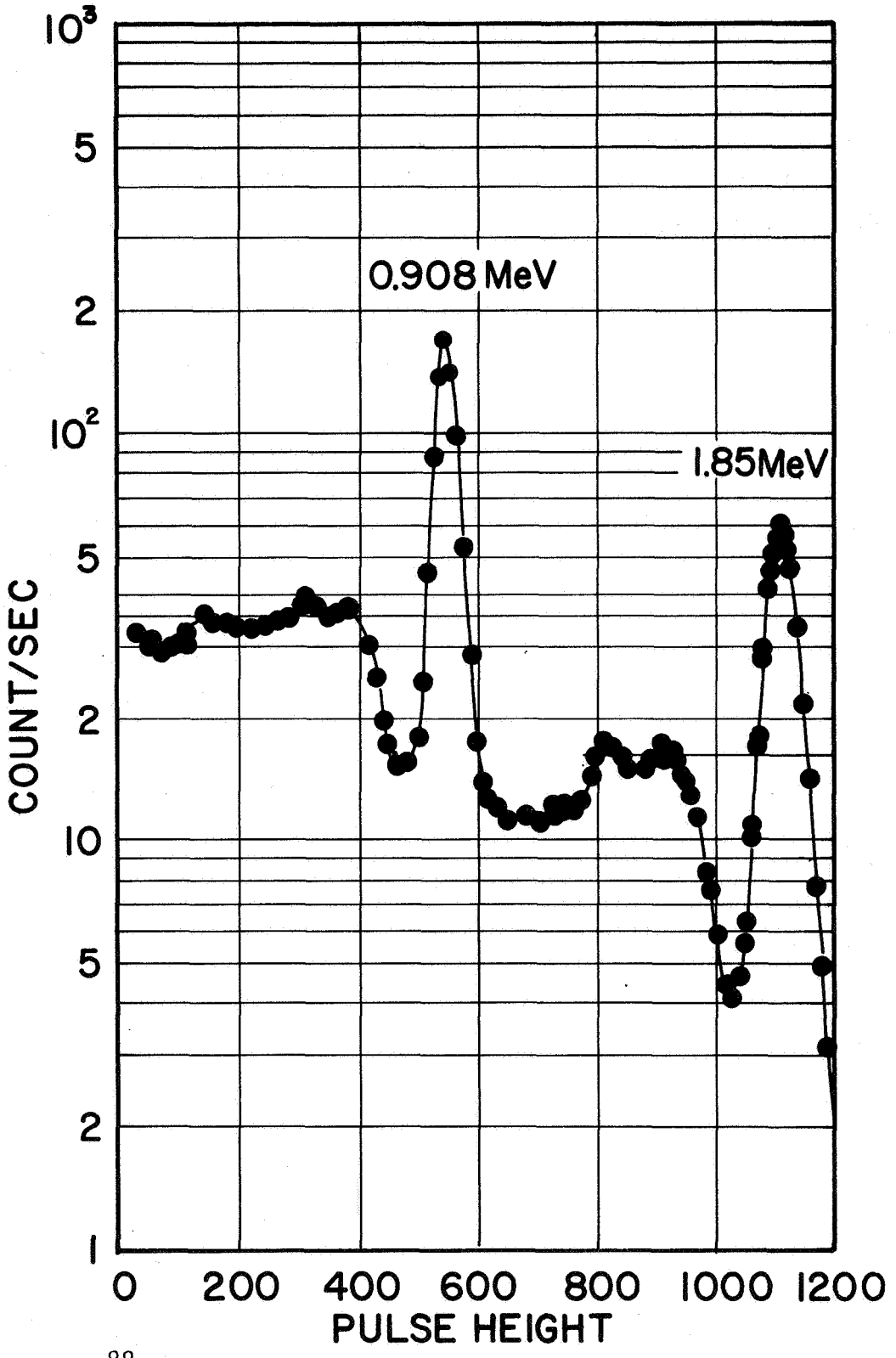

Figure 4-1 Typical Y^{88} Gamma Ray Spectrum Obtained with a 3" Dia x 3" Thick Thallium Activated Sodium Iodide Crystal

amplitude of the peak relative to the continuum decreases with increasing gamma energy and increases with larger dimensions for the detector. When many lines are present, unfolding the response of the detector is an involved task. A least squares method for deriving the true gamma distribution from the spectrum that appears in a multi-channel analyzer has been described by Trombka [15].

A modest detector system is shown in Figure 4-2. The detector includes a 3-inch dia. x 3-inch NaI(Tl) scintillator that is contained in a cylinder of CsI (Tl) crystal scintillator which acts as both a shield and a collimator when its signals are placed in anti-coincidence with those of the NaI (Tl). A thin disc of scintillating plastic that is optically coupled to the CsI (Tl) guards against charged particles within the field of view. This configuration has been used in balloon borne gamma experiments by Peterson [16] where it has proven to be quite effective as a shield and collimator. In addition to the collimator-shield function, the CsI (Tl) will reduce the compton continuum in the NaI (Tl) by absorbing some of the gamma recoils that escape. It may be beneficial to surround the entire assembly with a thin layer of material that has a high thermal neutron absorption cross section and a small gamma yield.

The CsI (Tl) crystal is particularly well suited to the space environment because of its ability to withstand shock, acceleration, and vibration plus large temperature changes. Its resolution is inferior to that of NaI (Tl), hence it is not to be preferred for spectroscopy, but is quite adequate when acting in anti-coincidence. Several photomultiplier tubes connected in parallel will view the light output of the CsI (Tl) and plastic. A single photomultiplier tube that is well matched to the crystal will suffice for the NaI (Tl). To achieve good light output stability the temperature of the NaI (Tl) should be maintained at a level that is greater than $0^{o}C$. Controlled heaters will be needed to provide the regulation.

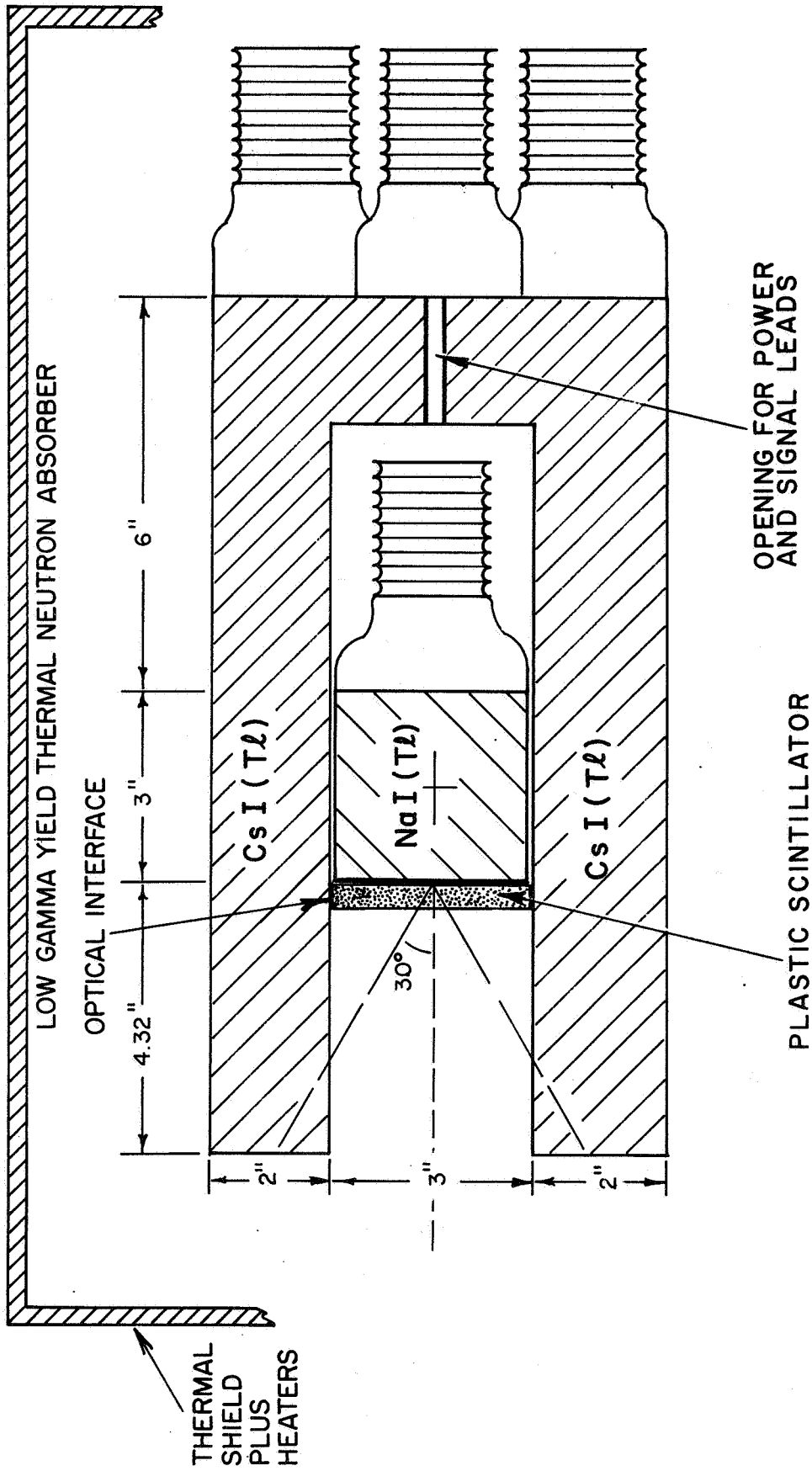

Figure 4-2 Gamma Ray Detector with Active Shield and Collimator

(b) Spatial Resolution Size and Weight - Design criteria for the measurement include spatial resolution that is approximately equal to that of altitude of the orbiting vehicle. This is accomplished by limiting the field of view of the detector with the CsI(Tl) active collimator-shield. Passive absorbers will not totally block gamma rays unless many mean free paths of material are used. However, interaction of cosmic ray primaries in the absorbers will generate more gammas. The active collimator will produce an anti-coincidence signal that vetoes any event in the NaI(Tl) whenever an interaction takes place that deposits a small amount of energy in the CsI(Tl) or plastic. Hence, compared to passive absorbers, fewer mean free paths of material are needed to limit the gamma acceptance and the passage or interaction of a cosmic ray particle is readily observed.

A field of view that is approximately a 60° cone is desired. However, partial penetration of the gamma through the collimator does not permit an angular acceptance that is as sharply defined as in for example the x-ray experiment. This geometry is shown in Figure 4-3. It is seen that gamma rays incident at angle θ pass through a thickness of material, y, in that it depends on x, the point at which it strikes the face of the (NaI(Tl) crystal. The relation between x, y, and θ is as follows:

$\theta < x < \ell \text{ Tan } \theta - t$	$y = t/\text{Sin } \theta$
$\ell \text{ Tan } \theta - t < x < \ell \text{ Tan } \theta$	$y = (\ell \text{ Tan } \theta - X) \sin \theta$
$\ell \text{ Tan } \theta < x < 3"$	$y = 0$

The effective area as a function of θ, the entrance angle of the radiation, cannot be expressed analytically. It must be evaluated numerically and is a function of energy. Calculated values of the effective areas as a function of θ are shown in Figure 4-4 for several energies. (In the calculation it is assumed that the plane of the detector is parallel to the lunar surface). The height and thickness of the collimator was determined by requiring a 2 MeV gamma that is incident at 30° towards the center of the front face of the crystal to pass through two mean paths of material.

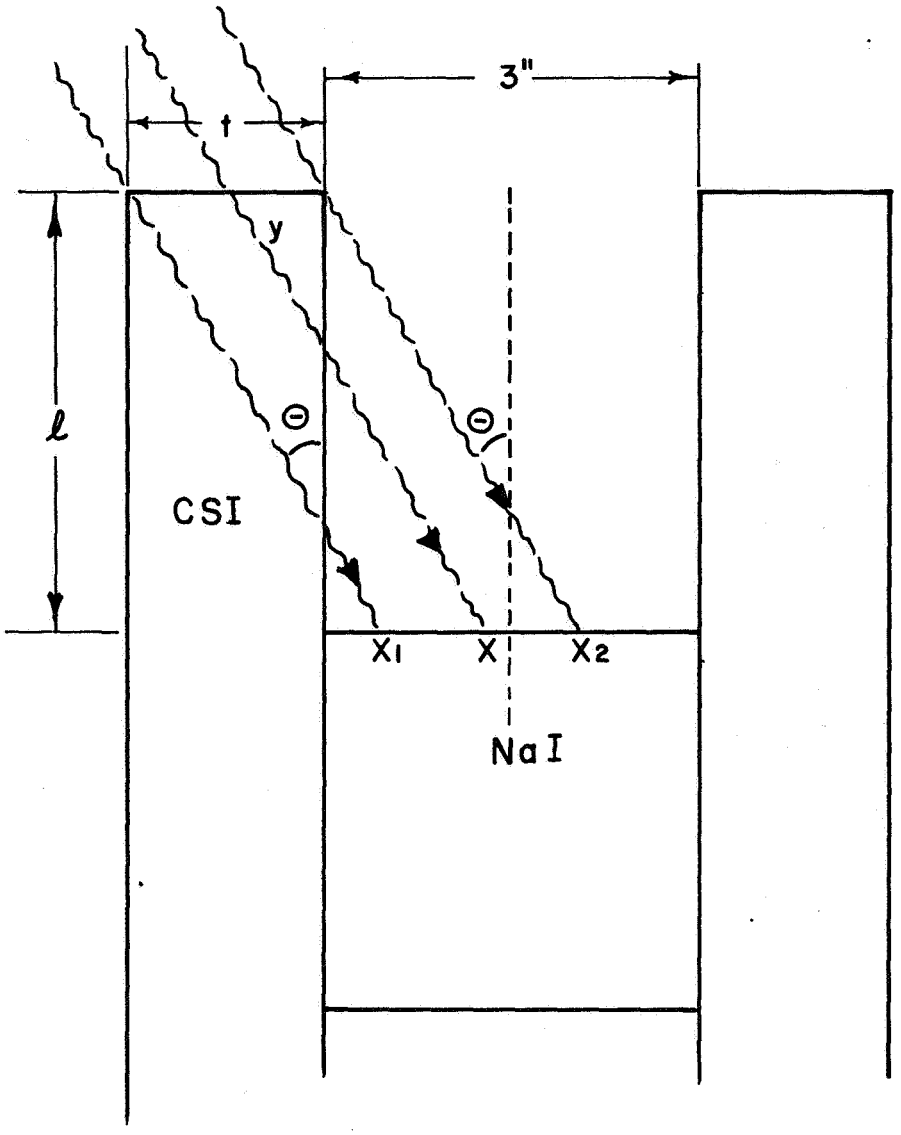

Figure 4-3 Geometry of Gamma Rays Entering Detector

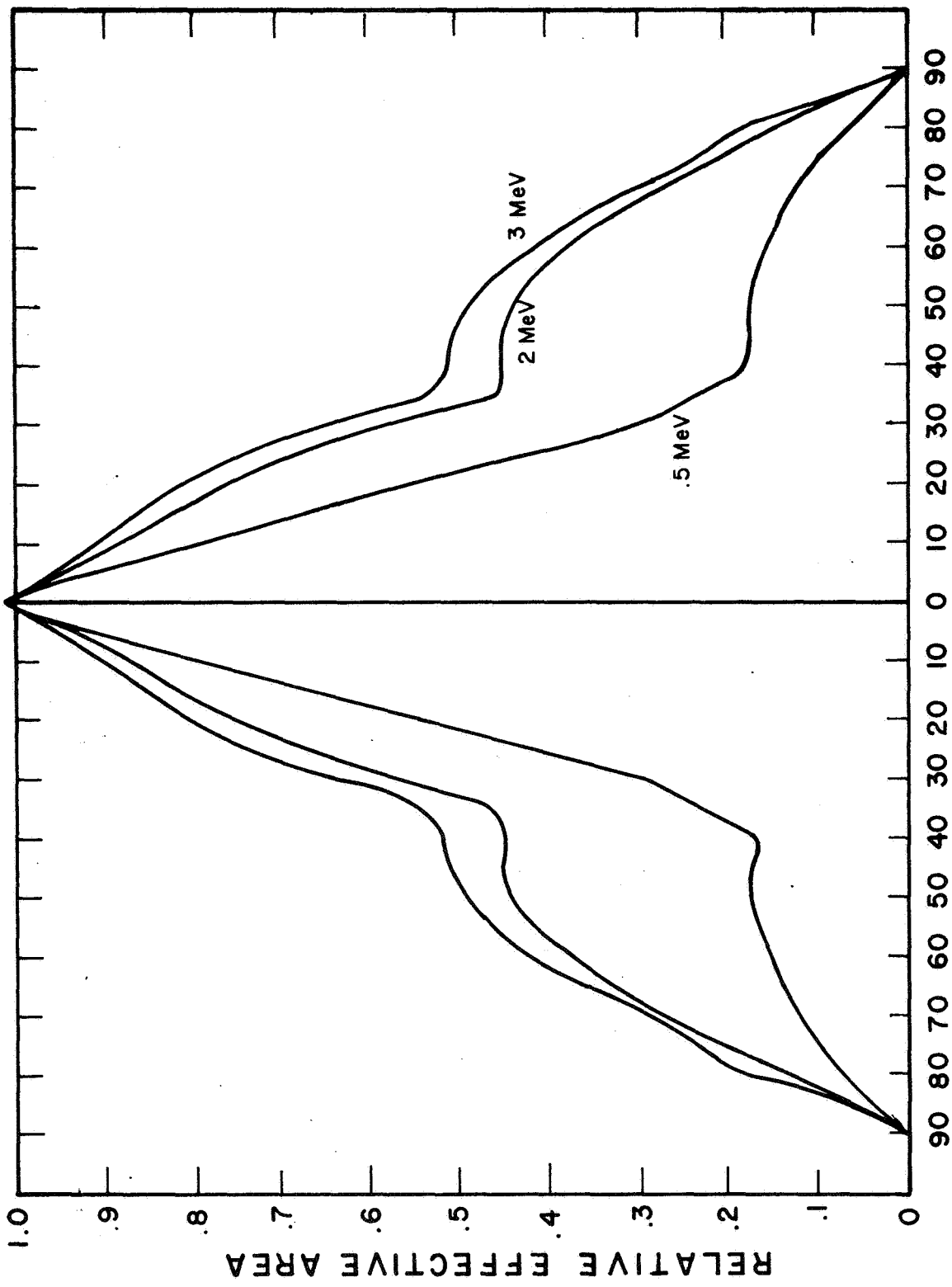

Figure 4-4 Calculated Response for Several Energies of Gamma Ray Detector Shown in Figure 4-3.

Note: The detector is presumed to be aligned with the local vertical of the lunar surface. The "gamma angle" refers to the angle between the radiation and the normal to the detector face as shown in Figure 4-2.

(c) Detector Weight - The dimensions of the CsI (Tl) shield determines its volume and hence its weight which represents most of the total detector weight. From Figure 4-4, the volume of the shield is equal to:

$$\pi \frac{(7)^2}{4} \times 2 + \pi (3.5)^2 - (1.5)^2) \, 11.5 \approx 400 \text{ in}^3 = 6300 \text{ cm}^3$$

$$\rho_{CsI} = 4.5 \text{ g/cm}^3$$

$$\text{Wgt}_{coll} = 6300 \times 4.5 = 28,400 \text{ g} = 62.1 \text{lbs}$$

$$\text{Vol}_{NaI} = 3(1.5)^2 \pi \times (2.54)^3 \approx 334 \text{ cm}^3$$

$$\rho_{NaI} = 3.7 \text{ g/cm}^3$$

Wgt = 2.7 lbs

Wgt 5 P.M. tubes + Voltage Distribution $\approx$ 10 lbs

Total Weight = 75 lbs

4.2.3 Electronics

A block diagram of the electronics logic is shown in Figure 4-5. All methods and techniques are well known in nuclear physics and have been previously used in space.

4.2.4 Expected Performance

(a) Estimate of Background Counting Rates--Results derived from the Soviet Luna 10 data for the lunar surface gamma ray contribution are shown in Figure 4-6. The scatter of the data points as they are shown by Vinogradov et al[8] are in most cases much less than what is expected from the indicated statistical errors. Very likely the authors have smoothed their results in some fashion. Figure 4-6 was obtained by operating on the

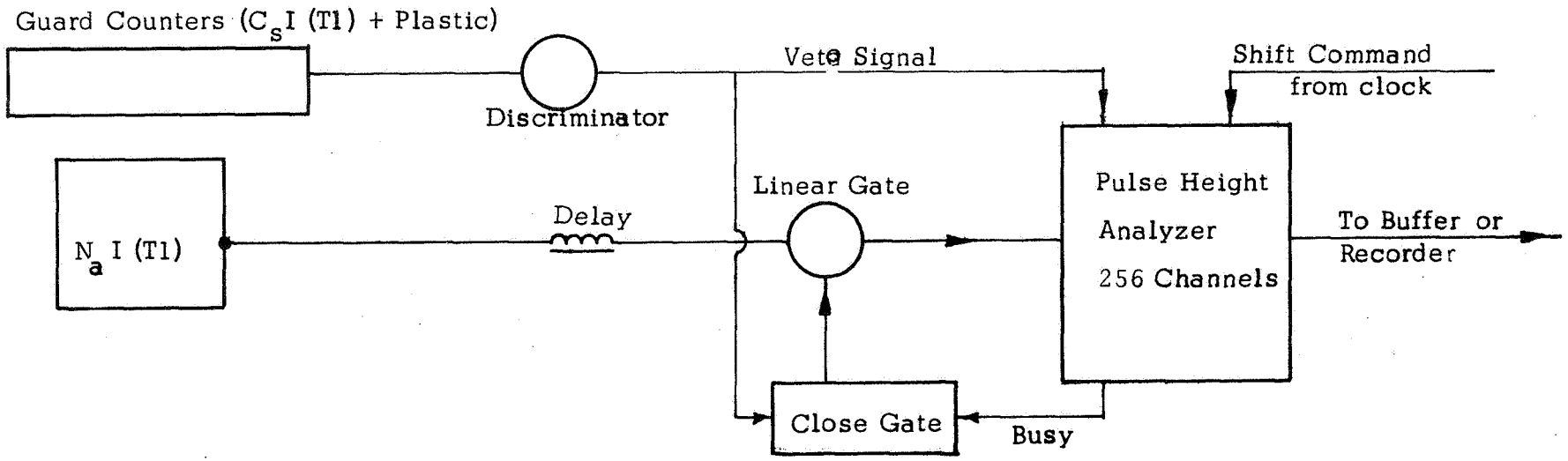

Figure 4-5 Functional Block Diagram of Gamma Ray Experiment

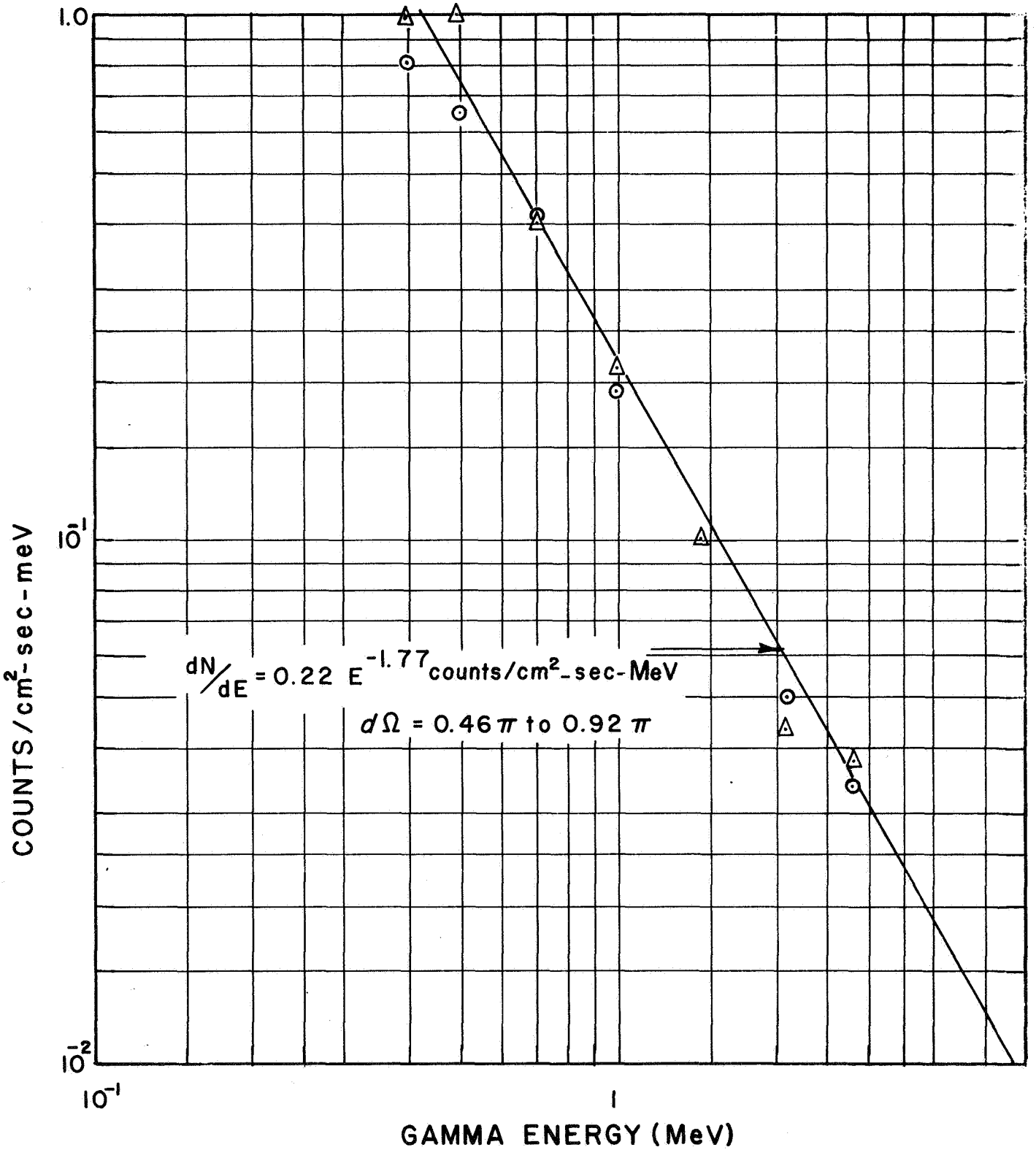

Figure 4-6 Gamma Ray Spectrum from Moon as It Would be Observed in a Low Resolution Detector.

Note: Points were derived by the summing and replotting of the results of Vinogradov et al[8] that are shown in Figure 2-2.

data shown in Figure 2-2 in the following manner: The first two points were plotted as given; the other points were summed in intervals combining 3, 5, 6, and eventually 7 points, and the average counting rate of the interval was plotted against the average energy of the interval. For example, the data in the bins at 6, 7, and 8 MeV was summed, divided by 3 and plotted against 7 MeV. All the data reprocessed in this manner is consistent with the expression:

$$dN/dE = 0.22\ E\ (MeV)^{-1.77}\ counts/cm^2 - sec\ MeV,\ (Moon)$$

$$0.4<E<3.2\ MeV$$

The solid angle is not given explicitly but the authors state that it varied between 0.9π (h=350 km) and 0.46π (h=1015 km) depending on h, the altitude above the surface. We assume the average value is 0.67π.

This is similar to the cosmic ray produced gamma background aboard OSO-1 and Ranger III: [17]

$$dN/dE = 0.38E^{-1.7}\ counts/cm^2 - sec - MeV,\ (Spacecraft)$$

where the solid angle is presumably 4π. This similarity between the moon and spacecraft suggests that the spectrum of cosmic ray produced background events, as it is observed in a low resolution detector (individual photopeaks and compton edges <u>not</u> identified), is not strongly dependent on the compostion.

In estimating the background that appears in the proposed detector it is assumed that these two spectra represent a continuous gamma ray distribution and that no lines are present. It may be naive to assume that these events are indeed all gamma rays. Neutrons undoubtedly constitue a significant fraction of the total. Hence, the reduction in background that is achieved by the use of an active-collimator shield may be overly optimistic due to its much lower effectiveness against the neutron component.

The surrounding passive components of the shielding that have a high thermal neutron absorption cross section may be useful. For purposes of the estimate, only the photopeak and not the compton edge of a line will be useful in obtaining its identification and strength. For the background continuum, there is no corresponding reduction because it is difficult to make a distinction between events that represent the photopeak for photons of a given energy and the compton continuum of another.

The background is calculated below keeping in mind that it is difficult to make a realistic estimate of the performance without knowing precisely what fraction of these events are neutrons and to what extent lines are present in the cosmic ray produced gammas. It is assumed that the field of view is a 60° cone ($d\Omega \approx 1$ ster-rad) and that detector is placed on a boom at a distance of 12 feet from the spacecraft.

Lunar Background, $dN_{BL}/dE\,dt$

$$dN_{BL}/dE\,dt = \frac{0.22}{0.67\pi} E^{-1.77} = 0.105E^{-1.77} \text{ counts/cm}^2 - \text{sec} - \text{MeV}$$

Spacecraft Background, $dN_{Bs}/dE\,dt$

It is assumed that the projected area of the first 20 grams/cm^2 of spacecraft material is 4 ft x 4 ft.

Hence,

$$d\Omega \approx (\frac{4}{12})^2 = 1.11 \times 10^{-1} \text{ ster.}$$

The thickness of collimator-shield material between it and the detector is one mean free path for gamma rays. Consequently, assuming the events are all gammas:

$$dN_{BS}/dE\,dt = \frac{0.38}{4\pi} \times 1.11 \times 10^{-1} \times .369 \times E^{-1.7}$$

$$= .0126E^{-1.7} \text{ counts/cm}^2 - \text{sec} - \text{MeV}$$

Total background, dN_B/dE

$$dN_B/dE\ dt = \frac{dN_{BL} + dN_{BS}}{dE\ dt} \approx 0.118\ E^{-1.77}\ \text{counts/cm}^2\text{-sec-MeV}$$

This estimate is probably too low because of the reduced effectiveness in shielding against the neutron component.

(b) Estimated counting rate from K^{40} above background -- In section 4.2.4(a) it was shown that for a 1% concentration of K, the counting rate is equal to:

$$dN\gamma/d\gamma, d\Omega = .052\ \text{photons/cm}^2\text{-sec-ster}$$

Effective area of detector, 3" dia x 3", = 50 cm^2

Efficiency of detector, = 0.40

Ratio photopeak to total counts, = 0.30

$d\Omega$, 30^o cone, = 1 ster-rad

Hence, the total counting rate is:

$$dN/dt = .052 \times 50 \times 0.40 \times 0.30 \times 1 = 0.312\ \text{counts/sec.}$$

At 1.46 MeV the energy of the K^{40} gamma, detector resolution is about 10% FWHM or 0.146 MeV. Within this 0.146 energy interval the background rate is:

$$dN_B/dt = 0.118 \times 50\ (1.46)^{-1.77} \times 0.40 \times (0.146)$$

$$= 0.175\ \text{counts/sec.}$$

At the end of 36 seconds of counting the total accumulation is:

$\Delta N = 0.312 \times 36 = 11.2$ counts for K^{40}

$\Delta N_B = 0.175 \times 36 = 6$ counts for the background within the FWHM

The peak should be visible above the estimated background.

(b) Estimated counting rates from thorium and uranium -- In the thorium series the counting and background rates from the combined (unresolved) 1.64 MeV and 1.59 MeV gammas should be comparable at a thorium concentration of 3 ppm to that of the 1.46 MeV gamma from a 1% potassium concentration. The 2.62 MeV gamma appears at an energy where the background has diminished by a factor of three. Hence, it should be easily distinguishable and also useful for indicating contribution of the 1.59 and 1.64 MeV lines.

The uranium series 1.76 MeV gamma should be visible for a concentration exceeding several ppm. It can get confused with the 1.64-1.59 thorium gammas. Information from the 2.62 MeV thorium gammas should be useful in unfolding these two contributions.

4.3 X-Ray Fluorescence Experiment

4.3.1 Fluxes and Background

The expected fluxes of fluorescent x-rays from the lunar surface were given in Figures 3-5 and 3-6. Under normal solar conditions there are significant yields of characteristic K radiation from O, Na, Mg, Al, and Si plus L radiation from Fe. Flares cause production of K, Ca, and Fe K radiation to an extent that is determined by the hardness and duration of the flare. In distinguishing between granitic and basaltic compositions, the most sensitive indicators are Mg, Fe, and Si. Under average solar conditions (April 1967), the Mg $K\alpha$: Si $K\alpha$ ratio is equal to above unity in basalt and about 0.09 in granite. The Fe content provides an independent check.

The most important background accompanying the fluorescent x-rays are solar x-rays back scattered from the lunar surface. The spectrum of these x-rays is characteristic of the incident solar flux and bears little relation to the chemical composition of the lunar surface. To the extent that good spectral resolution can be achieved, the effects of the scattered x-rays can be diminished. Calculation of the scattered flux shows that:

$$dN_{scat}/d\lambda\, dt\, d\Omega = 15 \text{ photons } \text{Å}^{-1}\, cm^{-2}\, sec^{-1}\, ster^{-1}$$

$$\text{at } \lambda = 8\ \text{Å}$$

where the assumed solar spectrum is the same as was used in Figures 3-5 and 3-6. In this wavelength region, unfiltered proportional counters have a full width at half maximum (FWHM) resolution of 40%. Hence, if one selects the FWHM region of an element such as Mg, Al, and Si on the basis of the proportional counter resolution, a contribution of $8 \times 0.4 \times 15 = 48$ photons/cm^2 -sec-ster from scattering is included.

This is comparable to the yield of fluorescent photons. Effective improvements in resolution by a factor of two can be achieved by balanced filter techniques (to be discussed below) resulting in a background reduction by a factor of two. The presence of strong lines in the solar spectrum would complicate matters somewhat if they occurred within the resolution interval of an element. Solar spectrum measurements do indeed show line emission; but the line density is high enough to allow its approximation by a continuous distribution. The one exception is flares which have been reported to exhibit the strong line emission characteristic of highly ionized iron.

Non x-ray background events will appear in the proportional counters while looking at the lunar surface. The principal source will be cosmic rays plus gamma rays produced in the moon or spacecraft which eject an energetic compton electron from the walls of the detector into the active gas volume. Recent improvements in the use of pulse shape discrimination promise at least a factor of 10 reduction in background at 8 Å and considerably more at 2 Å.[18] Judging from our experiments with sounding rockets above the earth's atmosphere the residual background from this effect should be minor.

4.3.2 Detectors

Two types of detectors appear to be appropriate for this measurement: filtered proportional counters for the radiation shorter than 10 Å; and a windowless detector for the very soft radiation from O, Fe, and Na.

(a) Proportional Counters

Thin beryllium can be used as the window in large area proportional counters. Sealed detectors having an effective area of over 100 cm^2 have been made from .001" Be. Individual units have been

flown several times on rockets and have enjoyed a long life in the laboratory. It is possible to fabricate detectors with .0005" windows but this would probably require a gas reservoir in parallel to maintain the pressure. The window transmission at the relevant wavelengths for the .001" and .0005" Be windows are given in Table IV-2.

TABLE IV-2
Window Transmissions

Element	λ_{K_α}	.001" Be	.0005" Be
Mg	9.9	.25	.49
Al	8.3	.40	.64
Si	7.1	.55	.78

The choice of the sealed .001" counters seems preferable. The sensitivity loss is significant only for Mg Kα; but, in addition to the simplicity of using a sealed counter, there is considerably more mechanical strength for protection against micrometeorites and lunar ejecta. It would be desirable to have separate .003" Be window counters for the harder fluorescent K x-rays from K, Ca, and Fe that are observable during solar flares. The thicker window will be essentially transparent to those radiations and offer added protection.

(b) Windowless Electron Multipliers

The softer radiation which includes OKa, NaKa, and Fe La will be observed in windowless multipliers of the magnetic or electrostatic type. An x-ray sensitive cathode shall be used to convert the x-rays. Such detectors offer an efficiency of about 10% which is sufficient in this situation. In spite of the name, a very thin aluminized organic film window will be used to exclude ultraviolet radiation and very soft charged particles.

(c) Filter Techniques

The resolution of proportional counters is about 40% FWHM at 8 Å. This is below what is needed to separate Mg, Al, and Si and K from Ca, although the Fe Kα radiation can probably be seen as a distinct peak. In addition, the background of scattered solar radiation will make resolution even more difficult. Absorption filters provide a means of separating the characteristic radiations and of reducing background effects. For example, consider the counting rates when thin foils of Si and Al are alternately placed in front of the detector. The Si has a discontinuity in its x-ray transmission at 6.74 Å; the Al at 7.95 Å max. which are the K edges of those materials. The thickness of the foils are calculated to have high transmission just below the edge and low transmission just above it. Hence, only Si Kα radiation plus x-ray background of about the same wavelength can contribute significantly to the difference when the two counting rates are subtracted. Other contributions to the background cancel upon subtraction. Similarly, with additional filters of Mg and Na, the Al Kα and Mg Kα lines can be isolated. The transmission characteristics of a likely set of filters are shown in Figure 4-7. For the K, Ca, and Fe group, filters of manganese, chromium, calcium, potassium, and sodium chloride can be used to facilitate the separation. In all cases, the resolution of the proportional counter serves to check the consistency of the results. The pulse height peak of each filtered interval should be consistent with its mean energy.

This technique can be used in conjunction with the windowless detector. Very thin filters of sodium, iron, manganese, chromium, and titanium (organic films with evaporated deposits) will enhance the OKα, NaKα, and Fe L lines. However, somewhat greater care is needed in the interpretation of the results because the L edges are multiple, and there is no energy resolution to check the overall consistency.

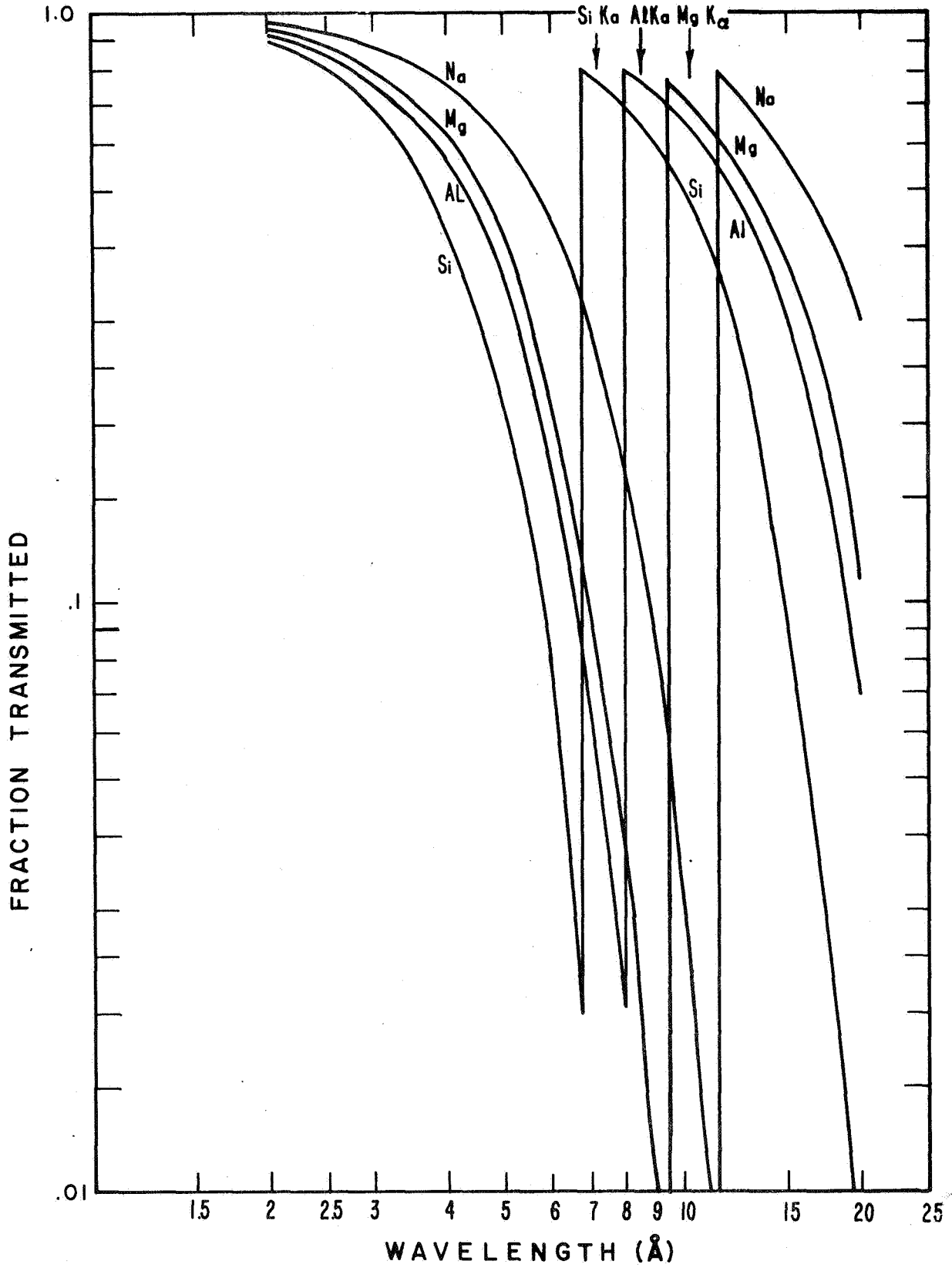

Figure 4-7 **The X-Ray Transmission as a Function of Wavelength for Several Metallic Filters of Selected Thickness.**

Note: The wavelengths of fluorescent x-rays of silicon, aluminum, and magnesium are shown.

A detector system utilizing several proportional counters plus a filter wheel that advances one position between periods of accumulation is shown in Figure 4-8.

(d) Spatial Resolution and Shielding

The discussion in Section (4.1) stated that the desired spatial resolution on the lunar surface would require limiting the detectors to a field of view of about $\pm 30^{\circ}$ in each direction. This can be accomplished with great ease by use of slat or tubular collimators made of 1/16" aluminum occupying a width of less than 1".

Shielding cannot be used to great advantage in the x-ray experiment. The major background will be scattered x-rays of the same wavelength originating from the region of interest. Pulse shape discrimination will be used with the proportional counters to vastly reduce the effects of cosmic rays. For the windowless multiplier a coaxial scintillation counter operating in anti-coincidence would reduce the effects of cosmic rays. The counter could easily be fabricated from plastic scintillator but it would be of some advantage to use CsI(Tl) as active shielding against the gamma background.

4.3.3 Electronics

Electronic circuits for the detection of soft x-rays in space have been developed in connection with the study of cosmic x-ray sources and the isotropic x-ray background. The lunar x-ray detector can incorporate all of those features. For the proportional counters, charge sensitive pre-amplifiers shall be used to preserve the energy information. Pulse shape discrimination shall be used to reduce the non-x-ray contribution to the background. Pulse height analysis will select the desired wavelength interval and reveal the overall consistency of the filter technique. A block diagram of the electronics logic is shown in Figure 4-9.

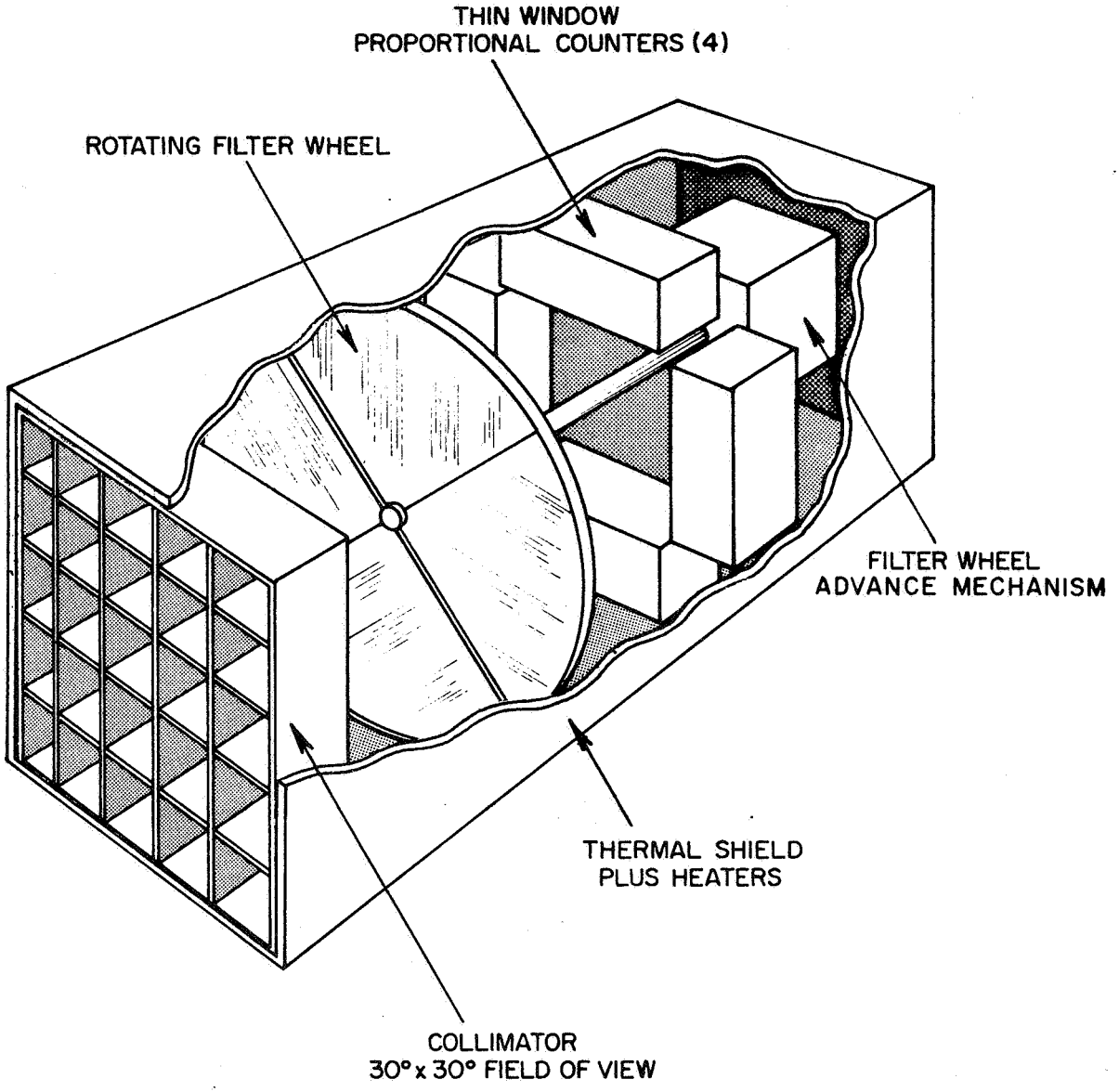

Figure 4-8 X-Ray Detector Consisting of Collimator, Proportional Counters, and Filter Wheel

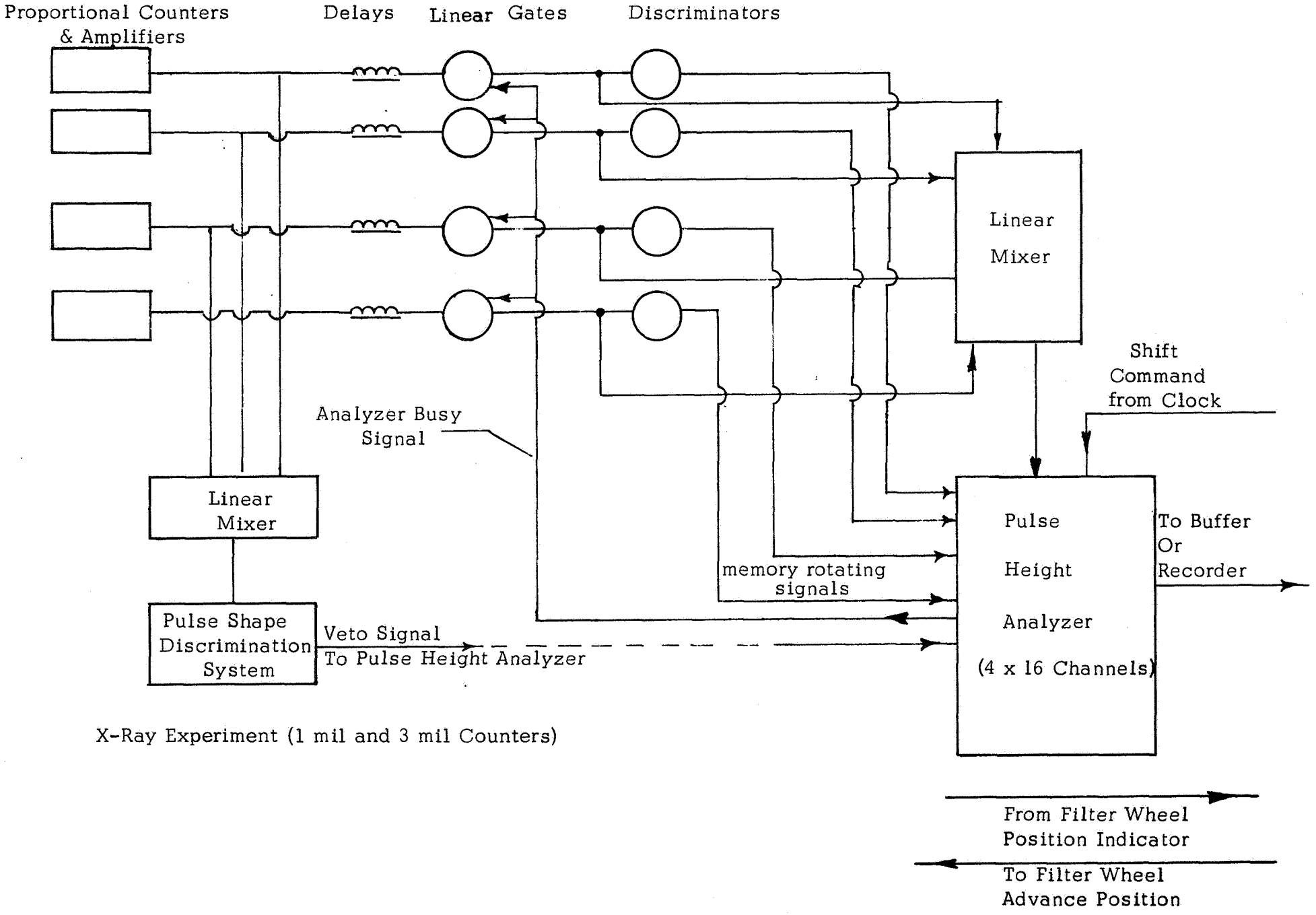

Figure 4-9 Function Block Diagram of X-Ray Experiment

4.3.4 Estimated Counting Rates

The counting rate at each wavelength, $N(\lambda)$, is equal to the product of the following quantities:

$Y(\lambda)$: yield of fluorescent x-rays at the characteristic wavelength in photons/cm^2-sec-ster.

$N(\lambda)$: detector efficiency, essentially the window transmission.

$d\Omega$: the solid angle acceptance as determined by the collimator.

A: the effective area of the counters.

$Y(\lambda)$ is given in Figures 3-5 and 3-6. $N(\lambda)$ is given in Table IV-2 for the proportional counter and is equal to about 0.1 independent of λ for the windowless multiplier.

$d\Omega \approx 1$ ster.

$A \approx 100$ cm^2 proportional counter

20 cm^2 windowless multiplier

$N(\lambda) = Y(\lambda)\, n(\lambda)\, d\Omega\, A$

The expected counting rates are summarized in Table IV-3.

TABLE IV-3

Expected Counting Rates

(Average Solar Intensity, April 1967)

Windowless Multiplier:			
Element	λ	Basalt $N(\lambda)$	Granite $N(\lambda)$
O	23 Å	620 counts/sec	860 counts/sec
Fe(L)	17	390	168
Na	11.9	48	84
Estimated background		100	100
Total counts		1160	1200
.001" Be counter:			
Mg	9.9	1250	180
AL	8.3	1400	1570
S	7.1	2500	4450
Estimated background in proportional counter resolution (with filter)		900	900
.003" Be counter:			
K	3.7	15	61
Ca	3.35	62	180
Estimated background in proportional counter resolution (with filter)		30	30

Element separation is achieved by subtracting the spectra with the various filters in place. Pulse height channels that are far removed from the element peak need not be considered, except as a background check. Consider the situation in the .001" Be counter

which has four possible filter conditions. Measurements are made in four equal time intervals.

Let N_1 be the spectrum with the Na filter in position.

N_2 be the spectrum with the Mg filter in position.

N_3 be the spectrum with the Aℓ filter in position.

N_4 be the spectrum with the Sl filter in position.

N_{12}, N_{13}, N_{14} be the spectra for Mg, Al, and Si alone in the absence of filters. These are the quantities to be found.

T_{12}^{11} be the transmission of the Na filter for MgKα radiation

T_{12}^{12} be the transmission of the Mg filter for MgKα radiation

T_{12}^{13} be the transmission of the Aℓ filter for MgKα radiation

T_{12}^{14} be the transmission of the Sl filter for MgKα radiation

T_{13}^{11} be the transmission of the Na filter for MgKα radiation

etc.

Hence:
$$N_1 = NB_1 + T_{12}^{11} N_{12} + T_{13}^{11} N_{13} + T_{14}^{11} N_{14}$$

$$N_2 = NB_2 + T_{12}^{12} N_{12} + T_{13}^{12} N_{13} + T_{14}^{12} N_{14}$$

$$N_3 = NB_3 + T_{12}^{13} N_{12} + T_{13}^{13} N_{13} + T_{14}^{13} N_{14}$$

$$N_4 = NB_4 + T_{14}^{14} N_{12} + T_{13}^{14} N_{13} + T_{14}^{14} N_{14}$$

where NB_i is the background spectrum for the i^{th} filter condition.

The spectra N_1, N_2, N_3 are our observables while the set of T's are known constants representing the properties of the filters. To determine N_{12}, N_{13}, N_{14}, one is required to solve several simultaneous equations. However, some of the T's are negligible. For example, in granite, the counting rate due to the Al Kα line is estimated by taking the spectral difference channel by channel for the aluminum and magnesium filters. The filter constants are those shown in Figure 4-7.

$$T_{12}^{12} = 0.75 \qquad T_{14}^{12} = 0.09 \qquad T_{13}^{12} = 0.03$$

$$T_{12}^{13} = 0.67 \qquad T_{14}^{13} = 0.05 \qquad T_{13}^{13} = 0.78$$

$$N_2 = NB_2 + 0.75\, N_{12} + 0.03\, N_{13} + 0.09\, N_{14}$$

$$N_3 = NB_3 + 0.67\, N_{12} + 0.78\, N_{13} + 0.05\, N_{14}$$

$$N_3 - N_2 = -0.08\, N_{12} + 0.75\, N_{13} - 0.04\, N_{14} + NB_3 - NB_2$$

or $$N_{13} = (N_3 - N_2 + NB_2 - NB_3 + 0.08\, N_{12} + 0.04\, N_{14})/0.75 \ .$$

Since $(N_3 - N_2) << (NB_2 - NB_3)$, the Al contribution is approximately the spectral difference between two filter wheel positions divided by 0.75. A necessary condition for the procedure to be correct is that the peak of the Al spectrum derived in this manner be properly located in a pulse height analyzer. The statistical error, σ_{13}, in the difference is approximately equal to $\sqrt{(N_2 + N_3)\ \Delta T}$, where ΔT is the number of seconds of accumulation. Hence:

$$\sigma_{13} = \sqrt{(NB_2 + NB_3 + 1.42\, N_{12} + .81\, N_{13} + .14\, N_{14})\ \Delta T}$$

from Table IV-3.

$$\sigma_{13} \approx \sqrt{3400\ \Delta T}\ ;\ N_3 - N_2 = 1000\ \text{sec}^{-1}\ .$$

The relative statistical error in the aluminum contribution is equal to

$$\sigma_{13}/N_{13}\ \Delta T = \sqrt{3400\ \Delta T}/1000\ \Delta T = \frac{.058}{\sqrt{\Delta T}}\ .$$

The relative error can be reduced to below 1% in 35 seconds of observation time.

Systematic sources of errors other than the statistical uncertainties will limit the precision of the measurement of the element concentrations. These are caused by effects that cannot be ascertained during the course of the experiment. One can only set limits on their possible variation by determining how sensitive the results are to these effects. The more important systematic sources of error are discussed below.

(a) Uncertainties in the Solar X-ray Flux

The relative yields of fluorescence lines are sensitive to the shape of the solar continuum and to the presence of characteristic lines. A solar strong line can increase the yield inordinately if it happens to lie just above a K or L edge of an element. In addition, the line will be scattered from the lunar surface into the detector, severely increasing the background in one filter position only. Hence, it is absolutely essential to monitor the solar continuum with a broad band detector and to detect the stronger lines.

One extreme approach is to incorporate a standard rock sample as part of the solar monitor. A counter and filter wheel arrangement similar to the main detector would view the fluorescence and scattered radiation from the sample. The elemental composition of the surface would then be expressed relative to that of the sample. However, this would require a system comparable in size to the main detectors. If the solar radiation is viewed directly, the wheel detector system could be reduced to arbitrarily small size. Laboratory work with simulated solar spectra and rock samples is needed in this area to define the limits of acceptability.

The precise solar spectrum may be available from an OSO satellite that will be in orbit at the time should it be needed. However, correlating data from two different spacecraft is an awesome task that should be approached only with a great deal of trepidation.

(b) Effect of Surface Porosity

The yields will be affected by the physical condition of the lunar surface. Relative elemental yields are affected less than the absolute values. The effects of sample preparation in x-ray fluorescence spectroscopy has been studied and results are available in the literature. However, laboratory work is also needed in this area.

Larger scale geometric effects such as the shadowing in cavities become important when the solid angle subtended by a cavity is less than that of the detector collimator. However, only the absolute but not the relative elemental yields are affected.

(c) Chemical Matrix Effects

The presence in large quantity of an unexpected element on the lunar surface can lead to misleading results. For example, a large amount of fluorine (in the form of NaF or $A\ell F_3$) would deplete the

quantity of outgoing MgKα more than Al or Si because of the energy variation of the fluorine absorption coefficient. Such an occurrence is extremely unlikely when it is noted that the elements considered in the experimental design dominate to a great extent in the earth's crust.

4.4 Alpha Particle Experiment

4.4.1 Fluxes and Background

The four possible sources of alpha radiation from the moon are:

1) The α-radioactive decay of the uranium and thorium impurities in the upper few milligrams of the lunar surface materials;

2) The α-radioactive decay of radon and thoron (and the daughter products) which have diffused out of the first few meters of lunar soil;

3) The α-radioactivity induced by the interaction of galactic cosmic rays with the lunar surface materials; and

4) The evaporation of protons and α-rays caused at times of solar flares by the interaction of flare-associated energetic solar protons and alphas with nuclei of the lunar surface constituents.

Of these four sources, the second and fourth are expected to be the most intense. Each of these sources will be considered in turn to estimate the expected specific source strength at the lunar surface.

Estimates of the natural radioactivity can be obtained by scaling directly from the average relative concentration of α-emitters in terrestrial materials or by assuming that the concentrations of these species are the same as those measured in the stony meteorites. The major species of interest are the isotopes of the uranium and thorium series. Table IV-4 gives a comparison of these estimates.

TABLE IV-4

Estimates of Terrestrial and Meteoritic Sources Of Alpha-Emission

Isotope	Igneous Rock *	Source Strength **	Chondrite *	Source Strength **
Th^{232}	3.9 - 13.45	$(1-4) \times 10^{-4}$	0.0396	1×10^{-6}
U^{235}	0.072 - 0.288	$(0.4 - 1.6) \times 10^{-4}$	0.000821	0.5×10^{-6}
U^{238}	0.992 - 3.98	$(1-4) \times 10^{-4}$	0.0113	1×10^{-6}

* Fractional abundance by weight (ppm)

** Source strength number of α's/cm^2-sec

The second column of Table IV-4 shows the concentration in parts per million by weight of the naturally occurring radioisotopes while the fourth column gives the same information for a chondrite. Typical energies of the α-rays emitted are about 5 MeV. This corresponds to a range in low Z materials of about 5 mg/cm^2. Using this and the known mean lifetimes of the isotopes, the surface α-activity of the moon can then be estimated. The third and fifth columns give the specific source strengths in number of α-rays emitted per cm^2 per second.

The mechanism of diffusion of radon through the upper surface layer of the moon and subsequent "painting" of the surface by the radioactive radon decay products has been suggested as a possibly important mechanism for producing sizeable surface activity. Recent measurements on earth samples of the radon and thoron diffusion allow definitive estimates of this effect to be made. The predominant isotopes of naturally occurring uranium (U^{238}) and thorium (Th^{232}) decay, produce long chains of radioactive isotopes. Tables III-1 and III-2 present these decay schemes and give the energies of the alpha, beta, and gamma-rays emitted in each decay. It is seen that the decay of the radium isotope (Ra^{226}) with a half-life of 1622 years produces an isotope (Rn^{222}) of the noble gas radon. Similarly, in the thorium series, Rn^{220} (Thoron) results from the decay of Ra^{224} which has a half-life of 3.65 days.

A series of measurements have been performed by Evans, Kraner and Schroeder of the concentration gradient and escaping flux of radon from many types of soil in widespread regions of the United States. The following model appears to account quite well for this process on earth. A fraction of the radon and thoron produced by the decay escapes the minerals into the interstitial voids in the soil. The gases then diffuse through these voids to the surface. Application of the appropriate diffusion equations to the experimental results establishes a value for the diffusion coefficient of radon in the various soils. The values obtained range from about 0.02 cm^2/sec to 0.1 cm^2/sec (compared for example with the diffusion coefficient of radon in air, 0.1 cm^2/sec). Estimates had to be made of the porosity of the soil so that these diffusion coefficients should be representative of radon. The differing values obtained can probably be related to atmospheric effects rather than to soil composition.

If the characteristics of the lunar surface layer (the porosity and uranium and thorium concentrations) are assumed to be similar to that on the earth, an estimate of the expected counting rate may be made.

The average observed value for the flux at a number of regions in the United States is approximately 5.0×10^{-17} curies/cm^2-sec. This corresponds to a Rn^{222} atomic flux of about 1 atom/cm^2-sec through the lunar surface.

If one assumes thermal velocities for the emerging Rn^{222} atoms, they will nearly all be trapped in the moon gravitational field, bouncing from the surface and taking excursions up to altitudes of kilometers, finally decaying with their 3.8 day half-life. If one assumes an equilibrium situation, the activity of the Rn^{222} and each of its daughters must be 1 decay/sec-cm^2. The daughter products will probably adhere to the surface. Approximately half of each of the decays would be observable from above since half would decay with the alpha emerging in the direction away from

the detector. Due to the shorter half-life of thoron (Tn, Rn^{220}), most of its decay will occur in flight, offering the possibility of good spatial resolution as compared to the radon activity.

The expected count rate due to the radon diffusion mechanism at an orbiting vehicle (note the assumed experimental parameters) is given in Table IV-5. The actual count rate could differ from this estimate for several reasons. Because of the vacuum conditions at the surface the porosity of the lunar surface may be high; if so, the radon flux leaving the surface would be greater than the estimate. On the other hand, if the lunar composition is basic or ultrabasic, then the concentration of uranium and thorium would be lower than that considered here and the count rates corresponding lower than the estimate.

The third source of alpha emission is the radioactivity induced by the interaction of cosmic rays with the material of the lunar surface. This effect is due to the direct proton reactions and capture of neutrons produced in nuclear stars. To estimate this source strength we must use as the cosmic ray source one-half of the omnidirectional flux in deep space to account for the shielding of the lunar surface. We must further assume that this flux level has been constant during the past eons. Strong departures from the present value may have occurred at times of occurence of nearby supernova.

Taking the composition of igneous rock as typical of lunar surface materials, it is possible to estimate the alpha activity produced by this mechanism by determining the number and kind of interactions which take place within a layer near the surface which is sufficiently thin to permit the exit of the emitted alpha-particles.

TABLE IV-5

Expected Counting Rates

Source of Activity	Counting Rate*	Spectrum
Natural (Igneous Rock)	0.0016-0.008 counts/sec	Degraded from few MeV
Radon (Thoron) Chain	80	Lines 5.48, 6.00, 7.68, and 5.30 MeV from Rn^{222} chain
Cosmic Ray Protons	0.01	Extended, 10 to 50 MeV
Solar Flare Protons	16	Extended, 10 to 50 MeV

*Counting rate in 100 cm^2 solid-state detector in 100 km altitude orbiter with field of view of one ster.

A quite simplified semi-quantitative calculation along these lines has been done by Hayakawa [19] based on the theoretical calculations of Metropolis and Dostrovsky. He predicts an alpha-particle albedo from the lunar surface of 2×10^{-4} particles/cm^2 - sec-ster in the vertical direction as a consequence of the interactions of the galactic cosmic rays. Typical energies are in the range 10 - 30 MeV. This yield produces a counting rate at lunar orbital altitudes of the same order of magnitude as that due to the natural activity of the lunar surface on the assumption of an igneous rock composition. Hayakawa notes that with the values for the mean intensity of non-flare-associated solar protons observed by Vogt, the quiescent flux of solar protons will produce as much albedo as the galactic proton component.

The fourth source is due to the evaporation of the alphas by the lunar surface constituents caused at times of solar flares by the flare-associated energetic solar protons. During a Class IV flare, protons are produced having energies between 10 and 1000 MeV. Measurements made using terrestrial neutron monitors, balloon flights and a few deep space probes have given some information concerning spectral shape and fluxes. The proton flux from a solar flare at the moon's surface (one astronomical unit) is typically 1000 times the galactic background; hence, we can expect during these times a specific activity of about one alpha/cm^2 -sec. The energies are in the range 10-30 MeV.

Two minor additional sources of alpha-emission are due to (n, α) reactions from solar neutrons and (α, α') reactions due to alpha-particles which are accelerated during a flare. No attempt has been made to estimate the expected activity.

4.4.2 Detectors

The alpha particle monitor will be a solid state detector. The silicon surface barrier detector is the most promising because of its excellent resolution and essential simplicity.

Alpha-particle spectroscopy is accomplished by allowing the particle to lose all its energy in the so-called depletion region of the detector. This region is created in the vicinity of the junction of the semi-conductor when a reverse bias is applied. Particles lose energy via electron-hole pair production and these carriers are subsequently collected as they drift in the electric field in the depletion region.

Surface barrier detectors with collection areas as large as several cm^2 are available commercially. Since the anticipated total collection area is 100 cm^2, several detectors connected to a common amplifier will be arranged in a mosaic.

4.4.3 Electronics

The pulses from the detector will be directed to a charge-sensitive amplifier, then to a discriminator and finally to a pulse height analyzer. If the major source of the alpha-particles is the radiogenic noble gas radon, the energy of the alpha-particles emitted in the various radon decay chains range from 5.30 to 7.68 MeV. The depletion depth in silicon, required to stop the most energetic of these is less than 50 microns. This value corresponds to a reverse bias voltage of about 30 volts.

High resolution is required at least in the vicinity of the alpha-particle lines. A pulse height analyzer should be used that provides a sufficient number of channels so that the strength of the lines above the background can be estimated. A block diagram of the electronics logic is shown in Figure 4-10.

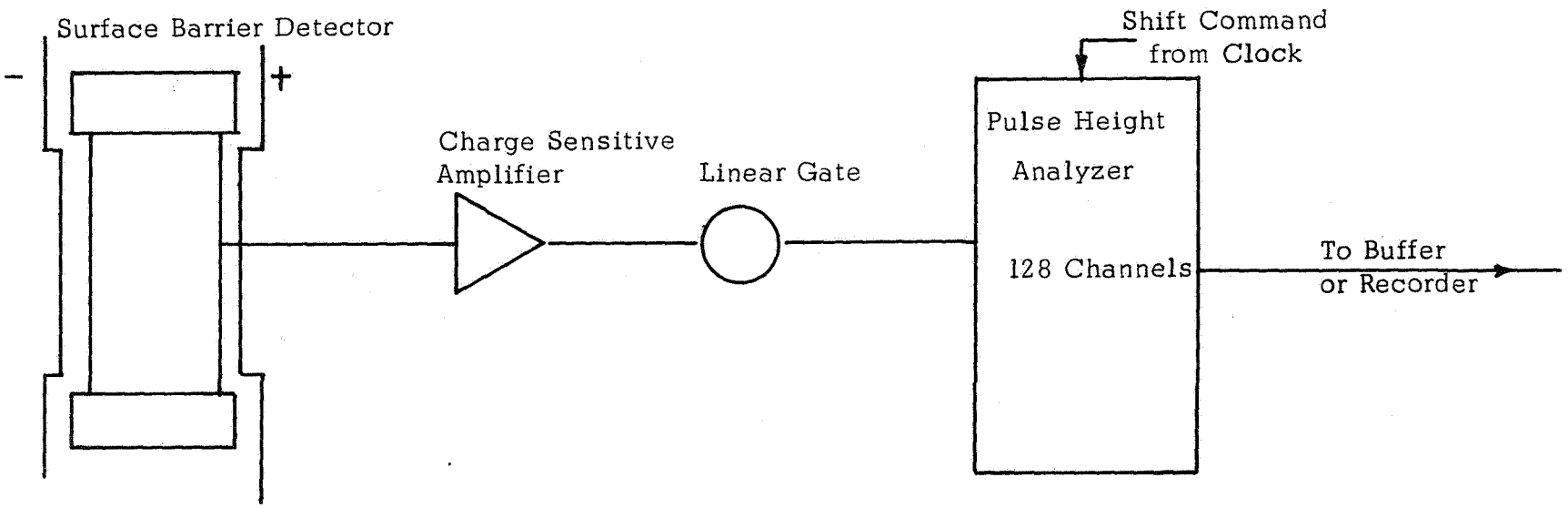

Figure 4-10 Functional Block Diagram of Charge Particle Experiment

4.4.4 Expected Performance

Unlike the x-ray and gamma-ray measurements, the alpha-particle experiment does not have the benefit of previous space experience for making a realistic estimate of its performance. Nevertheless, it is instructive to look at the alpha-particle flux found in the environment created by the settling of the Surveyor V spacecraft. The background situation prevailing at the site is shown in Figure 4-11.

In comparing the background measurements of Turkevitch et al[20] to the counting rates predicted for the alpha-decays of radon and thoron, care must be exercised. First, from Fig. VII-7 of this report, the counting rate rose from 0.1 c/sec in the "background" position to 2 c/sec in the "lunar surface" position, an increase of twenty in the counting rate. This increase occurs as the device is lowered so that the alpha-source is moved from about 56 + 7 cm above the soil to 7 cm above the soil. The alpha-detectors have a field of view with a half angle of about 30°. The alpha-sources are collimated so that when the detector head is on the surface, the detectors see alpha rays back-scattered through 174°. The total activity of all six alpha sources is $2/75 \times 10^{11}$ dist/min or 4.6×10^{9} dist/sec, while on the ground 2 α/sec are seen or an efficiency of $\sim 2/(5 \times 10^{9}) = 4 \times 10^{-10}$ which, of course, includes the solid angle of the alpha-source for emission of the alpha's into the designed solid angle. From the description of the instrument[14], 2.2% of the alpha's produced are emitted through the orifice in the source-holder. Hence, an efficiency of about 2×10^{-8} is indicated when the sampler is in the operating position. For the "background" position and from solid angle considerations, the counting rate over a smooth plane should drop by a factor of 60 to 80 i.e., $\sim (7/50)^2$ to $(7/63)^2$. The fact that the lunar surface is not a smooth plane could result in a factor of 3

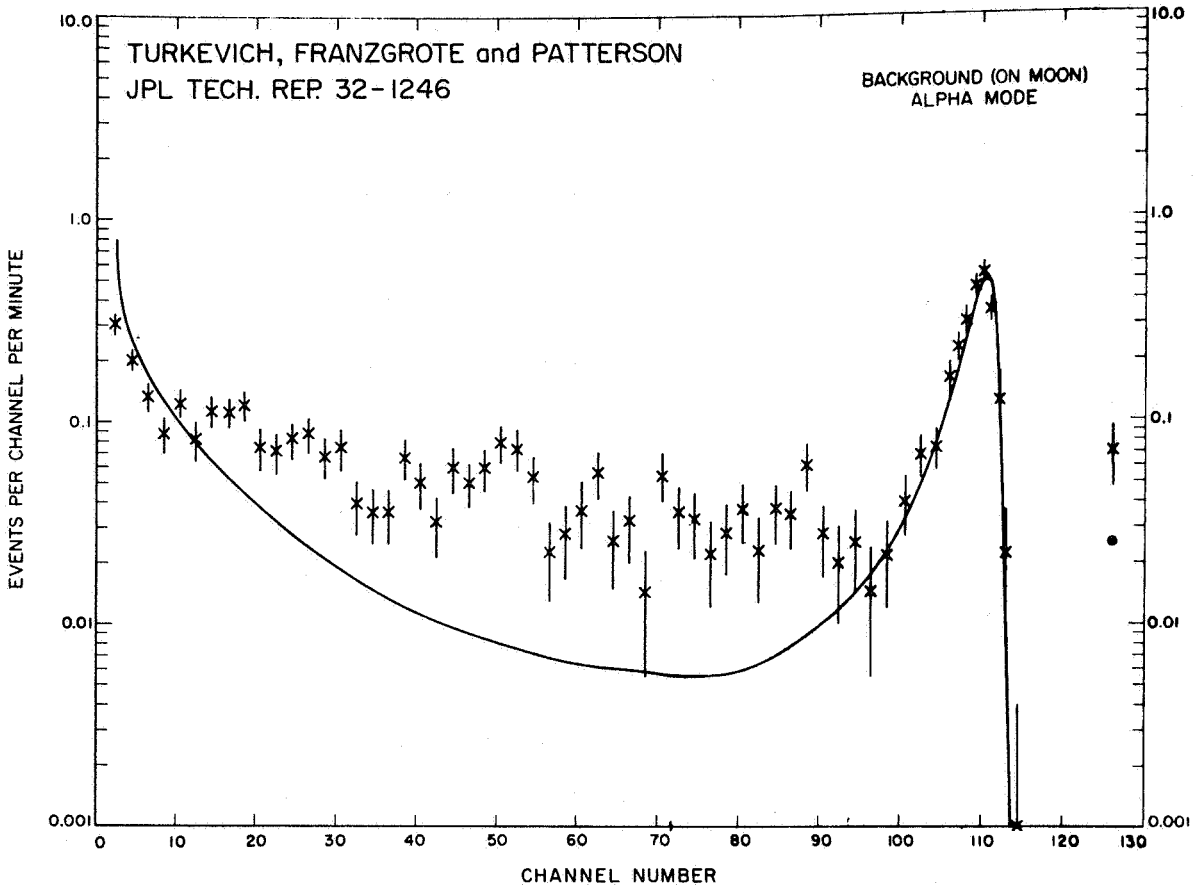

Figure 4-11 Alpha Particle Background at Surveyor V Landing Site.

Note: The continuous curve is the predicated background calculated on the basis of surface radioactivity and cosmic ray production. The points are the observed background.

or 4 increase in the reflectivity. Hence, the "background" seen by Turkevitch could easily be due principally to scattered alpha's from the source.

Second, the alpha-counting rates predicted by the radon estimates were for a detector flown above the radon atmosphere which may have a height of~ 6 to 10km. The total counting rate expected is of the order of 1.9 α/cm^2 -sec for such a 2π detector. For a detector 56 cm from the lunar surface, it will see only the small amount of radon which decays below it within its field of view and the daughter products of radon that are painted out on the surface. For the latter, we have at most 1 α/cm^2 -sec into 4π Sr; hence, if the detector solid angle is 1 ster then we would see 0.08 α/cm^2 - sec. For a detector the size of Turkevitch's (0.2 cm^2) we would expect 0.016 α/sec or about 1 α/min which is higher than what is seen in the resolution width of a line by a factor of about 40. However, if the radon daughter products are not uniformly spread over a smooth surface, then this factor of 40 is perhaps not too significant. Even if the Surveyor results are given, the most pessimistic interpretation from the point of view of detecting alphas, the upper limits to the fluxes are still sufficiently high for a significant measurement.

4.5 Neutron Albedo Experiment

4.5.1 Fluxes and Background

Lingenfelter, Canfield and Hess (LCH) [13] have calculated in detail the cosmic ray induced neutron leakage spectrum for several model lunar compositions. The results show a variation with the mineral type and a strong sensitivity to the hydrogen content. Figure 4-12 reproduced from (LCH) demonstrates the expected leakage for several compositions, including for chondritic material two different values of the hydrogen/silicon atomic ratio.

The accuracy of the H/Si absolute measurement is limited by two factors: (1) the statistical precision of the slow to fast neutron ratio (which depends on the duration of the mission), and (2) the accuracy with which the thermal-neutron cross section for absorption is known. This latter factor depends on the composition of the lunar surface, and in particular, on the concentration of the atoms such as in iron. This information will be obtained from the gamma-ray and x-ray experiments of the integrated experiment package.

The diffusion analysis by LCH shows that hydrogen may be detected by such an experiment if $H/Si \approx 0.05$. This is the composition of chondrites, and corresponds to 0.3% of water (by weight).

Alternatively, an amount of water in excess of 0.25 gm/cm^2 in the upper 100 gm/cm^2 of the lunar crust will be detectable. This is the equivalent to 2.5 mm of H_2O in otherwise dry rock, if the water is in the uppermost foot of material. It is interesting that granite has an H/Si ratio of 0.1, twice the minimum detectable.

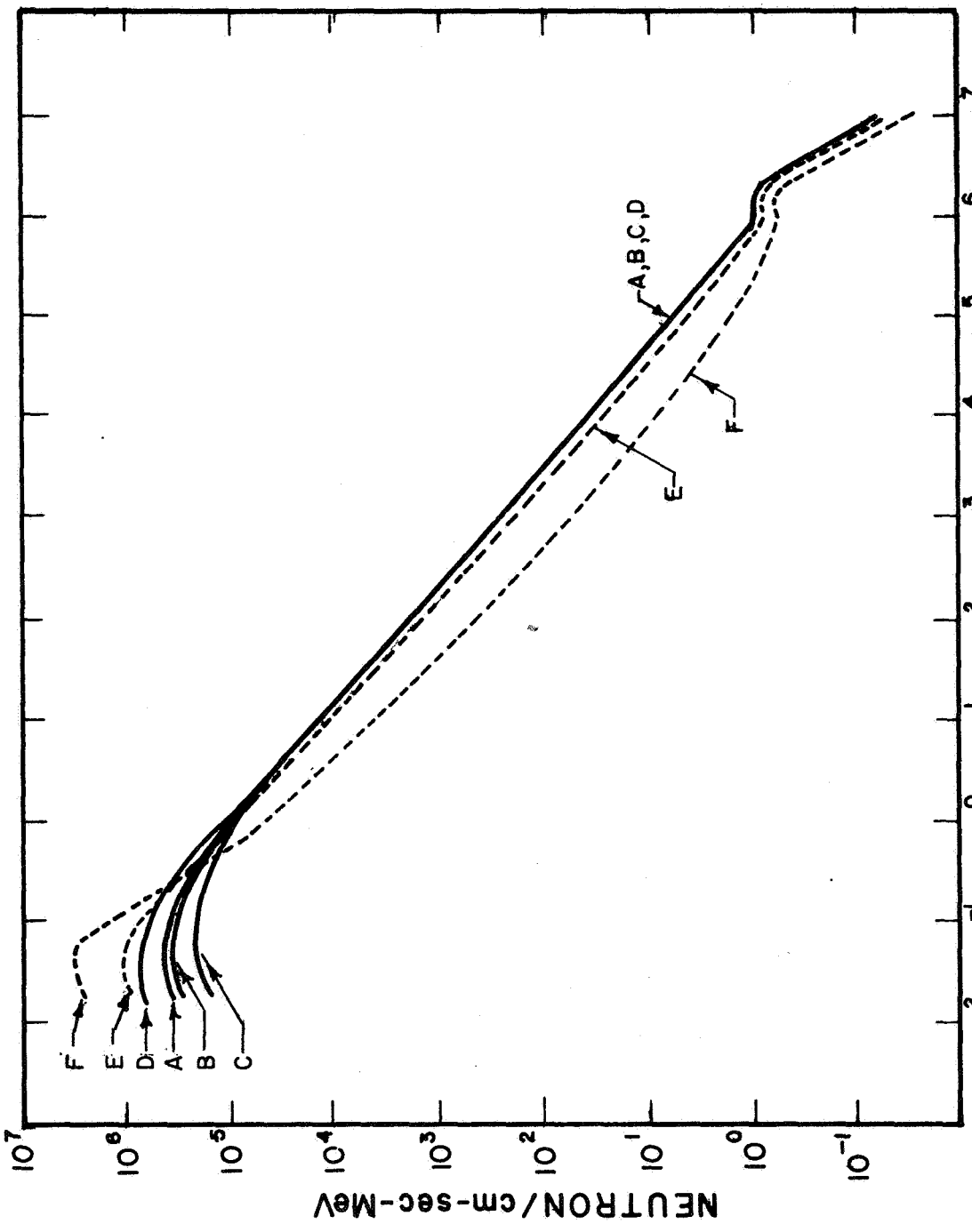

Figure 4-12 The Calculated Neutron Equilibrium Leakage Spectrum for the Lunar Surface for Compositions A, Chondritic Material; B, Chondritic Material with a 10 Per Cent Increase in the Total 1/v Capture; E, Chondritic Material with 0.1 H/Si Atom; and F, with 1.0 H/Si Atom. Reproduced from Lingenfelter, Canfield and Hess [13].

The figure of H/Si ≈ 0.05 assumes the thermal-neutron cross section to be uncertain to ± 50%, for the material in the lunar crust. If only a ± 20% uncertainty exists, then H/Si will be known to about ± 30%, if we find it to be somewhere around 0.1.

Finally, statistical precision is not expected to be a serious limit on the accuracy of measuring H/Si. The relatively high neutron fluxes that we expect for the moon should allow us to measure the (slow/fast) neutron ratio to ± 9% in 30 seconds, the sampling time. If H/Si is about 0.1, this will only contribute a 9% uncertainty to the latter ratio. Thus, it seems clear that the relative measurements (prospecting) will be comparatively easy to make and that absolute information on the hydrogen concentration in the lunar surface may also be obtained. These data may then serve as an index to the presence of water.

4.5.2 Neutron Detectors

(a) Slow Neutron Detector

Two unmoderated proportional counters filled with BF_3 are proposed as the slow-neutron detector. The two counters are identical in all respects except for the isotopic enrichment of the boron in the filling gas. One of the two tubes contains 96%B^{10}; the other counter uses 10%B^{10} and 90%B^{11}. The B^{11} isotope does not appreciably interact with neutrons, but B^{10} does interact, in accordance with the B^{10} (n, α) Li^7 nuclear reaction. A proportional counter may be used to select the pulses due to the heavily-ionizing alpha particle and lithium nucleus. The reaction has a 1/v dependence in the cross-section, where v is the velocity of the neutron. Hence, the counter primarily responds to slow neutrons.

The difference of the counting rates is a measure of the slow-neutron density. If $\underline{n}$ is the counting rate due to slow neutrons in a counter filled with 100% B^{10}, and $\underline{b}$ is the background counting rate due to charged particles, then

$$A = 0.96\ \underline{n} + \underline{b}$$
$$B = 0.10\ \underline{n} + \underline{b},$$

where A and B are respectively the two measured counting rates. The solution of the two simultaneous equations yield the desired quantity, $\underline{n}$, which may then be related to the density of slow neutrons, ρ. The pair of counters thus provides an absolute value for ρ, in units of neutrons cm^{-3}.

(b) Fast Neutron Detector

Fast neutrons are detected through the ($\underline{n}$, $\underline{p}$) elastic scattering process. A fast neutron interacts with a proton in a special organic scintillator, imparting some of its energy to the (charged) proton and causing a pulse of light. The light is then detected by a photomultiplier tube. A relatively simple (32 channel) pulse-height analysis is conducted on board the spacecraft, in order to relate the counting-rate to a flux; self-contained data processing electronics will perform this latter function.

In the range of energies from 1 MeV to 15 MeV, a scintillator also responds to charged particles such as cosmic rays and also to gamma rays through the Compton process. These spurious responses may be eliminated, however, by completely surrounding the organic scintillator with a thin layer of inorganic scintillator, CsI (Tl). Charged particles traversing this "phoswich" assembly also cause pulses to be generated in the inorganic layer; this may be differentiated from signals that occur in

the organic material through pulse-shape discrimination (PSD). The PSD technique thus allows charged particles to be rejected by the system.

Mention was made of the "special" nature of the organic scintillator. Some organics display PSD between neutrons and gamma rays (protons and electrons); this property is employed in the fast-neutron detector to establish a device that responds uniquely to neutrons in the presence of other radiation types.

4.5.3 Electronics

Standard techniques shall be used in the logic circuits that select a proper event and reject background. The circuits shall be quite similar to those used in the x-ray and gamma-ray experiments. A block diagram appears in Figure 4-13.

4.5.4 Expected Performance

The expected performance is based on the calculations of LCH. Figure 4-14 which has been reproduced from that article shows the ratio of counts in the two neutron detectors (as a function of the hydrogen/silicon atomic ratio) of the materials counters "a" and "b" are like the detectors described in sections (a) and (b) respectively, above.

It is strongly recommended that this experiment, like the gamma, be evaluated at a high energy proton accelerator.

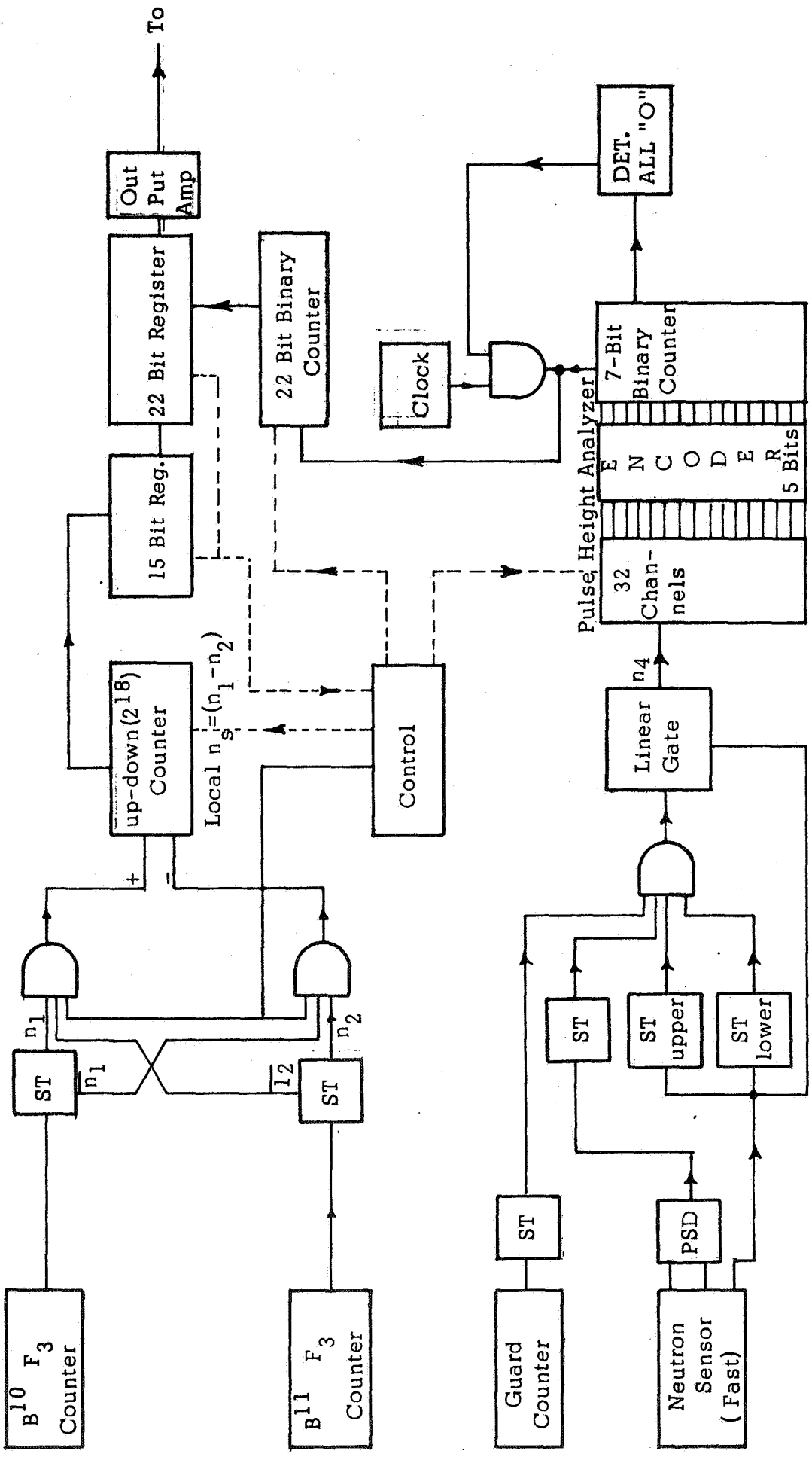

Figure 4-13 Functional Block Diagram of Neutron Experiment

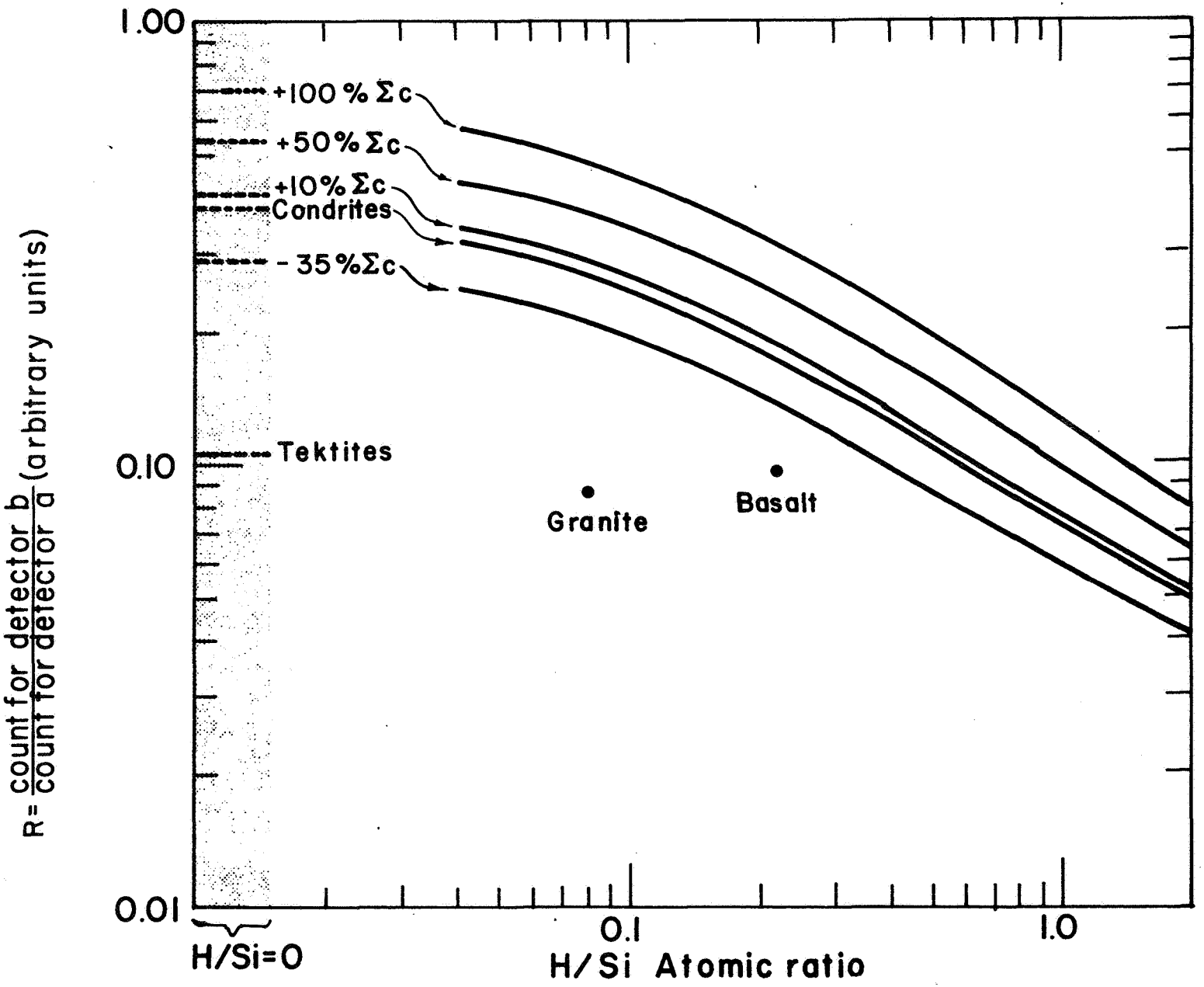

Figure 4-14 Calculated Neutron Counting Rate Ratios in Detectors (a) and (b).

Note: Detector (a) is presumed to have an energy sensitivity varying as 1/v, e.g. a B^{10} F_3 proportional counter detector, (b) has a flat response at higher energy. The neutron flux is the cosmic ray induced leakage spectrum from the lunar surface. Reproduced from article by Lingenfelter, Canfield and Hess[13]

4.6 Observational Aspects of Lunar Radiations

This section considers the observations that are made during one orbit of the mission. A lunar orientation would provide the ideal attitude positioning for most of the experiments. To achieve this kind of attitude control would require a gravity gradient stabilization system or its equivalent. In practice it may be difficult to implement such a system in a lunar orbiting vehicle in a way that is compatible with the experiments. A gravity gradient stabilization system would require booms that lie along the radial line to the lunar barycenter, fore and aft of the spacecraft. On the other hand the experiments desire a tangential boom direction for unobstructed viewing of the lunar surface. A second preference would be a solar referenced system in which the vehicle attitude or a platform containing the experiments rotates with respect to the solar direction in several discrete steps throughout the course of an orbit. This would be a "quasi-lunar" orientation, a compromise between the desirability of viewing the lunar surface in the normal direction and the capabilities of most currently available spacecraft.

All of the experiments will be designed to have a field of view that can be approximated by a cone whose full opening angle is about 60°. In a purely solar pointed stabilization mode three effects take place during the orbit that greatly reduce the observational efficiency when the spacecraft is off the sun-moon line. It is assumed that the spacecraft is in a lunar polar orbit.

(1) The angle, θ, between the normal to lunar surface and the center of the field of view changes.

(2) The area of lunar surface that is covered by the field of view is changing. This means that the spatial resolution is continually changing being at minimum when the

spacecraft, moon, and sun are co-linear and broadening toward the lunar poles.

3) The solid angle subtended by the detectors will decrease towards the poles when the lunar surface no longer fills the field of view of the detectors.

The situation is shown in Figure 4-15 for an orbit whose altitude is 0.08 lunar diameters. Because of the first effect, the detection efficiency will decrease as the angle θ, shown in the sketch below, increases:

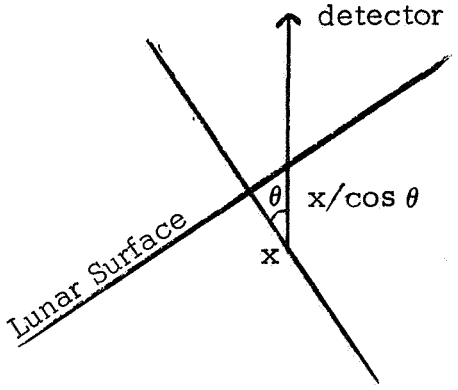

For radiation having a linear attenuation coefficient of μ in the lunar material the total amount per unit area leaving the surface at an angle is proportional to:

$$\int_0^\infty e^{-\mu x/\cos\theta}\, dx = \frac{\cos\theta}{\mu}$$

Consequently, a purely solar stabilization mode will result in a very poor coverage of the lunar poles in a single orbit. In part, the continual observation of the poles during many orbits compensates. Hence, it would be desirable to re-orient the spacecraft attitude or at least that part which contains the detectors at discrete intervals so as to re-align the field of view with the lunar surface. Figure 4-15 illustrates such a change in an attitude occurring when the spacecraft is 60° off the sun-moon line.

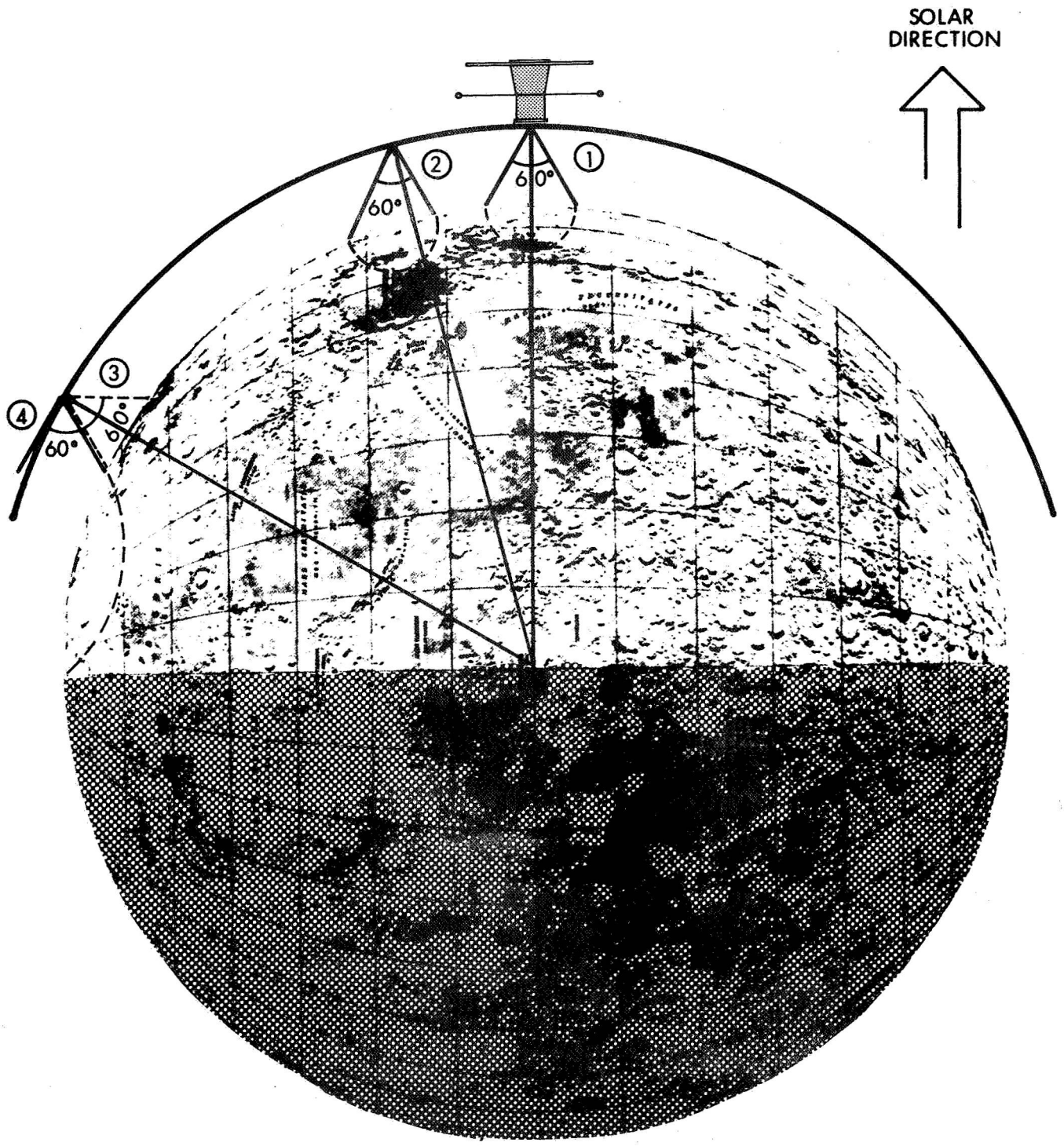

Figure 4-15 Coverage of Lunar Surface From Orbiting Vehicle With Detectors Limited to 60° Cone-Shaped Field of View

Throughout the orbit a total of 6 changes would occur if the data are taken on the darkened side of the moon. This amounts to a complete attitude cycle in one orbit. It would be desirable to make the attitude change more often to increase the counting efficiency, and to keep the coverage of the surface as uniform as possible. Attitude changes would also be beneficial in making assessments of the background. Attitude changing capability would be limited by the characteristics of the spacecraft. To change the entire spacecraft would be simplest from the experimenter's point of view and best for assessing background. However, large torques would be needed which can be achieved possibly only through the use of gas jets. This has obvious limitations in a mission where there are several attitude changes in an orbit. If the attitude changes are restricted to smaller and lighter experimental platforms perhaps much less jet action will suffice. The mechanical problems of changing the orientation of a massive gamma detector at the end of a long boom are of course formidable. Perhaps a system of lightweight counterpoises could be arranged that require only electric power and no jet action in the reorientation of a platform. All the experiments except the x-ray are independent of the solar illumination of the surface. Useful data can be obtained on the dark as well as the sun lit side.

Spin stabilization of the vehicle would result in less efficient coverage of the lunar surface and would place a great burden upon the data handling. With the desired 60^{o} field of view useful data would be obtained during only one-sixth of the spin period with a concommitent loss in sensitivity. More significantly there would be the formidable problem of selecting the data which accumulates when the instruments are looking at the moon from the surfeit of "off-lunar" measurements.

Hence, a spinning vehicle needs more telemetry capability. There is a need to know the spin axis orientation and the rotation angle with respect to the lunar surface at all times. Sun sensors could be used on the sunlight portion of the orbit. Star sensors are needed at other times.

4.7 Expected Results

4.7.1 Resolution of Spectral Lines

It would be interesting if the lunar surface merely exhibited variations in the spectral quality and total quantity of emitted radiation. However, the measurements are qualitatively superior if spectral lines are identified in the gamma, x-ray and alpha fluxes. In that case it is possible to derive quantitative data for the abundance of certain elements. Estimates of the primary fluxes and backgrounds given above indicate that the measurement should succeed in this respect.

Instrument resolution is the principal limitation in the unfolding of the counts as they appear on a pulse height analyzer into the true primary spectrum. If a strong line can be identified and the instrument response is well understood its strength can be determined and its contribution may be subtracted from the total count distribution. As a result, perhaps more lines can be identified and the process repeated. When individual lines are not resolved the decomposition lacks uniqueness.

In both the gamma and x-ray experiments the background from the lunar surface will consist of a large number of lines plus a continuum. As discussed above, there are fairly good estimates of the continuum from experimental data. Knowledge of the line contribution is lacking. For the gamma-ray experiment the lines are produced in the decay of highly excited states formed in many generations of cosmic ray processes. In the x-ray experiment the lines originate in the scattered solar spectrum. Difficulty will arise if there exists strong lines whose separation from the lines of interest is less than the detector resolution. To the extent that knowledge of the detector response permits, quantitative methods of analysis which examine the shape and symmetry of line profiles can be used to estimate or set limits upon the background contamination.

4.7.2 Figure of Merit of Detector Systems

The figure of merit of the detector system is the statistical error in the determination of the strength of a line within a given accumulation time. If it is possible to trade off effective area or efficiency against resolution or reduced background, one chooses the configuration that leads to the smallest relative error. In general, the selection is governed by a combination of the strength of the expected line and the amount of background that will appear within its resolution width. The optimum configuration depends on the situation. In these measurements not much choice is available. Decreasing detector size does not lead to an improvement in resolution or background. In fact, exactly the opposite occurs at least for the gamma experiment. Hence, it is desirable to use as large a detector as the spacecraft can support.

4.7.3 Background Measurements, Auxiliary Monitors and Measurements

Correct interpretation of the fluxes recorded during these observations depends on knowledge of the radiation incident on the moon and of certain spurious (background) effects from the moon and the spacecraft. Even in the case of the gamma measurements, where the bulk of the radiation originates in naturally occurring radioactive material and lunar albedo and no dependence on solar activity is expected, there may be a substantial background caused by solar cosmic rays which must be accounted for--if only for the purpose of stating that it is negligible. In general, one can distinguish two kinds of auxiliary measurements. One, as in the case of the fluorescence x-ray measurements, is the observation of the primary incident radiation; in this case the solar x-ray flux gives rise to the secondary radiation from the moon. The other kind of

measurement can be categorized as on-off moon to assure oneself that the measured radiation is, in fact, originating from the moon. Because of the diversity of measurements to be performed, an equally diverse set of auxiliary measurements are involved, some of which involve independent detectors and others simply use primary detectors in an other-than-moon oriented mode.

The following incident radiation can be identified:

(a) Solar X-Rays - These comprise the source function for the fluorescence x-ray measurement. Since the solar x-ray flux varies with time, in both intensity and spectrum it is necessary to monitor the x-ray flux continuously and with some form of broadband spectral resolution.

(b) Solar Cosmic Rays - Fluxes of energetic protons from the sun are highly variable and can contribute a substantial gamma and alpha background when incident on the lunar surface. It is thus necessary to monitor this flux of particles. The galactic cosmic rays, which are the principal source of the lunar neutrons and an important source of gamma-ray background, do not vary on the time scale of this mission, and need not be monitored.

(c) Spacecraft Produced Background - The material comprising the spacecraft can be a source of background, which is why certain experiments are mounted on booms. Measurements made before and after the booms are extended permit an assessment of the fraction of the background that is attributable to the spacecraft. The formalism for evaluating the effect of extending the boom is that the solid angle of the spacecraft, as seen at the detector, is reduced when the boom is extended.

(d) Solar Wind and Trapped Radiation - The omnipresent solar wind comprises a flux of the order of 10^8 particles/cm^2-sec of low energy (~1 keV) protons and even much lower energy electrons. These can give rise to low energy radiation from the lunar surface. In addition, the moon will traverse the tail of the earth's magnetosphere once per month and be exposed to trapped radiation; namely, both electrons and protons varying in energy from keV to MeV. Both of these kinds of radiation need to be monitored.

These monitoring functions can be performed with modest detectors since only very large fluxes produce measurable effects from the lunar surface. However, a variety of detectors is required; namely, proportional counters for measurement of the solar x-ray flux, a plasma probe for the solar wind, and solid-state detectors for energetic protons and electrons. The detectors are not large but their placement is critical.

(e) "On-Off" Lunar Measurements - A variety of on-off observations can be identified. These are:

1. Day-Night Differences. When the spacecraft is in the moon's shadow (night) certain incident radiation is blocked, principally the solar x-ray flux, the solar wind and the bulk of the solar cosmic ray flux. In the case of the fluorescence x-ray measurement, the blockage should be complete and counts recorded at night constitute background.

2. Attitude Variation. Variation of the attitude of the spacecraft can be used to estimate what fraction of the detected radiation can be attributed to the lunar surface. If at some point the spacecraft is rotated to an orientation in which the detectors no longer have a view of the moon, the persistent events are within limits, a measure of the background. They are due to cosmic ray interactions in the spacecraft or

effects from the magnetosphere. However, these are qualifications. Some lunar radiation may penetrate the collimator of the gamma experiment which is not perfectly opaque. This is true to an even greater extent in the the neutron experiment. Off the lunar surface the x-ray detectors are exposed to the isotropic cosmic x-ray flux which is normally occulted by the moon. Capability of the attitude variation should be included in the performance characteristics of the spacecraft.

3. Measurements During Various Phases of Mission. It is important to have counting rate data during all phases of the mission; i. e., during mid-course and before booms are deployed, and all elevations above the moon and at all orientations with respect to the moon. It is important to avoid a constraint whereby no data can be obtained at any time during some moon-related phase of the operation of the spacecraft. It is necessary to know the spacecraft orientation and its orbital parameters as a function of time.

5.0 SPACECRAFT SELECTION

5.1 Physical Characteristics of Experiment

Some of the relevant characteristics of the detectors that comprise the experiment are listed in Table V-1. The data rate requirement (BPS) is based on a 30 second count accumulation time along with the counting rate data presented in Sections 3.0 and 4.0. The assumption in calculating these rates is that counts are accumulated for 30 seconds into the primary registers of the pulse height analyzer and then read out during the subsequent 30 seconds. Intermediate buffer registers for the primary registers allow continuous accumulation of counts. The lengths of the individual registers (bits/channel) vary according to the expected accumulated count; for the present purpose, it is assumed that for a given detector the total accumulated count is divided equally between all channels of the pulse analyzer. In actual practice the register lengths can be optimized according to the expected spectral distribution of counts. As shown the register can accumulate four times the anticipated rates (two extra bits/channel). No attempt has been made to reduce the bit requirement by techniques of data compression. In certain instances, particularly with the gamma-ray and alpha detectors, it may be possible to accomplish considerable bit saving by restricting the readout to the most relevant portions of the pulse height spectrum.

A conceptual block diagram of the experiment is shown in Figure 5-1. The largest single block of electronics comprise the count registers and the associated input-output circuits. Approximately 1200 independent registers are required containing a total of about 10^4 bits. The registers are actually in the form of core storage; thus the bit requirement is not excessive. While each of the detectors requires independent signal conditioning, much of the pulse analysis electronics is time shared by all the detectors, thereby reducing the overall complexity.

A more detailed breakout of the experiment electronics is shown in Figure 5-2. The signal conditioning associated with each of the detectors

TABLE V-1

EXPERIMENTAL PHYSICAL CHARACTERISTICS

AND PARAMETERS

Experiment	Weight Lbs	Power Watts	Size Approx.	Data Rate BPS	Experiment Description	Requirements (All Exp. 30 sec. Acquisition Time)
γ-Ray	75	10	300 in^3 on boom 150 in^3 Elec.	70	256 Chan. (PHA) 9 Bits/Chan.	A/C Shield, 10"x20" N I Crystal Mount on boom
X-Ray	25	10	12"x12"x7"(2) 6"x6"x4" (1)	30	128 Chan. (PHA) 9 Bits/Chan.	(8) 16 Chan. Analyzers, one each per quadrant of a circle, behind radiation filters(2 units)
α/P/CR	15	4	7"x7"x2"	15	128 Chan. (PHA) 7 Bits/Chan.	Solid State Detector 100 cm^2
Neutron	10	3	430 in^3 boom 120 in^3 Elec.	3	32 Chan. (PHA) 7 Bits/Chan.	Boom Mounted
Solar Monitor	3	3	5 in^3 Detector 10 in^3 Elec.	3		Sun Oriented. May be mounted on Solar Panel
Charged Particle Monitor	2	2	5 in^3 Detector 10 in^3 Elec.	2		
Infrared	TBD	TBD	TBD	1	TBD	
Mass Spectrometer	5	4	200 in^3	2	10 Chan.	
TOTAL	135	36		126		

Note: Table parameters do not include those of Data Processing, RF Communications and Recorder

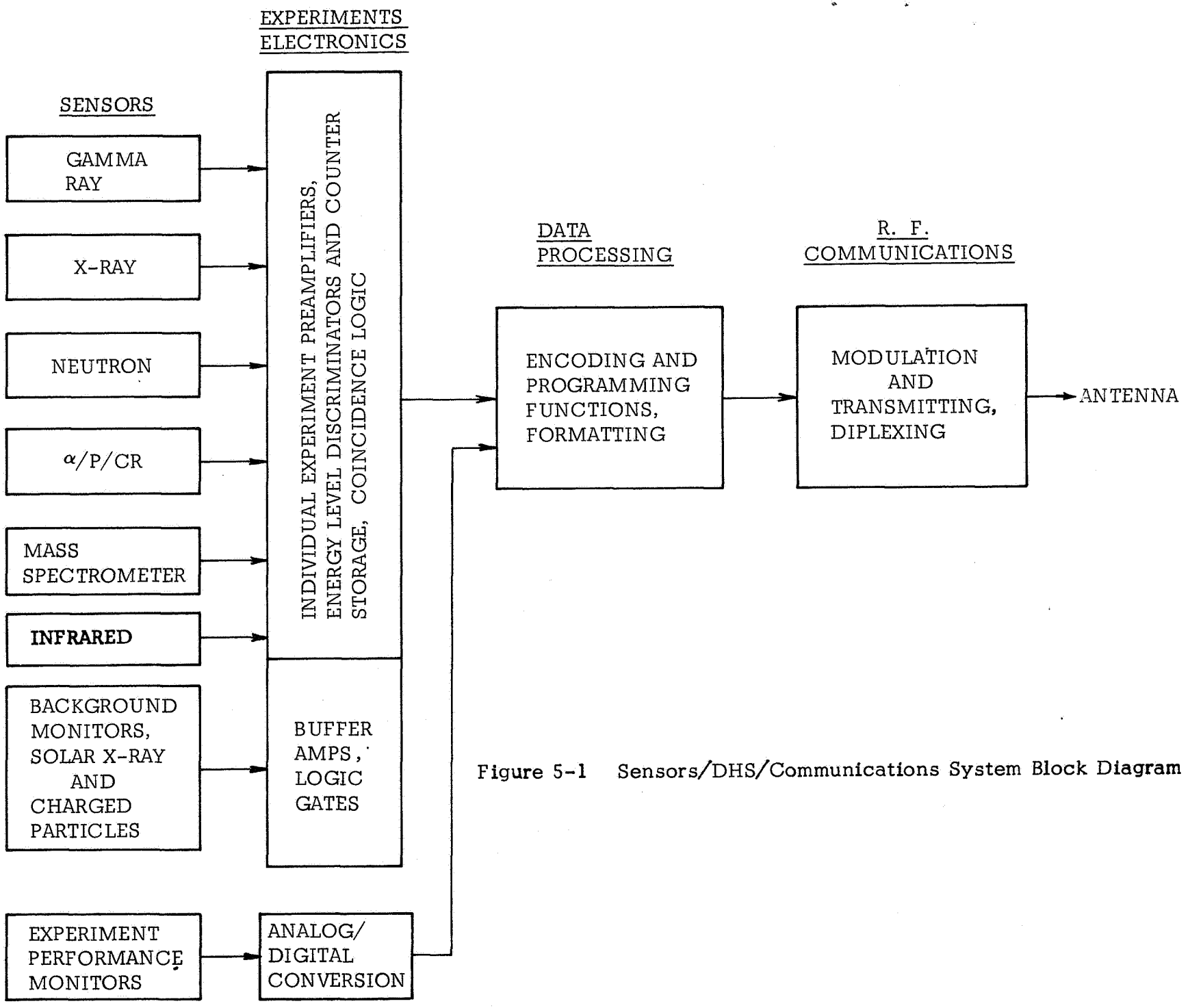

Figure 5-1 Sensors/DHS/Communications System Block Diagram

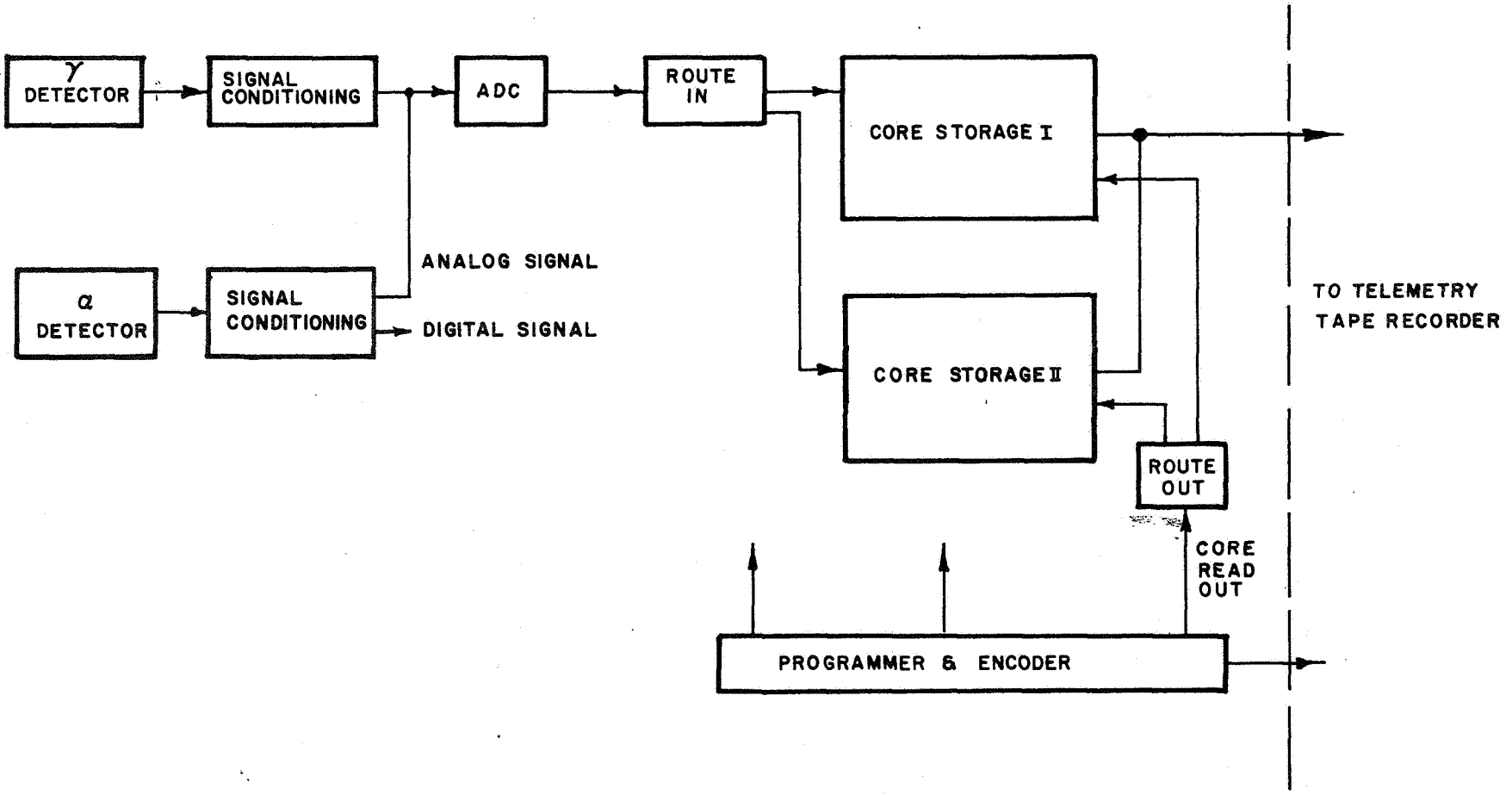

Figure 5-2 Logic Block Diagram Experiment Processing Electronics

is basically a low-noise, charge-sensitive preamplifier, although the actual requirements vary somewhat from one detector to the next. At least one group of detectors, the X-ray proportional counters, require two channels of signal conditioning in order to allow for pulse shape discrimination. One of the channels preserves the amplitude of the signal; the other is processed to yield a signal whose amplitude is proportional to the rise time or the width of the counter signal. This processing can comprise a zero-cross technique, followed by a time-to-height conversion. In addition, each of the detectors utilizes some kind of guard counter whose output is used to veto time-coincident signals from the primary detector.

Beyond the signal conditioning, analog signals are sent to an ADC (analog to digital converter) whose output is a bit stream that represents a number that is proportional to the amplitude of the analog signal. Several of the detectors can be processed by a single ADC, the digital signal out of the signal conditioner being used to sort the output of the ADC. The number of bits comprises a register address and a count is accumulated into storage at that address. Two core storages are used, one into which counts are being accumulated for some time period, the other, which had accumulated counts from a previous time period, from which the register contents are being shifted to telemetry or to a tape recorder for subsequent transmission to earth. The use of two independent, but identical, storage units allows virtually continuous accumulation of detector data. The routing of counts is controlled by a programmer. A possible mode of operation is that data is accumulated into one storage for 30 seconds while the other is being read out; and, in the next 30 seconds, the first is read out and data is accumulated in the other. The readout would be destructive.

Data processing systems of the kind described above have been developed and flown on various space missions, being known generally as multichannel analyzers. One system has been developed specifically with

the requirements of a mission of this kind by the Spacetac Corporation under Contract NAS5-11099 and has been described in detail by Streeter[21].

5.2 Environmental Constraints

With the possible exception of the infrared detection system and the mass-spectrometer which are not well defined at this time, none of the detectors or electronic subassemblies require any unusual environmental conditions. Detectors of the kind being proposed here have flown on virtually every kind of space mission. They can be made to tolerate broad ranges of temperature, vibration and ambient pressure. In addition, the effluvium from rocket motors and the normal outgassing of the spacecraft material can be contended with by providing programmable doors for the most critical detectors. The latter device may be necessary to protect certain very thin filters, such as are contained in the x-ray fluorescence experiment and the alpha particle detector, from the degrading effects of micrometeorite bombardment. The flux of micrometeorites is discussed in Appendix A.

One critical area, which is not usually encountered in spacecraft design, is the problem of onboard radioactive material. The detectors utilized in these observations are extremely sensitive to nuclear radiation, and certain sources of this radiation may be overlooked. One well-known source of gamma-rays are certain high-quality optical elements utilizing rare-earth and heavy element inclusions. These may contain naturally occurring radioactive materials as well. Another potential source is thorium, which is sometimes used as an alloying element to increase the strength of aluminum and magnesium. The materials utilized in the spacecraft must be carefully examined to eliminate the possibility of excessive radiation. It should be emphasized that the problem here is not one of physical damage to the detectors as may be encountered for instruments that need to operate for long periods of time in the radiation belts, but rather an increase in counting rate that adds to experimental data and could degrade the quality of the results.

5.3 Spacecraft/Experiment Electrical System

A conceptual block diagram of the spacecraft electronic interface with the experiment system is shown in Figure 5-3. Clearly the arrangement is a conventional one regarding power, telemetry and command subsystems. The requirements for commands will not be excessive.

5.4 Mounting and Orientation Considerations

As indicated in Table V-1, certain detectors, namely, the neutron and gamma ray detector, need to be mounted on booms in order to reduce the effect of radiation originating in the spacecraft. The basic reason that these, and not the other detectors need to be removed from the spacecraft is that the background to which they are most sensitive can penetrate large amounts of matter; thus they are sensitive to neutrons or gamma rays produced almost anywhere in the spacecraft. For the other detectors no significant advantage accrues from their being mounted on booms and away from the spacecraft. The reduction in background factor achieved by boom-mounting is given, approximately, by the expression,

$$f = A/4\pi R^2$$

where f is the ratio of spacecraft background out at the end of a boom of length R to that measured at the spacecraft itself. The quantity A is the projected cross section area of the spacecraft. For a typical situation $R \approx 10$ ft and $A \approx 25$ ft^2, f becomes the order of 1/50.

The actual mounting position is dictated by the requirement that the detectors have a clear view of the moon. This is intimately connected to the mode of orientation control of the spacecraft. This latter factor is discussed at length at Section 6.0.

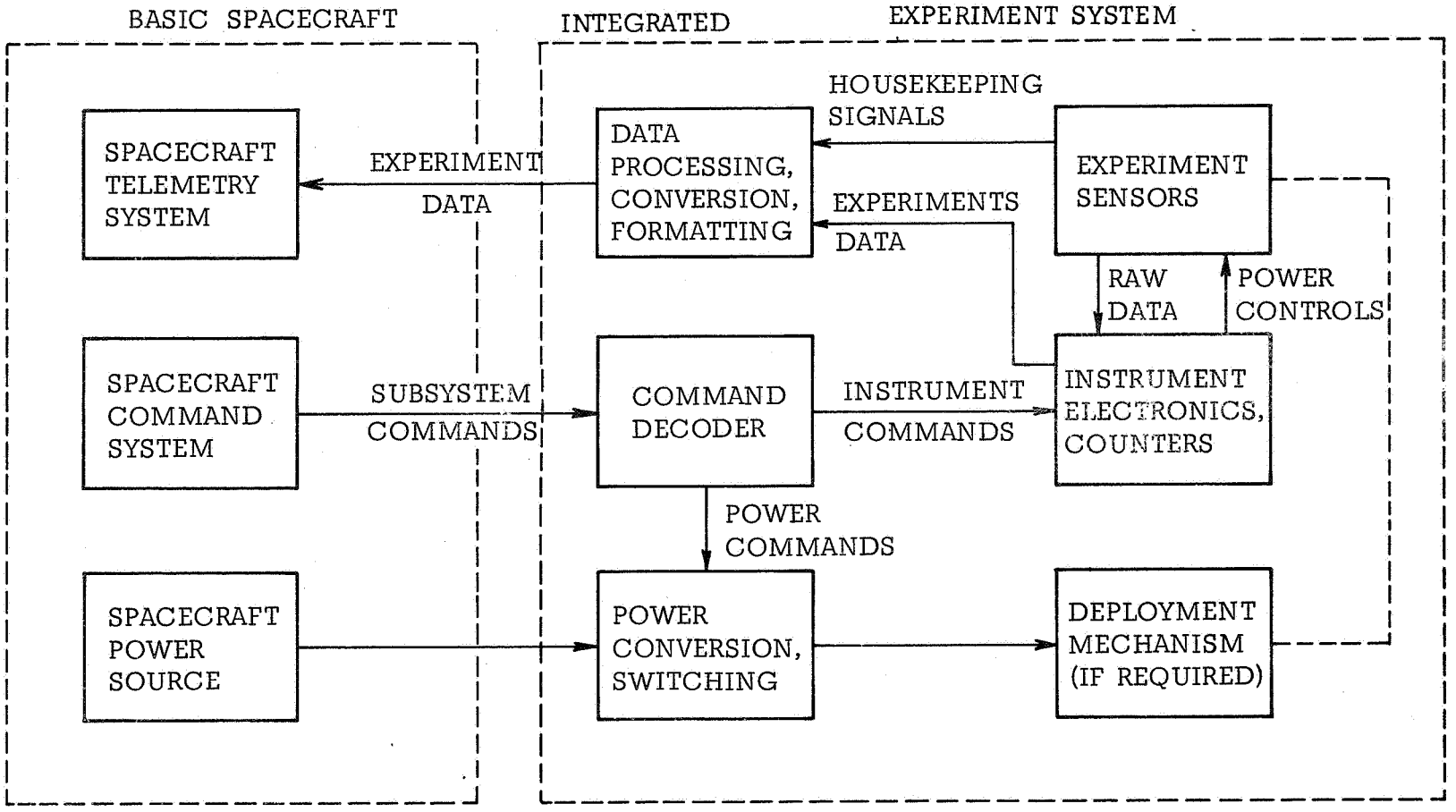

Figure 5-3 Spacecraft/Experiment System Electronic Interface Block Diagram

5.5 Possible Spacecraft

Table V-2 lists a number of existing spacecraft and their characteristics. Also listed in the final column are the requirements on the spacecraft which would be imposed by the integrated radiation experiment discussed here. Briefly, the possibilities are:

5.5.1 Pioneer

Although Pioneer's weight-carrying capability and power capacity are modest, a minimal type of mission may be carried out. Pioneer has been updated to include a restartable rocket engine.

5.5.2 Anchored IMP

IMP's capabilities are minimal for the mission, and probably could not carry all the instrumentation. It does have a fairly extensive data handling system.

5.5.3 Lunar Orbiter

This successful and versatile spacecraft is clearly the most suitable and preferred vehicle to carry out the mission.

Neither Pioneer nor A-IMP can achieve polar orbit from an equatorial orbit. The new Pioneer, with the added engine, can, from mid-course, choose a polar orbit, then deboost. However, if either of these be carried (within the Apollo Service Module) and launched during mid-course, they may be inserted into polar orbit. Apollo will provide the extreme accuracy of orbit insertion needed, since the moon acts as an amplifier of guidance errors.

Lunar Orbiter has demonstrated lunar orbiting capability on its own, polar or equatorial. A proposal has been put forward recently to launch Lunar Orbiter also by Apollo Service Module which can be done with minor reconfiguration and actually may result in a slightly increased payload capability.

TABLE V-2

SPACECRAFT CHARACTERISTICS

FUNCTION	THESE SPACECRAFTS MUST BE CARRIED BY APOLLO SERVICE MODULE TO ATTAIN ACCURATE LUNAR ORBIT. ANCHORED IMP - (D) Goddard S/C Manager, Prime Cont. Booster: Thrust Augmented Delta (TAD)	PIONEER (VI) ARC S/C MANAGER TRW Systems S/C Prime Cont. Booster: Thrust Aug. Improved Delta	PROPOSED MODIFIED LUNAR ORBITER Launched & Deployed by Apollo Service Module	LUNAR ORBITER, (I-V) Boeing S/C Prime Booster: Atlas-Agena D	APPLICATIONS TECHNOLOGY SATELLITE Booster: Atlas - Agena D / Atlas - Centaur(Prop) Goddard S/C Man., Hughes S/C Prime	MARINER 5 JPL Spacecraft Prime, Exp., NASA Lewis Research Center Booster: Atlas-Agena D	INTEGRATED LUNAR RADIATION PACKAGE REQUIREMENTS
COMMUNICATIONS	PFM/PM, 7 Watt Transmitter, 136.02 MHZ, Command Rec. 148.26 MHZ Sens. -115 DBM., Bit Rate 29.6 Antenna Omni-Directional in Plane of Ecliptic	S Band, 2292mhz telemetry, Chan. 6A & 7A. 2 recvrs on board for commands, 2)110 MHz chans. 6B, 7B. 2 low gain Omni Antennas, & (1) dish high gain; all designed for max. rad. in plane of ecliptic ± 5°. 2 power amps (TWT) 7.7 watts each, either may be selected, either receiver may be selected. PCM/PSK/PM, Data Storing or Real Time Mode can be GND selected, also choice of 512, 256, 64, 16, 8 Bits/Sec.	A Reconfigured Lunar Orbiter will fit in Sector one of the Apollo Service Module. It is expected to be Deployed from the ASM during Mid-course, Thence to attain Polar Orbit, independently. The capabilities of the Orbiters are retained.	50 BPS for performance TEL, 400 MW XMTR, using Omni-Direct, Antenna (Lo Gain). Beamwidth ± 60° About x-z Plane (Earth-Moon). Second Antenna Dish Type for video, 10° solid angle, 10 Watt Xmtr. Ant. Steerable About Boom Axis only (Y) in 1° increments, L.O.S. Moves in Xz Plane. Video: 250Kc BW. Removing Photo subsystem & redundant measurements yields 304 Bits available for science experiments, & still fit within L.O. standard frame.	(4) 2 Watt Transmitters, which includes 2 for science exp., and 2 for house-keeping. In addition, S/C acts as a re-peater for microwave signals, and trans-mits TV pictures generated on board. S/C also relays voice communications at 135.6 MHz.	Dual Transmitters, single receiver, telemetry and command subsystems, High & Low Gain on Antennas. 10.5 Watt TWT, 6.5 Watt, Xmtrs. Bit rate 33 1/3, and 8 1/3. S Band for telemetry	Estimate between 1.25 & 200 BPS (3 Exp.) error rate 10^{-4}, must use Apollo Frequencies, (S Band). Data format, Command Formats to be de-termined. γ-Ray Experiment 3 KB/SEC (Real Time Transmission) supplementary Bits not included. See Experiments Re-quirements Table.
PROPULSION - ORBIT CHANGE CAPABILITY	Will Allow: Inclination To Be Changed By 34°, Apolune To Be Changed To ∞, Inclination & Apolune To Be Relatively Selected Between Mentioned Limiting Values, Once.	None at present. Proposed system has unlimited restart capability. This will allow incremental variation of incl. from 0 - 34°, incr. var. of Apolune from circu-lar to ∞, incremental variations of above within limiting values above.	See L.O. 1-5	1000 Meters/Sec total ΔV Capability. Restart Capability. Propellant is used for cis-lunar Mid-Course corrections, Deboosting into Lunar Orbit, and various orbit inclination, and phasing changes. 100LB Thrust Engine, 700 Secs operation total, approx. This capability sufficient to transfer from equatorial orbit to 35° inclination only, at Moon.	6250 LB Thrust Motor to transfer from Elliptical to circular orbit, altitude 23000 miles, Earth.	50.7 LB Engine for Mid-Course corrections. (June "67)	Capability required for Polar Orbit. Near Circular Orbit preferable, Perilune approx. 50 Km, at Lunar locations to be determined. Orbital changes other than inclination may be desired.
PRIME POWER	S/C Normal Load 2.2 AMPS At 18.3 Volts. Average Power of Array 50 Watts. Has an 11 AH Battery.	Total to S/C 51-60 Watts, 30 Watts of this is for TWT. 24 to 33 Volts. Has a 2 AH Battery, switched on Bus by GND Command.	See L.O. 1-5	26.6 to 31 Volts, on Solar Cells. 22 to 27 on standby battery, 12 AH. Depth of Discharge must not exceed 40%. Array Delivers AVG of 300 Watts to present S/C System. Orbit Sun/Shadow Ratio must be ≈ 4:1 or larger.	185 Watts on Solar Cells and Batteries. Cells located around sides of 56 in. Dia Cyl.	370 Watts on Solar Cells & Batteries.	N.A.
POWER ALLOTTED TO EXPERIMENTS	6.7 Watts, Peak, Initially 4.3 Watts, AVG, End of Life	9 to 18 Watts	See L.O. 1-5	100 Watts	Data Unavailable.	90 Watts	46 to 64 Watts approx. (Extra required for Encoder, conditioning and Xmtr.)
ATTITUDE STABILIZATION & CONTROL	Spin Stabilized, 20 RPM. Uses 2 Digital Sun Sensors Plus 3 Moon-Earth Telescopes to Generate Data. Analyzed on GND, Fixes Spin Axis in Space.	Nitrogen Jets, 4 sun sensors to Orient Spin Stabilized Probe, 60 RPM, Spacecraft- Sun Line, 90° ± 2°, Must also be 90° ± 2° S/C - Earth Line for Dish Ant. Attitude corrections are not required once stabilized, except for Perturbations (Rad. Press) (Possible). 1 jet, 1 Nitrogen Bottle Req. 1 Yr. Life.	See L.O. 1-5	Locks on Sun in Pitch &Yaw using sun senosrs, stabilizes in roll by sensing Canopus. 3 Axis Gyro stabilized (IRU) when sun or Canopus not visible. Attitude Oriented to point down over target ± 0.2° of local vertical. Has power cap, for 3 Axis Maneuver every 1/2 hour, 30 days, or Low Activity for 11 mos. Orbiter Team has demonstrated capability in finding & using other celestial sources for references in space over a year.	Spin stabilized at 100 RPM. Redundant Gas Subsystems for attitude control. Spin Axis wobble measured to 0.001°, Damping employed to remove wobble.	Redundant 6 Nitrogen Gas Jets, 3 Gyros, Canopus Tracker, 2 Sun Sensors, Earth Sensor, Planet Sensor.	Capability of changing attitude ± 90° frequently is required. Mission lifetime minimum, 90 days, maybe as long as 1 year.
COMMAND CAPABILITY	10 Commands, 2 are used for XMTR on-off. The remainder are concerned with Flight Hardware (Dynamics)	57 Commands. Has 2 Decoders, Command Message 23 Bit Word.	See L.O. 1-5	Command Word 26 Bits Long. Flight Programmer (or computer) can store 128 words (21 Bits Each). Reserved for telemetry, 8-20 Bit word storage. Computer can issue 120 commands. Photo Sub-System takes 27 commands, at 20 Bits each from storage. 6 other operational codes are available, at 15 commands/code.	Command Capability Extensive	Number of Commands not available. Has on board computer and programmer.	On-off, calibrate, for Each experi-ment. Tel. Mode Real Time or Stored, Format Selection; typical. Assume 20 commands total.
WEIGHT, VOLUME AVAILABLE	Total S/C, 130 LBS [(IMP-F, 163LBS) Experiment, 50LBS (51 LBS Exp.)]	Total S/C, 140 Lbs Experiments, 35 Lbs.	See L.O. 1-5	Total S/C, 850 LBS Photo Subsystem 150 LBS, when removed, will yield experiment space of 30" x 30" x 20" High Approx.	Total S/C 1550 LBS	Total S/C 540LBS	56 LBS for Exp, +51 LBS Tape Rec. for "Minimal" Exp, 220 LBS Exp. + 77 LBS for Recorder for "Max" experiment. Extra requ'd for En-coder, Xmtr.
ANTENNA	See "Communications" Above	See "Communications" Above	See L.O. 1-5	(1) Low Gain Omni, (1) High Gain Dish 10° Solid Angle.	Phased Array experiment ant, 8 whip antennas on top, 8 VHF Phased Array Ant. on bottom. Electronically Despun antenna yields 10 times normal effective radiated power.	High Gain Ellipse, and Low Gain Omni-Directional, Plus UHF Dipole Array.	Parabolic maybe required for High Bit Rates at Lunar Distance, Omni for "Off Attitude" and Low Bit Rates.
ON BOARD DATA STORAGE	In the Encoder Module: (3) 16 Bit Accumulators, (1) 12 Bit Accumulator, (4) 20 Bit ACC., (2) 24 Bit ACC.	15,232 Bits. Readout is Destructive, & cannot be interrupted. Register must be cleared before new Read-in is begun.	See L.O. 1-5	See Flight Programmer Above	No Data Available	Tape Recorder	Tape recorder may be required for periods when Earth is occulted, or when tracking station coverage is not 24 hours long, or RF Link is off.
TYPICAL EXPERIMENTS	7 Active: Ionizing Radiation, or Lo-Energy Electron/Proton Fluxes & Monitoring Cosmic Ray Events; Thermal Ion Plasmas; Distribution of > 40KEV Elect; Meas. of Plasma Flow; Magnetometers (2);	Pioneer VI (2) CR DET, (2) Plasma Detectors, (1) Magnetometer, (1) Radio Propagation (Passive)	NONE	None. Spacecraft designed to carry a 150LB Photographic Subsystem.	Supra-Thermal ion detector, magneto-meter, Omni-Directional Electron-Proton Detector, Multi-Element Particle Telescope, Electron Magnetic Deflection Spectrometer.	UV Photometry, trapped radiation, Magnetic Field, Solar Plasma, Dual Frequency Propagation Experiment, 423.3 & 49.8 MHz.	(1) γ-Ray, (1) X-Ray, (1) Neutron, (1) α/p/CR (1) IR (1) Mass Spectrometer.
LIFETIME	1 Year	1 Year	1 Year, Moderate Use of Nitrogen.	1 Year, with moderate use of Propellants.	3 Years	6 Months +	1 Year Desirable
TEMPERATURE CONTROL	———	57°-105°F (Spacecraft never in Shadow)	To Be Determined	Passive, Experiments are protected, Temp. Range + 100° F to -12° F.	———	Thermal Louvers, Deployable Sunshade, insulation, Paint Patterns.	Varies with experiment requirements. Exact figure to be determined.

6.0 FLIGHT REQUIREMENTS, SPACECRAFT ATTITUDE AND ORBITAL PARAMETERS

6.1 Basic Plan of the Experiment

As shown in Figures 6-1 and 6-2, the basic experiment configuration involves one group of detectors mounted within the body of the spacecraft with a view of the surface, and other instruments mounted on a boom, away from the spacecraft. Assuming that the detector is nominally pointed down, the instantaneous view area on the moon is a function of the detector field of view and the altitude of the spacecraft above the lunar surface as is shown in Figure 6-3. By instantaneous view area is meant the area of moon from which radiation can reach the detector. Another relevant factor is the time for the detector to traverse the view area. In a near-moon orbit, the orbital velocity will be about 1.7 km/sec; thus, in 30 seconds, the detectors will sweep out a swath of the moon's surface of 50 km length. This is comparable to the diameter of the view area if the satellite is 50 km above the surface for a detector with a $\pm 30^{\circ}$ field of view.

The detectors can be made to view the surface continuously only if the satellite or detector can be made to point toward the center of the moon. In general, the spacecraft axes will be fixed in inertial space and the moon's surface will be viewed only during a portion of the orbit as shown in Figure 6-4 where the area ABCD comprises the fraction of the surface seen during a single pass. During other times, if the spacecraft is in a fixed inertial mode and if the detectors are not pivoted, the detectors will view out into space. From one orbit to the next, different segments of the moon will be viewed because of the rotation of the moon about its axis.

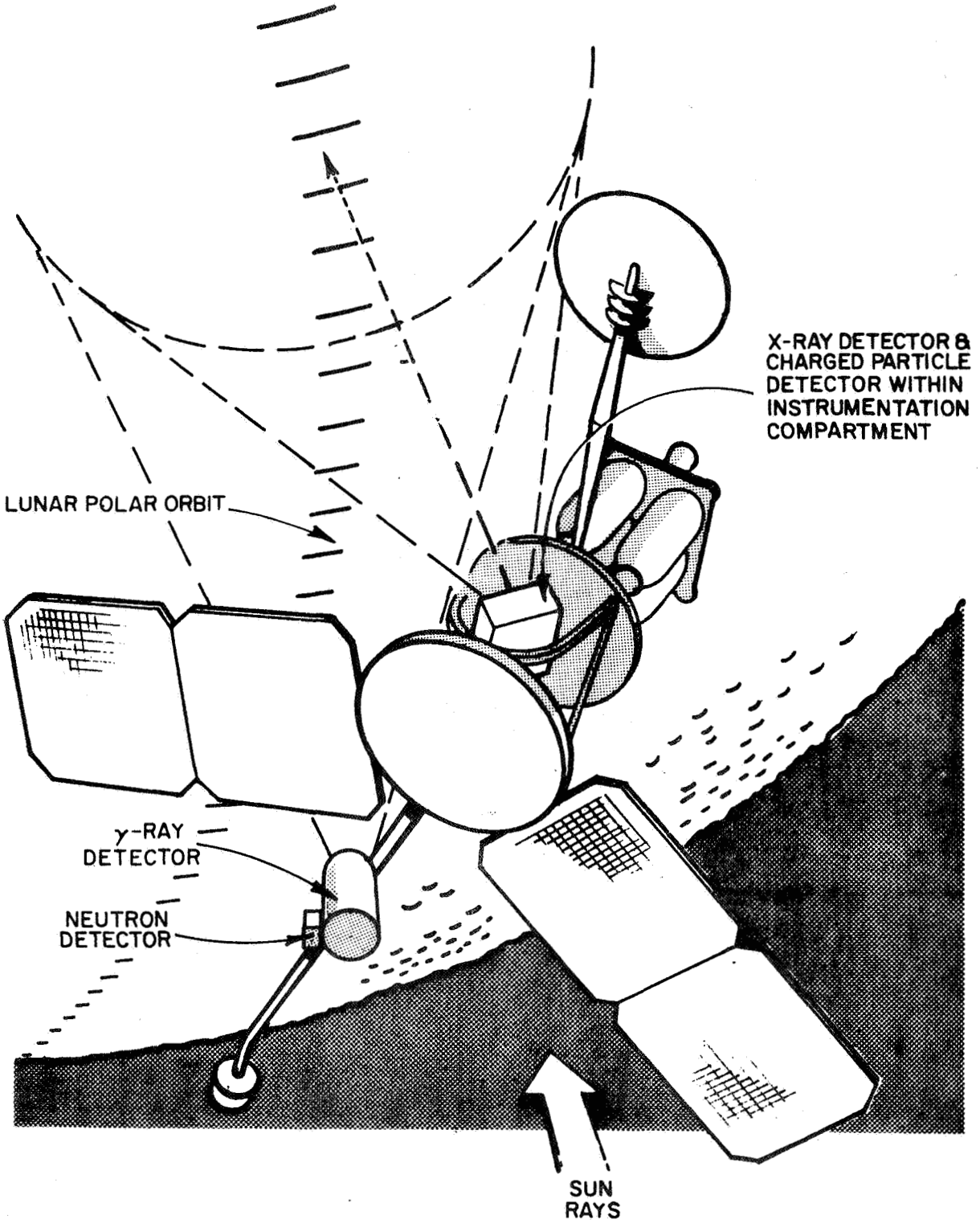

Eigure 6-1 Conceptual View of X-ray Fluorescence Data Sensing from Orbiting Satellite

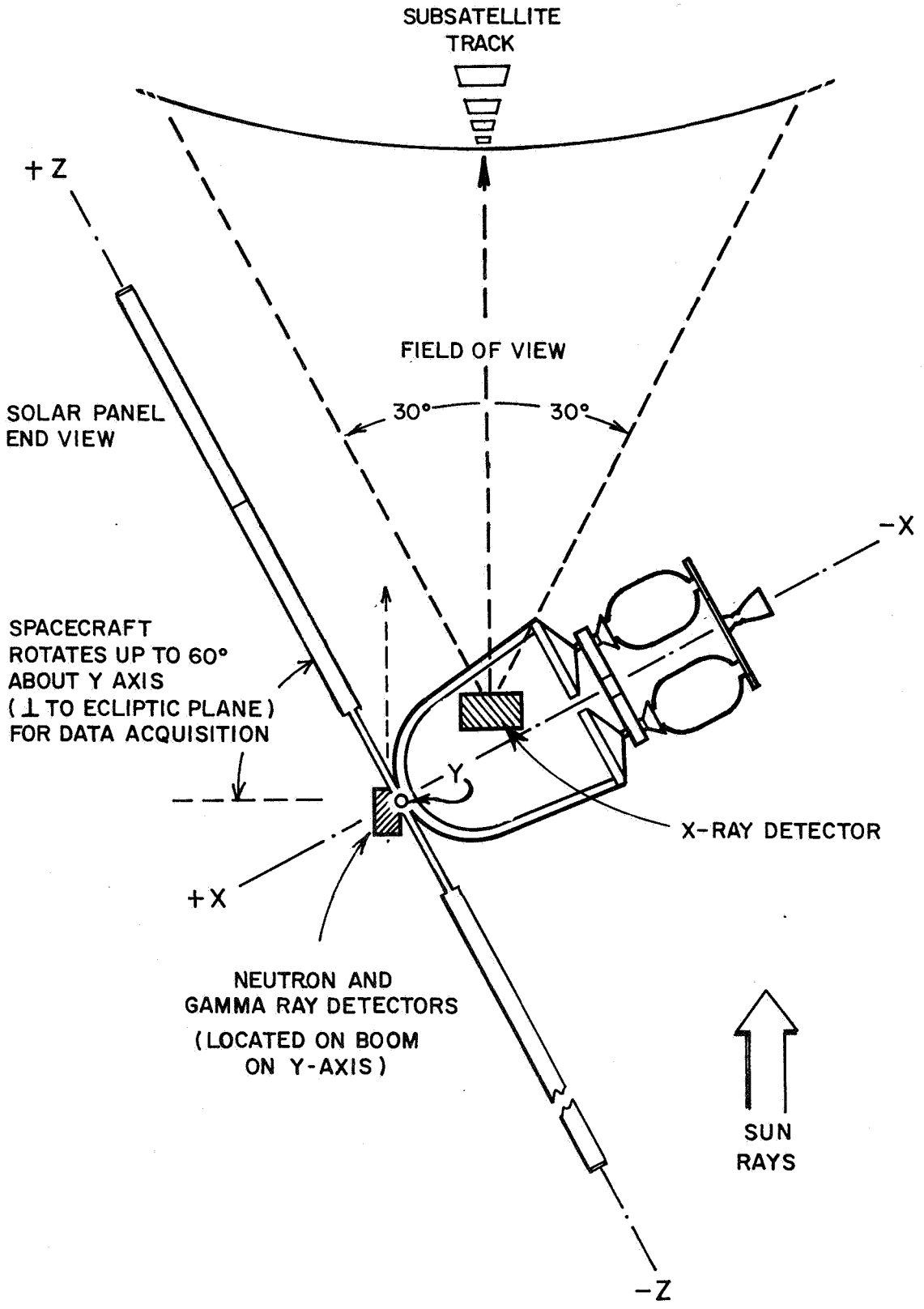

Figure 6-2 Plan View of Orbiting Satellite

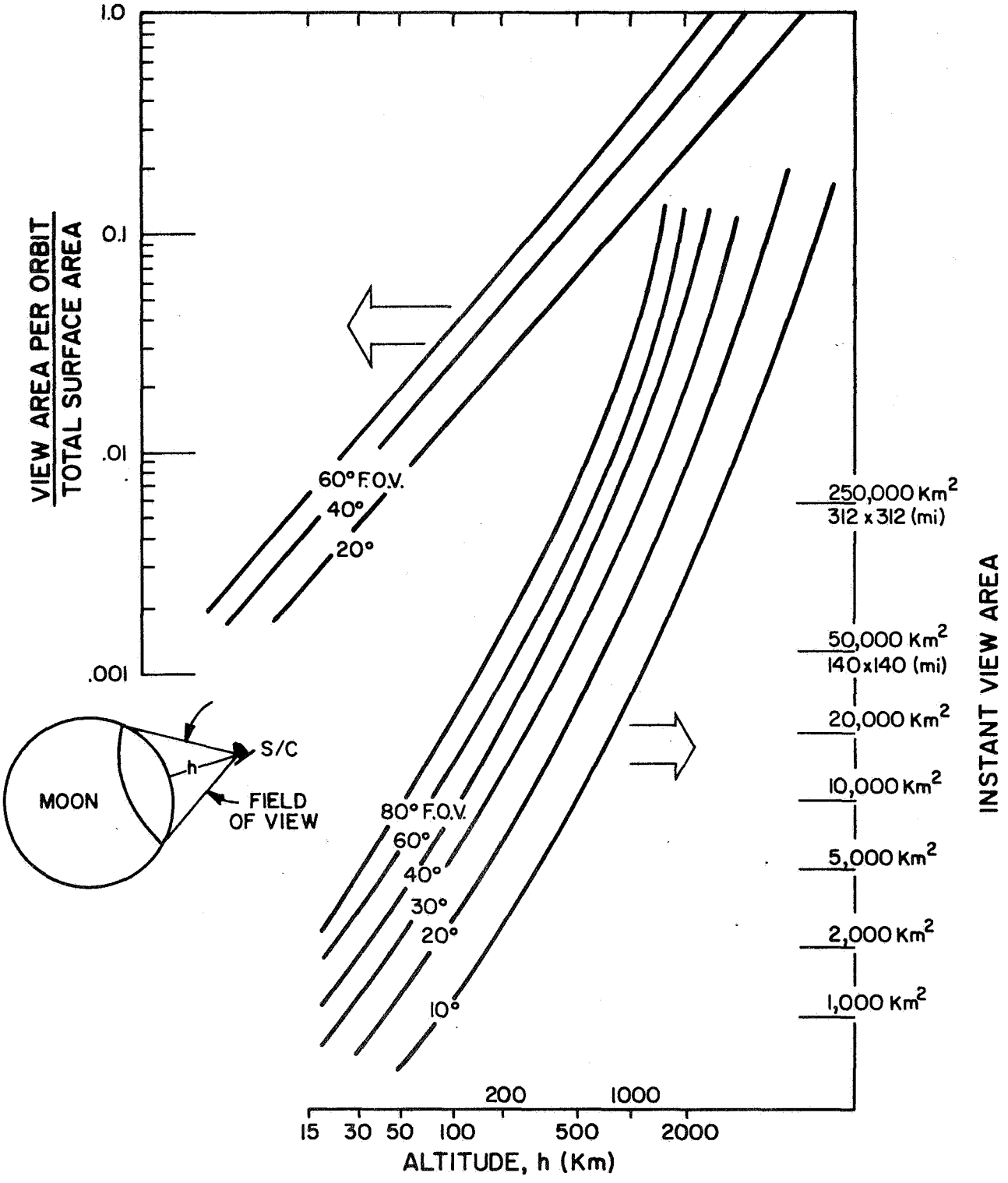

Figure 6-3 View Area Parameters

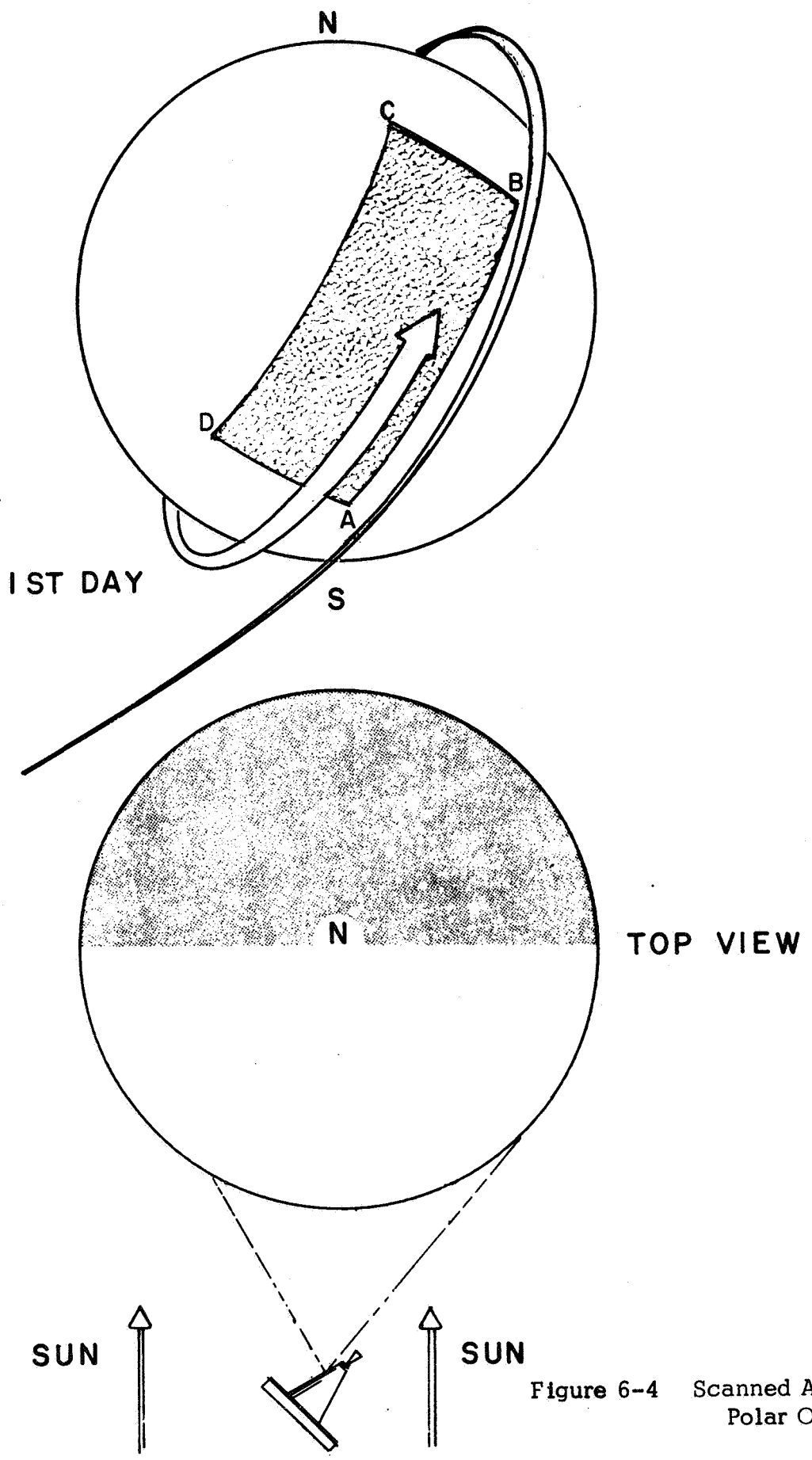

Figure 6-4 Scanned Area for Equator-Polar Orbit

6.2 Spacecraft Stabilization Modes

Three kinds of stabilization modes of the spacecraft can be identified; namely,

(1) Spin stabilized, in which the vehicle spins around the principal axis of interia. In the vicinity of the moon, perturbing torques should be virtually negligible (only gravity-gradient torques and solar pressure effects are present). Both Pioneer and IMP are spin-stabilized. The spin axis which is fixed in inertial space, can be reoriented by use of gas jets, as is the case with Pioneer.

(2) Inertially or quasi-inertially stabilized, in which the vehicle is fixed in space by use of an active control system. In order to be capable of performing guidance maneuvers, a vehicle must have such a stabilization system. The system need not be truly inertial (i.e., with respect to the stars), but, as is the case with Lunar Orbiter, may have one axis fixed on the sun (quasi-inertial). In the latter case the vehicle makes one full rotation around the axis normal to the ecliptic plane during a year, corresponding to the motion of the earth's in its orbit around the sun.

(3) Moon Oriented, in which one axis is directed toward the center of the moon at all times. Such a system, which does not exist on any of the available spacecraft, would require either a gravity-gradient control system or an active control system that utilized sensors that could generate orientation signals off the moon's limb.

6.3 Detector Orientation

The basic consideration in detector orientation is that the detectors be mounted on the spacecraft so that they view the lunar surface for a significant fraction of the total time available for the mission.

In the case of the moon-oriented spacecraft stabilization mode, the detectors could view the moon continuosly. In the sun-oriented mode the situation is more complex, and the fraction of time on the moon depends on the orientation of the orbit plane with respect to the moon and to the sun. In order to be specific, we consider first the sun-oriented mode, as is the principal means of stabilization of the Lunar Orbiter. The amount of the surface swept out per orbit is as described in Section 6-1. This is shown again in Figure 6-5, which shows a sun-oriented satellite at various points in its orbit around the moon, with the sun-line along the X-axis. The detectors are presumed to be perpendicular to the solar direction. During approximately half the orbit the detectors view the surface; however, in principle, the spacecraft could perform a roll maneuver around the X-axis, still preserving the sun-orientation and view the remaining half of the moon. In this case, the equatorial regions of the moon are viewed at glancing angles. This particular stabilized mode, without any attitude changes, results in very poor coverage of the equatorial regions.

6.4 Orbital Effects

6.4.1 Lunar Rotation

Ignoring precessional effects, the orbital plane of the spacecraft is fixed in inertial space; thus, since the moon rotates in inertial space with a 27 day period, the moon will rotate within the orbit by about 13°/day or about 1.9°/orbit. What this means is, simply, that from one orbit to the next, the moon will move by 1.9° beneath the spacecraft. For example, in Figure 6-4, the area ABCD will displace by 1.9° around the moon. Since the angular width of ABCD is much greater than 1.9°, a large number of orbits or even several days is required before an entirely new piece of the moon is in view. Thus, the lunar rotation

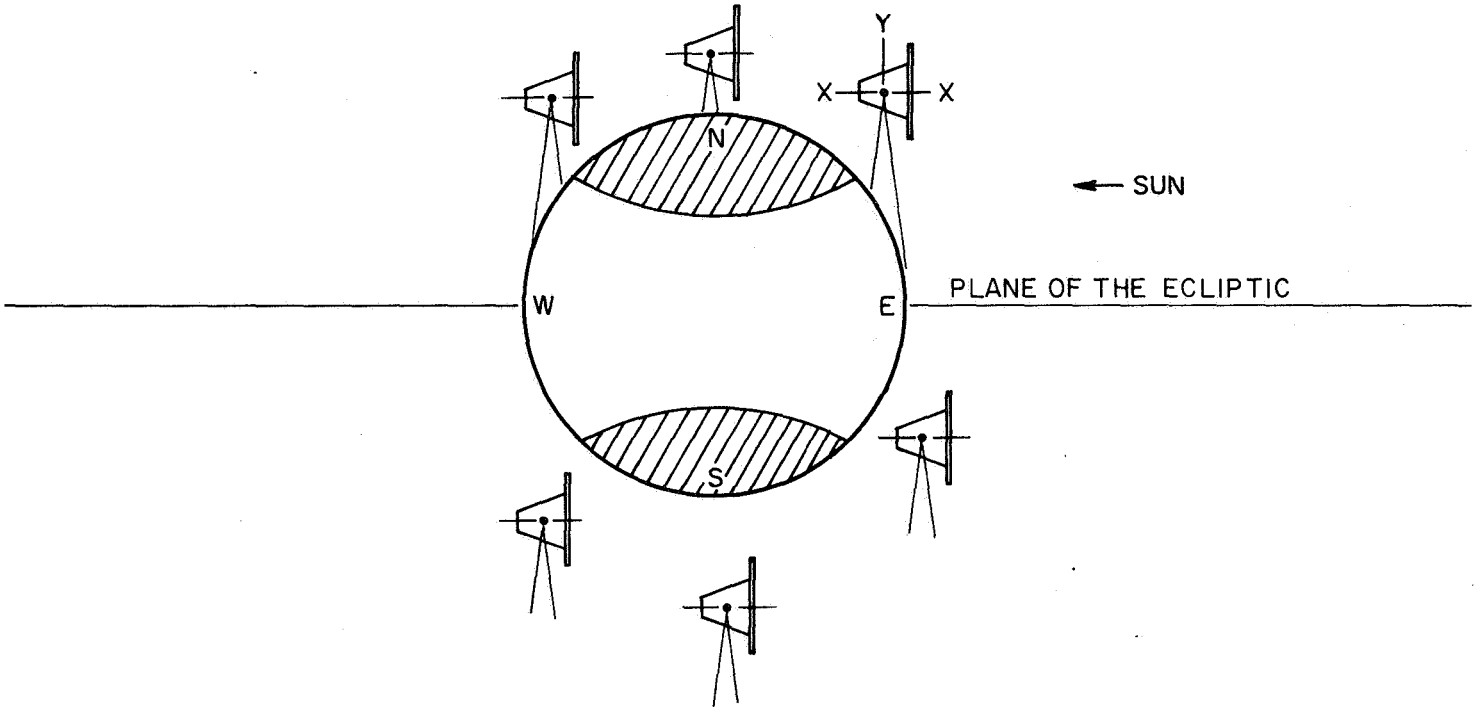

Figure 6-5 Scanning of Polar Regions with Detector Axes Fixed in Perpendicular Orientation to Solar Direction.

Note: Areas that receive best coverage are shaded

provides a means of viewing the entire lunar surface even though a small fraction of the moon is viewed per orbit. This is shown in Figure 6-6, where a polar orbit around the moon is considered. During the month the point X on the lunar surface will make one rotation within the orbit plane and will be directly below the spacecraft twice during the month.

6.4.2 Changes During the Year

During the year, a sun-oriented satellite will make one full rotation in inertial space as shown in Figure 6-7. The orbital plane on the other hand is fixed in space. The effect of this can be seen in Figure 6-6 if one imagines the sun carried around the earth. The moon-orbiting spacecraft will rotate with respect to the orbital path as this happens. Depending on how the detectors are mounted in the spacecraft, during certain times of the year, different portions of the moon can be viewed with maximum efficiency. For example, in discussing Figure 6-5, it was noted that for the configuration shown the polar regions were viewed with high efficiency (near normal incidence) and the equatorial regions with low efficiency (glancing angles of incidence). Three months later, however, the situation will reverse itself.

6.4.3 Effect of Orbit Inclination

In Figures 6-5 and 6-6, the spacecraft was taken to be in a near polar orbit around the moon (inclination close to 90°). For low-inclination orbits the effects related to the lunar month and the earth year are similar. There is one important difference between low and high inclination orbits; namely, the total fraction of the lunar surface that can be observed. For a polar orbit, it is possible to view the entire lunar surface at one time or another. For a low-inclination orbit, only

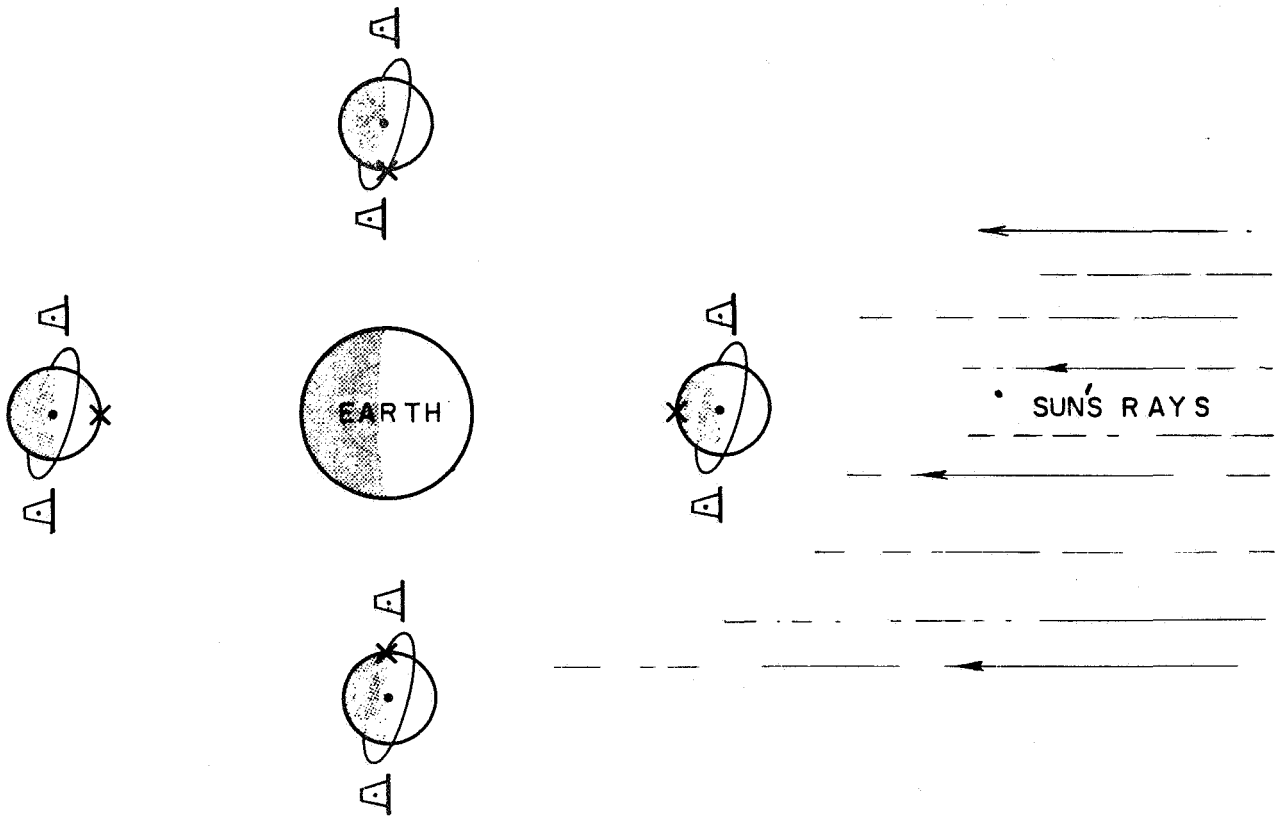

Figure 6-6 View Looking Down on Pole
(one lunar month)

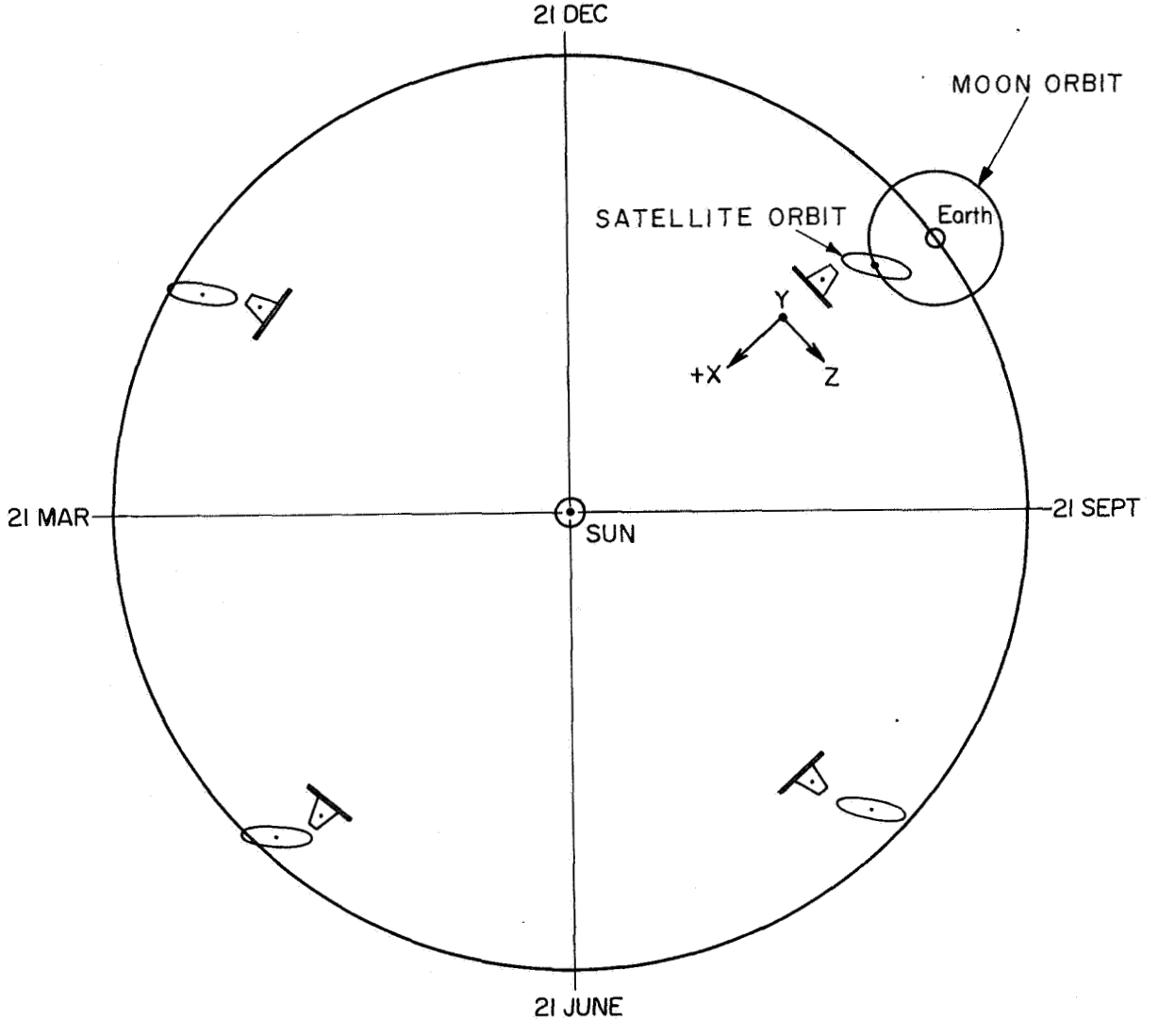

Figure 6-7 Satellite and Orbital Relationships Over Solar Year

a band, centered on the lunar equator, will be viewed. The choice of orbit inclination depends very much on the mission objectives and other parameters relating to the mission. For example, only certain spacecraft can be placed into a near-polar-orbit around the moon.

In general it would be desirable to place the satellite, carrying the integrated experiment package, into a polar orbit. Such an orbit makes the entire lunar surface accessible for observation.

During a short-duration mission (approx. one month) a low-inclination orbit might be desirable since the maximum time is spent on or near the equator and will include the lunar landing sites. During a longer mission, the high-inclination orbits would be desirable. For a given mission, assuming the total observational time is fixed, the time per unit area of the moon will be inversely proportional to the inclination. Smaller inclination results in less area of the moon sensed in the same total time than a high-inclination, and a correspondingly large amount of observing time per unit area. Thus, depending on the sensitivity of the individual experiments, it might be desirable to have a low-inclination orbit in order to maximize the information on a small fraction of the lunar surface.

6.4.4 Methods of Increasing Moon-Viewing Time

Clearly, using fixed detectors on a sun-oriented spacecraft, less than half the available mission time is actually spent in gathering data. Several means of overcoming this deficiency exist. One is to continuously reorient the spacecraft to maintain the detector near normal to the lunar surface. This could be done on a programmed basis, rather than relying on a moon sensor. The principal disadvantages are the fuel requirements for such extensive maneuverings, and the fact that less time is spent on the sun with a subsequent loss of power.

Another technique is to mount the detectors on a pivotable platform which could be continuously reoriented to point down toward the surface. This introduces certain mechanical complications but does allow for normal sun acquisition. It is not likely that either technique would allow an increase of viewing time to 100% but a substantial improvement over the simple fixed orientation case could be achieved.

6.5 Sun Inclination

The principal impact of the sun inclination is on the spacecraft power subsystem. The Lunar Orbiter nominally requires a 4 : 1 sun/shadow ratio which, in the case of a near-moon orbit, can be achieved only if the spacecraft is in a polar orbit during certain times of the year (See Figure 6-6); namely when the orbit plane intersects the terminator. However, this is an unfavorable operation with respect to the experiment since the view area simultaneously contains both sunlit and shadowed portions of the moon. Since the background in several experiments is a function of the solar illumination, data obtained during such an orientation may be difficult to interpret. In general, only 1 : 1 sun/shadow can be achieved. If the spacecraft attitude is changed during the orbit to keep the detectors moon-oriented this ratio is reduced even further to about 0.64 : 1; however, the solar paddles would be set to optimize the input power for a given mission. In a near-moon orbit, there is no means to avoid an unfavorable sun/shadow ratio. There are means of conserving power; for example, turning off the experiments during unfavorable viewing times.

At least one experiment, the X-ray fluorescence observations, requires near-normal incidence and detection of X-rays for maximum data. It is possible, by choosing the time of launch, that favorable sun angles are achieved for certain times and for certain regions of the moon.

6.6 Other Orientation Considerations

The low gain antenna boom points along the line of sight of the Canopus sensor (approximately). The antenna is designed to have maximum radiation in the X-Z plane, so that the earth is in view at all times (ignoring occulting by the moon). The Z axis is the photographic viewing axis (Orbiter I - V, Figure 6-2). Neutron radiation sensing equipment must be along the Y axis. The antenna need not be relocated.

It is not certain at this time whether the parabolic antenna, of the Lunar Orbiter will be needed. If not, the gamma-ray experiment may be mounted on the boom in its place, instead of on the low gain antennas as shown. The configuration will be arranged to keep the center of gravity along the central axis.

When the Lunar Orbiter is torqued to remain on the Sun during the year, the Canopus reference is lost (Canopus being 15^{o} off normal to Ecliptic Plane). The craft is then stabilized by use of its inertial reference unit in a limit cycle mode ($\pm 10^{o}$). The field of view of the Canopus sensor is such that the star reference is available for approximately 30 days, only. The reference unit will have to be updated at intervals. This can be done either by the use of the narrow beam of the parabolic antenna or by acquiring another celestial reference (such as Jupiter). Both methods have been used successfully by the Lunar Orbiter team at Goldstone.

In the existing Lunar Orbiter configuration enough fuel is carried for moderate two-axis maneuvering for one year (drifting is allowed about the roll axis.) Three-axis control is sufficient for only a fraction of a year. Two-axis control uses 0.01 lb nitrogen per day. A maintained three-axis reference uses 0.03 lb per day. For each

commanded maneuver, nitrogen consumption is 0.02 lb in roll, 0.01 in pitch, and 0.01 in yaw. Expenditure of gas, and therefore spacecraft lifetime, is very dependent upon the mission plan. Previous Lunar Orbiters carried a 10.5 lb supply of nitrogen for attitude maneuvers.

6.7 Data Handling System

As discussed in Section 5.1 the experiments require about 125 BPS, although this can probably be reduced to below 100 BPS by using some appropriate data compression techniques. Depending on the mission, it might be advantageous to consider the use of a tape recorder. As an example, it would seem feasible to dump 2×10^6 bits into the Goldstone tracking facility at a rate of about 500 BPS for 65 minutes. That many bits constitutes about 5 hours of viewing time on the moon. The advantage of the tape recorder is that it allows accumulation and transmission of data obtained during the time that the spacecraft is on the far-side of the moon and out of direct radio contact with the Earth. The other advantage is that it reduces the total listening time at the tracking facility.

Other data system parameters must be considered and analyzed. As the study proceeds and the mission fundamentals crystallize, numerical values will be added. These parameters are tabulated in Table VI-1.

TABLE VI-1

Data System Parameters

System Performance Reqmnts. or Standards	System Design Specification
a. range 239,000 Stat. Mi.	1. Transmitter freq. Apollo downlink JPL
b. capacity	2. Trans. power
c. error bit rate 10^{-3}	3. antenna gain, coverage
d. reliability	4. modulation method, deviation, subcarrier frequencies
e. interference	5. noise figure
f. accuracy of measurements	6. peak pulse amplitude
g. quantizing error	7. bandwidth
h. analog data: SNR, peak value accuracy, harmonic distortion, time correlation, mean square error	8. telemetry format 9. ground station characteristics, antenna gain, noise temp.
i. data baseband, bit rates	10. number of formats, ground commandable
j. analog data spectral characteristics	
k. sampling rate requirement (aliasing, etc.)	
l. simultaneity requirements	
m. data storage requirement	

7.0 CONCLUSIONS AND RECOMMENDATIONS

7.1 Overall Program Conclusions

The principal conclusion of this study is that remote sensing of the moon by an orbiting integrated experiment package, consisting of at least a gamma, x-ray, charged particles, and neutron experiments, can produce significant results. The expected performance of modest detectors deployed aboard lunar orbiting vehicles that are similar to spacecraft that have already been used, would result in a geochemical mapping of the moon with a spatial resolution that is equal to the orbital altitude.

It is useful to consider what sequence of missions might evolve from this program, given this general capability of geochemical mapping and the scientific interests of the various groups. The scientific objectives can be restated as follows.

1. Geochemical map of the surface with a certain spatial resolution. The abundant light elements can be detected by the x-ray fluorescence technique, and the natural radioactive elements by gamma ray and alpha particle spectroscopy. Other techniques are sensitive to different aspects of the composition.

2. Study of transient phenomena. Certain phenomena, such as gas releases, are known to occur with short time periods. The composition of the material comprising these phenomena must be of great significance in interpreting the phenomena.

3. Detailed study of small regions. Certain regions of the moon appear to be of high intrinsic interest. It should be possible during certain missions, to devote a sizeable fraction of the observational time to a detailed study of those regions.

A sequence of missions intended to carry out these objectives in an orderly and logical sequence, could comprise the following:

a) Initial Mission. This would be the first of the series, and its basic configuration would be as described in this report. Aside from gathering whatever useful geochemical information was possible, this mission is needed to get precise information on the background and a measure of efficacy of the several observational techniques to obtain abundance data.

b) Intermediate Mission. Depending on the degree of success and sophistication of the initial mission, this mission would extend measurements of the first by the use of different orbits, different configurations of detectors, etc.

c) Ultimate Mission. It would be presumed that the early missions have derived sufficient information to permit detailed geochemical experiments. The ultimate mission would be capable of the highest spatial and spectral resolution possible with existing spacecraft systems. It might also be required to provide monitoring of certain regions known to be the sites of transient phenomena, and it also might be necessary to point at selected regions in order to permit detailed studies to be carried out.

d) Extension to Other Planets. The geochemical sensing techniques and the spacecraft systems developed here could have a direct application to other planets, although the presence of a gaseous atmosphere limits the attainable information. In the case of Venus, information could be obtained only about its atmosphere. For Mars, on the other hand, the gamma rays from the surface would penetrate the very thin atmosphere of that object. The atmosphere of Jupiter, although thick, may be chemically differentiated as is indicated by the striking color differences. Jupiter, however, may have a very high radiation level caused by a trapped particle belt.

The interest generated in these kinds of investigations will depend very much on the success of the early missions. It may be, for example, that virtually no chemical differences occur over the moon's surface, in which case very sophisticated advanced missions would not appear attractive.

On the other hand, it is entirely possible that advances in detector technology and other circumstances may combine to make these measurements sensitive to small chemical differences of great significance.

7.2 Definitions of Areas of Work

If it is accepted that a future goal is a geochemical survey of the lunar surface using a cluster of instruments in a moon-orbiting vehicle, then we can define a series of activities necessary to the attainment of that goal. For convenience, we distinguish three different areas of work: namely, Experiment, Integration, System. Ultimately, a hardware phase,which will not be discussed here,is required that entails the development of a flight qualified engineering prototype and subsequent flight unit and backup unit of the experiments integrated with the spacecraft. Preliminary to the design and development of flight hardware a number of phases can be identified which lead to detailed scientific and engineering specifications and other required documents for the program. In the three above-named areas the work entails:

1. Experiment

a) Realistic estimates of counting rates and background based on the most reasonable assumptions regarding the lunar environment. Use must be made of experimental data where it exists. Laboratory simulations can be made to yield certain relevant data.

b) Estimates must be made of the precision with which chemical abundances can be determined, based on assumptions of detector size, viewing time, etc. This study established trade-off parameters necessary to achieve a proper balance between the several instruments.

c) Laboratory simulations of the response of the detectors in the lunar environment must be performed in order to verify, as nearly as possible, the results of (a) and (b).

d) Detectors must be studied to establish their exact capabilities, to specify operating characteristics, and to make improvements where that is necessary or possible.

e) Analytical techniques must be established to handle observational data.

2. Integration

a) Establish which are the most relevant lunar element abundances to be determined and set guidelines for choosing detection of those elements.

b) Study theoretical aspects of certain lunar phenomena, such as "gardening" by meteoritic impact and diffusion of radioactive gases.

c) Determine what background radiation must be measured and specify group of detectors to determine that background.

d) Study the interrelationships between the data from the various detectors, how chemical abundances might be determined from data given by two or more detectors, how the data from one might provide information on the background of another, etc.

e) Study the relationship to other lunar research and suggest possible areas of investigation which might aid in the interpretation of the data.

f) Identify common elements of hardware between the several instruments.

g) Establish the requirements on the mission.

3. System

a) Establish the basic geometry and configuration of the spacecraft: the view angles and fields of view of the instruments, placement on the spacecraft, and the basic attitude control requirements.

b) Specify a common electronic hardware subsystem needed by the scientific instruments.

c) Specify weight, power and volume of the experiments.

d) Identify and specify the necessary spacecraft subsystems: power, communications, command attitude control, propulsion, etc.

e) Perform trade-off studies on the various spacecraft and mission characteristics; i.e., effect various modes of attitude control on return data.

7.3 Recommendations for Future Work

The present study has covered a number of these items in varying degrees of detail. For a next phase we recommend that work continue along the following lines:

1. Experiments Area. More complete simulation of the observations, both by the use of computers and by laboratory studies. It will be necessary to use breadboard or prototype detectors. These studies are best performed by the individual experimenter who will be ultimately responsible for conducting the separate measurements of neutrons, x-rays, gamma-rays, etc. It will be necessary to maintain close liaison between the individual experiments

2. Integration and Systems Area. This work must necessarily lag somewhat behind the definition phase concerning the experiments. The emphasis at the present time must be the designation of trade-off parameters regarding the individual instruments, the mission parameters and the basic observational requirements. This work, at least initially, must be performed in close collaboration with the experimenters.

If priorities are to be assigned it is clear that emphasis should be placed on work in the experiments area and in that portion of the integration involving interrelationships between experiments. However, it is also important that a decision be made at the earliest possible moment on the spacecraft to be assigned to the program and what constraints may exist on the mission itself.

The primary experimental areas in which the group at AS&E has been traditionally interested are the x-ray and the alpha observations. For the x-ray experiment it is felt that simulation studies using computers and selected laboratory results could yield much of the information necessary to fully define the instruments. The ultimate need is for laboratory measurements with simulated solar x-rays and cosmic ray beams to clarify the actual

performance. For the alpha experiment a prototype consisting of a matrix of silicon barrier charged particle detectors should be constructed and evaluated in a high energy proton background environment. Unfortunately, not much can be done in the laboratory to predict the effectiveness of the radon diffusion process on the moon. Too little is known about the lunar porosity and the gaseous diffusion rates through soil samples in the ultra high vacuum. It should also be possible to make more detailed trade-off studies. One example is the attitude changing capability of the spacecraft versus the weight of the payload that can be carried. With regard to other detectors, prototypes should be constructed for the various experiments and tested under as close to actual conditions as possible. For the gamma ray and neutron experiments, which would be performed by other groups of experimenters, this means measurements at a medium energy proton accelerator such as the NASA 600 MeV synchro-cyclotron with irradiated rock samples. Only a very small intensity is needed so that evaluation can be conducted as a "parasite" experiment. However, great care is needed in simulating the space environment and the experiment geometry.

REFERENCES

1. Luna Science and Exploration, 1967 Summer Study, Santa Cruz, Cal. July 31 - Aug. 13. Directed by W. N. Hess. NASA SP-157

2. NASA 1965 Summer Conference on Lunar Exploration and Science, Falmouth, Mass. July 19-31. NASA SP-88

3. N. Ness (private communication)

4. R. G. Strom and G. Fielder, "Multiphase Development of the Lunar Crater Tycho," Nature 217, 611 (1968)

5. B. Middlehurst, "An Analysis of Lunar Events," Review of Geophysics 5, 173 (1967)

6. See for example B. Hapke, Science 159, 76 (1968)

7. Surveyor V
   A. Turkevitch, E. Franzgote, and J. H. Patterson. Science, Nov. 3, 1967, 631
   Surveyor VI
   _____. JPL Tech. Rep. 32-1262 Jan. 10, 1968
   Surveyor VII
   (Results have not yet been published but have appeared in the form of publicity releases.)

8. A. P. Vinogradov, Yu. A. Surkov, G. M. Chernov, F. F. Kirnozov, and G. B. Nazarkina, "Gamma Investigation of the Moon and Composition of the Lunar Rocks." 10th meeting of COSPAR, London 1967

9. H. W. Kraner, G. L. Schroeder, G. Davidson, and J. W. Carpenter, Science 152, 1235 (1966)

10. P. F. Gustafson and S. S. Brar The Natural Radiation Environment, p. 499, Ed. by J. A. S. Adams and W. M. Lowder. Rice University Semicentennial Publication, University of Chicago Press, Chicago 1964

11. Fichtel, C. E., D. E. Guss, K. W. Ogilvie Solar Proton Manual, NASA Tech. Rept. TR-R169, 1963

12. W. M. Neupert, W. Gates, M. Swartz, and R. Young, Ap. J. 149, L79 (1967)

13. R. E. Lingenfelter, E. H. Canfield, and W. N. Hess J. G. R. 66, 2665 (1961)

14. A. Turkevitch, K. Knolle, R. A. Emmert, W. A. Anderson, J. H. Patterson, and E. Franzgrote. Rev. Sci. Inst. 37, 1681 (1966)

15. J. I. Trombka "A Numerical Least-Sequence Method for Resolving Complex Pulse Height Spectra" NASA X-641-67-184, April 1967

16. D. B. Hicks, L. Reid, Jr., and L. E. Peterson, "X-Ray Telescope For an Orbiting Solar Observatory" I. E. E. E. Transactions on Nuclear Science 12, 54 (1965)

17. L. E. Peterson, "Gamma Ray Production by Cosmic Rays Observed on OSO-1" USCD-SP-68-1, July 1967

18. P. Gorenstein and S. Mickiewicz "Reduction of Cosmic Background in an X-ray Proportional Counter through Rise Time Discrimination" to be published. Rev. Sci. Instr. June 1968.

19. S. Hayakawa "Albedo Radiation from the Moon and the Planets" Space Research III, W. Priester Ed. North Holland Publishing Co., Amsterdam 1963.

20. A. Turkevich, E. Franzgrote, and J. H. Patterson, JPL Tech Rep. 32-1426, Nov. 1, 1967.

21. G. R. Streeter, " A Completely Portable Battery-Powered Multichannel Analyzer, " submitted to 15th Nuc. Sci. Symp., Montreal, Canada, September 1968

APPENDIX A
SATELLITE ENVIRONMENT

1.0 MICROMETEOROIDS

Certain of the instruments are particularly sensitive to the impact of micrometeorites. Thin filters used in the x-ray experiment can easily be penetrated by small particles. Other detectors utilize aperture windows of thin materials as well. The effect of penetration varies with the detectors. In certain instances, the pinholes caused by meteorite puncture will render the device somewhat sensitive to visible light; in other cases, such as with the gas-filled proportional counters, a single puncture would render the detector inoperable.

Clearly, it will be necessary to make the best possible estimate of micrometeorite flux in order to properly specify minimum thicknesses of various materials. Fortunately, the micrometeorite flux is one of the more intensively studied phenomena relating to outer space, and a broad literature is available on the subject.

The most relevant characteristic of the meteroid flux is the average number as a function of the mass of the meteoroid which is shown in Figure A-1. The figure also demonstrates the range of uncertainties. The plotted curves represent different regions, in the vicinity of the moon (the value of β_2 can be taken to be ~ -1.0).

The other relevant features of the micrometeorite flux are:

1. Distribution of the velocities.
2. Diurnal and annual variations.
3. Lunar "splash" particles.

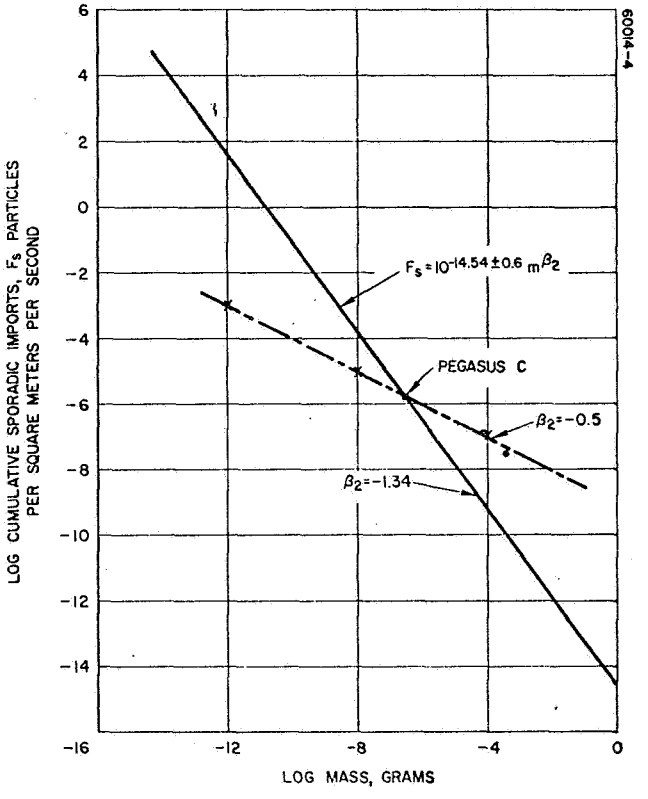

Figure A-1 Variation of Sporadic Meteoroid Flux

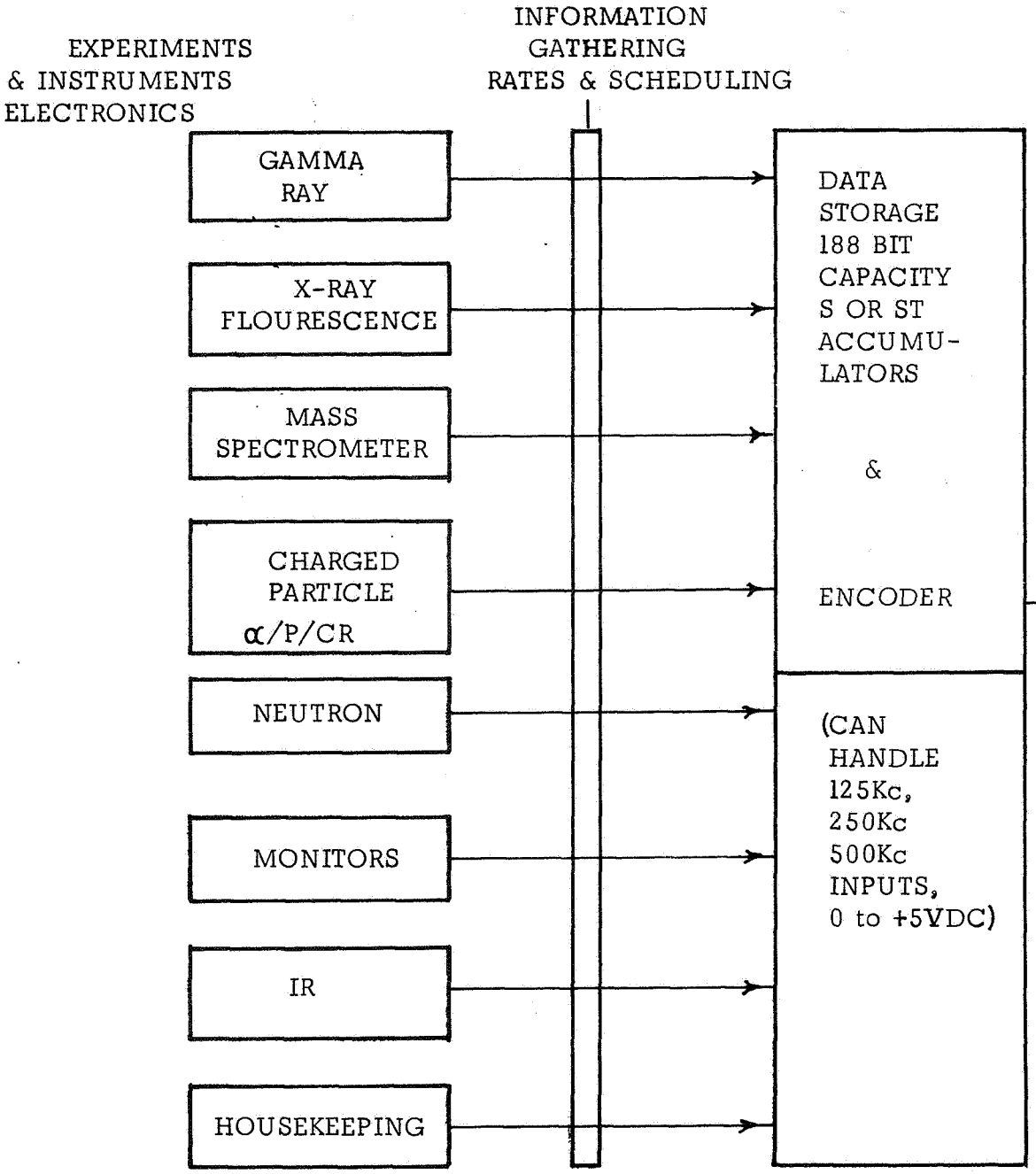

1. BASIC ACCURACY 32 BITS
2. READOUT EVERY 40.96 SECS
3. MINIMUM DEAD TIME 1.28 SECS

ENCODER & BUFFER
STORAGE CAPABILITY
A/IMP

A/IMP STORAGE CAPABILITY
(MODELS D & E)

APPENDIX C

TABLE OF ABUNDANCES

Constituent	Peridotite (ultra-basic rock), %	Basaltic rock (basic rock), %	Inter-mediate rock, %	Granitic rock, %	Crust, %	Shale, %
SiO_2	43.5	48.5	54.5	69.1	58.7	58.1
TiO_2	0.8	1.8	1.5	0.5	1.2	0.7
Al_2O_3	2.	15.5	16.4	14.5	15.	15.4
Fe_2O_3	2.5	2.8	3.3	1.7	2.3	4.
FeO	9.9	8.1	5.2	2.2	5.2	2.5
MnO	0.2	0.17	0.15	0.07	0.12	
MgO	37.	8.6	3.8	1.1	4.9	2.4
CaO	3.	10.7	6.5	2.6	6.7	3.1
Na_2O	0.4	2.3	4.2	3.9	3.1	1.3
K_2O	0.1	0.7	3.2	3.8	2.3	3.2

% of Atoms

	Granite	Basalt	Ultra Basalt
0	60.0	56.5	57.1
Na	2.7	1.7	.4
Ng	.6	4.5	18.5
41	7.3	7.9	1.0
Si	23.2	16.3	14.6
K	2.6	.7	.1
Ca	1.4	5.5	1.6
Mn	.1	1.1	.2
Fc	2.1	5.7	6.5

APPENDIX D

INFRARED EXPERIMENT

Experimental objectives and instrumentation description for a possible Infrared Experiment will be supplied later.

Results of recent sounding rocket observations are presently being evaluated.

APPENDIX E

MASS SPECTROMETER EXPERIMENT

Experimental objectives and instrumentation description for the Mass Spectrometer Experiment will be supplied later.